

AD-A066 726

MICHIGAN UNIV ANN ARBOR DEPT OF PHYSICS
NONLINEAR OPTICAL POLARIZABILITIES OF MOLECULES. (U)
JAN 78 C K MILLER

F/G 20/3

UNCLASSIFIED

AFOSR-TR-79-0365

AFOSR-77-3225

NL

1 OF 2
ADA
066726



AFOSR-TR- 79-0365

LEVEL *11*

(4)
B.S.

AD A0 66726

DDC FILE COPY

Nonlinear Optical Polarizabilities of Molecules

CHARLES KENNETH MILLER

PROFESSOR JOHN F. WARD, Chairman

January 1978

Supported in part by:
U.S. Air Force Office of Scientific Research

DDC
APR 2 1979
C



Department of Physics

Approved for public release;
Distribution unlimited.

AIR FORCE OFFICE OF SCIENTIFIC RESEARCH (AFSC)
NOTICE OF TRANSMITTAL TO DDC
This technical report has been reviewed and is
approved for public release IAW AFR 190-12 (7b).
Distribution is unlimited.
A. D. BLOSE
Technical Information Officer

79 03 30 068

UNCLASSIFIED

SECURITY CLASSIFICATION OF THIS PAGE (When Data Entered)

REPORT DOCUMENTATION PAGE		READ INSTRUCTIONS BEFORE COMPLETING FORM
1. REPORT NUMBER 18 AFOSR-TR-79-0365	2. GOVT ACCESSION NO.	3. RECIPIENT'S CATALOG NUMBER
4. TITLE (and Subtitle) NONLINEAR OPTICAL POLARIZABILITIES OF MOLECULES,	5. TYPE OF REPORT & PERIOD COVERED Interim Rept.	
7. AUTHOR(s) Charles Kenneth Miller	6. PERFORMING ORG. REPORT NUMBER	
9. PERFORMING ORGANIZATION NAME AND ADDRESS Department of Physics University of Michigan Ann Arbor, MI	8. CONTRACT OR GRANT NUMBER(s) AFOSR 77-3225	
11. CONTROLLING OFFICE NAME AND ADDRESS AFOSR/NP Bolling AFB Wash DC 20332	10. PROGRAM ELEMENT, PROJECT, TASK AREA & WORK UNIT NUMBERS 2301 A1 61102F	
14. MONITORING AGENCY NAME & ADDRESS (if different from Controlling Office) 12 136p.	12. REPORT DATE Jan 78	
	13. NUMBER OF PAGES 133	
	15. SECURITY CLASS. (of this report) unclassified	
	15a. DECLASSIFICATION/DOWNGRADING SCHEDULE	
16. DISTRIBUTION STATEMENT (of this Report) Approved for public release; distribution unlimited.		
17. DISTRIBUTION STATEMENT (of the abstract entered in Block 20, if different from Report)		
18. SUPPLEMENTARY NOTES		
19. KEY WORDS (Continue on reverse side if necessary and identify by block number)		
20. ABSTRACT (Continue on reverse side if necessary and identify by block number) A review is given of the relation between microscopic and macroscopic forms of electric tensor properties of both second and third orders. The Second Harmonic Generation process in a focused laser beam for a particular dc field geometry is also reviewed, and the treatment is extended to include anomalously dispersive gases. Hyperpolarizabilities and hyperpolarizability ratios have been measured for the molecules H_2 , N_2 , O_2 , CO , NO , CO_2 , SF_6 , NH_3 , H_2S , H_2O , $(CH_3)_2O$, and CH_3OH . The results are presented and compared with theoretical and		

UNCLASSIFIED

SECURITY CLASSIFICATION OF THIS PAGE(When Data Entered)

experimental data from other sources. Agreement with most other gas-phase experimental data is good, and where this is not the case, we believe our data to be the more reliable. Special points of interest are discussed for several of the molecules.

ABSTRACT

NONLINEAR OPTICAL POLARIZABILITIES
OF MOLECULES

by

Charles Kenneth Miller

Chairman: John F. Ward

The technique of dc-electric-field-induced second-harmonic generation (dcSHG) has been used to investigate higher-order polarizabilities (hyperpolarizabilities) of molecules in gases and vapors, and a model has been developed to describe trends in dipole moments, polarizabilities and hyperpolarizabilities for series of structurally related molecules.

A review is given of the relation between microscopic and macroscopic forms of electric tensor properties of both second and third orders. The dcSHG process in a focused laser beam for a particular dc field geometry is also reviewed, and the treatment is extended to include anomalously dispersive gases.

The experimental apparatus comprises a Q-switched ruby laser, optical components, detectors, and signal processing electronics, as well as a gas-handling and pressure measurement system which permits temperature-dependent gas-phase observations on substances which are

This document has been approved
for public release and sale; its
distribution is unlimited.

79 03 30 067

liquids at room temperature. A review is made of the various experiments by which the second- and third-order polarizabilities, ratios of hyperpolarizability components, and wave-vector mismatches are measured.

Hyperpolarizabilities and hyperpolarizability ratios have been measured for the molecules H_2 , N_2 , O_2 , CO , NO , CO_2 , SF_6 , NH_3 , H_2S , H_2O , $(CH_3)_2O$, and CH_3OH . The results are presented and compared with theoretical and experimental data from other sources. Agreement with most other gas-phase experimental data is good, and where this is not the case, we believe our data to be the more reliable. Special points of interest are discussed for several of the molecules.

The ability to work in the vapor phase with substances which are liquids at room temperature has enabled the acquisition of hyperpolarizability data on several halogenated methanes which are liquids at room temperature. Such data are now available for all molecules of the form CX_nY_{4-n} , $n = 1-4$, $X, Y = F, Cl, H$.

Correlations of electric tensor properties among molecules of similar structure are discussed. The familiar Bond Additivity Approximation is reviewed and applied to the dipole moments, linear polarizabilities, and hyperpolarizabilities of the set H_2O , $(CH_3)_2O$, and CH_3OH , and to the set of halogenated methanes. A model of molecular electric tensor properties is developed in

which electrostatic dipolar inter-bond interactions are accounted for in a self-consistent manner. A simplification of the model is applied with limited success to the set of halogenated methanes, and trends in the sizes of various interaction terms are noted.

NONLINEAR OPTICAL POLARIZABILITIES
OF MOLECULES

by

Charles Kenneth Miller

A dissertation submitted in partial fulfillment
of the requirements for the degree of
Doctor of Philosophy
(Physics)
in The University of Michigan
1978

Doctoral Committee:

Professor John F. Ward, Chairman
Professor Gordon L. Kane
Professor Emmett N. Leith
Professor T. Michael Sanders, Jr.
Professor Gabriel Weinreich

ACCESSION for	
NTIS	White Section <input checked="" type="checkbox"/>
DOC	Buff Section <input type="checkbox"/>
UNANNOUNCED	<input type="checkbox"/>
JUSTIFICATION	
BY	
DISTRIBUTION/AVAILABILITY CODES	
Dist.	Full and/or SPECIAL
A	

To My Wife, Diane
From the Darkness of Alone
to the Light of Together

To My Wife, Diane
From the Darkness of Alone
to the Light of Together

ACKNOWLEDGEMENTS

I am pleased to express my gratitude to Professor John F. Ward for suggesting this research program and for his advice, suggestions, and encouragement throughout its course. His thoroughness, patience, and sound physical intuition have been an inspiration to me in my work.

I am especially grateful to my wife Diane for her hours of typing and proofreading, and for her continued optimism and support.

Many other people have helped me in this endeavor. I wish to thank Irving J. Bigio for teaching me about the experimental apparatus, and I would like especially to thank my friend and lab co-worker Arlee Smith for his ready cooperation and counsel. I am grateful to Professor Brian J. Orr for his substantial contributions to the work on bond interactions, and to John Magerlein and Professor T. Michael Sanders, Jr., for their advice on bridge measurement techniques and for their inexhaustible supply of equipment. My appreciation goes to the men of Paul Halloway's instrument shop, particularly Ernst Lueder, for construction of apparatus and for design advice. A word of thanks goes to Connie Barker for her extra efforts in typing the final draft.

Finally, the financial support furnished by the Air Force Office of Scientific Research is gratefully acknowledged. **Grant no. AFOSR-77-3225**

TABLE OF CONTENTS

	Page
DEDICATION	ii
ACKNOWLEDGEMENTS	iii
LIST OF TABLES	vi
LIST OF FIGURES	vii
CHAPTER 1. INTRODUCTION	1
CHAPTER 2. THE THEORY OF DCSHG IN MOLECULAR GASES	6
2.1 Microscopic Hyperpolarizabilities ..	6
2.2 Relating Microscopic and Macro- scopic Hyperpolarizabilities	10
2.3 dcSHG in a Focused Beam	14
CHAPTER 3. THE DCSHG EXPERIMENTS	20
3.1 The Experimental Apparatus	20
3.2 Experiment Descriptions	28
3.3 Data Analysis and Typical Data	36
CHAPTER 4. EXPERIMENTAL RESULTS FOR ASSORTED SMALL MOLECULES	43
4.1 Experimental Parameters, Data, and Derived Quantities	44
4.2 Discussion of Results for Particular Molecules	51

	Page
CHAPTER 5. EXPERIMENTAL RESULTS FOR SOME HALOGENATED METHANES	59
CHAPTER 6. CORRELATION OF ELECTRIC TENSOR PROPERTIES AMONG SIMILAR MOLECULES	67
6.1 The Bond Additivity Approximation	68
6.2 The Interacting Segment Model	85
6.3 Application of the ISM to Electric Tensor Properties of the Halogenated Methanes	91
CHAPTER 7. SUMMARY AND CONCLUSIONS	109
APPENDIX	112
REFERENCES	120

LIST OF TABLES

Table		Page
1	Experimental parameters and data for assorted non-dipolar molecular gases	45
2	Experimental parameters and data for assorted dipolar molecular gases	46
3	$R^{(3)}$ and $\chi_{ }^{(3)}$ for assorted molecules	47
4	$R^{(2)}$ and $\chi_{ }^{(2)}$ for assorted dipolar molecules ..	49
5	Dawes approximation predictions for $\chi^{(3)}$ of H_2 , N_2 , and O_2	54
6	Experimental parameters and data for the halogenated methanes	60
7	$R^{(3)}$ and $\chi_{ }^{(3)}$ for the halogenated methanes	62
8	$R^{(2)}$ and $\chi_{ }^{(2)}$ for the halogenated methanes	64
9	BAA applied to α and $\chi_{ }^{(3)}$ for H_2O , $(CH_3)_2O$, and CH_3OH	72
10	Bond angles and bond radii for the halogenated methanes	93
11	Contributions to fitted ISM values of μ for the halogenated methanes	101
12	Contributions to fitted ISM values of α for the halogenated methanes	102
13	Contributions to fitted ISM values of $\Delta\alpha_K$ for the halogenated methanes	104
14	Contributions to fitted ISM values of $\chi_{ }^{(2)}$ for the halogenated methanes	105

LIST OF FIGURES

Figure		Page
1	Electrodes and interaction region	17
2	Schematic diagram of experimental apparatus	21
3	Room-temperature and high-temperature gas-handling systems	25
4	Capacitance manometer	26
5	Typical subrun and typical $ \chi^e $ run for NH_3	37
6	$\chi_{ }^e$ versus $1/T$ for NH_3	41
7	BAA applied to μ for H_2O , $(\text{CH}_3)_2\text{O}$, and CH_3OH	74
8	BAA applied to $\chi_{ }^{(2)}$ for H_2O , $(\text{CH}_3)_2\text{O}$, and CH_3OH	76
9	BAA applied to α for the halogenated methanes	78
10	BAA applied to $\chi_{ }^{(3)}$ for the halogenated methanes	79
11	BAA applied to μ for the halogenated methanes	81
12	BAA applied to $\chi_{ }^{(2)}$ for the halogenated methanes	82
13	Interaction between neighboring polarizable dipolar bodies	83
14	ISM applied to μ for the halogenated methanes	97
15	ISM applied to α , $\Delta\alpha_K$ and κ^2 for the halogenated methanes	98
16	ISM applied to $\chi_{ }^{(2)}$ for the halogenated methanes	99
17	Signal vs density for binary mixtures ...	119

CHAPTER 1

INTRODUCTION

The response of an isolated molecule to a strong electric field is of considerable theoretical and experimental interest. The ability to predict linear and nonlinear polarizabilities, which are measures of this response, is a stringent test of molecular orbital calculations, and accurate data are necessary for comparison. A knowledge of these values is also necessary to the experimentalist who may, for example, wish to separate out the effects of interparticle interactions in the polarizabilities of condensed phases. We have measured nonlinear polarizabilities of a number of molecules with the aid of the strong optical electric field of a focused ruby laser beam, and we have developed a model which is useful in correlating the permanent dipole moment and linear and nonlinear polarizabilities in groups of similar molecules.

A molecular system subjected to a (time-dependent) electric field E possesses an electric dipole moment $\mu(E)$. Disregarding for the moment the tensorial nature of the interaction, the relationship can be written

$$\mu(E) = \mu + \chi E \quad (1.1)$$

in which μ is the permanent dipole moment and χ is the electric dipole polarizability. χ is, in general, a

function of the applied field, and if it is analytic for a range of E , then in that range equation 1.1 may be written

$$\mu(E) = \mu + \alpha E + \chi^{(2)} E^2 + \chi^{(3)} E^3 + \dots \quad (1.2)$$

where α and $\chi^{(1)}$ are independent of E (the frequency dependence of α and $\chi^{(1)}$ is suppressed here; a more general equation will be presented in chapter 2). The linear polarizability α is responsible for the familiar dielectric properties of matter. For applied fields of optical frequency, α is manifested in such linear optical effects as the deviation of the linear index of refraction from 1 and Rayleigh scattering. A complete discussion of these phenomena can be found in reference 1. The quantities $\chi^{(n)}$, $n \geq 2$, are the nonlinear polarizabilities, or hyperpolarizabilities. Non-zero values of these coefficients imply that the induced dipole moment has terms proportional to second and higher powers of the applied field, and therefore that it may have components at frequencies which are sums and differences of the applied field frequencies. Effects due to these higher-order terms in the induced moment fall under the classification of non-linear optics.

Until the early 1960's, available optical electric fields of any particular frequency were small in magnitude, and effects due to the products of these fields were virtually undetectable; thus, observed "nonlinear optical"

effects were limited to those in which the optical polarization was at the same frequency as the incident optical field, and the higher order terms in $\mu(E)$ contained products of the optical field with dc fields. Examples of such processes are the (dc) Kerr effect and the linear electro-optic effect.² With the advent of powerful lasers, strong electric fields become available at optical frequencies, permitting the observation of non-linear optical phenomena of many types.³

Of interest in this dissertation is dc-electric-field-induced second-harmonic generation (dcSHG) in molecules in the gas phase. In dcSHG, the $\chi^{(3)}E^3$ term of equation 1.2, in which the field has components at optical frequency ω and at zero frequency (dc), yields a polarization with a component at the frequency 2ω . The dcSHG process was first studied in gases by Mayer *et al.*⁴ Subsequently, more accurate measurements were made by Finn⁵ and by Bigio,⁶ and the experiments described herein are in part an extension of these. We have expanded studies of the non-linear properties of a group of halogenated methanes^{5,6} to include CCl_4 , CHCl_3 , CH_2Cl_2 , CH_3Cl , CCl_3F , and CCl_2F_2 , so that data are now available for all twelve molecules of the form $\text{CX}_n\text{Y}_{4-n}$ with $n = 1-4$ and $X, Y = \text{F}, \text{Cl}, \text{H}$. In addition, a number of other small molecules were investigated: H_2 , N_2 , O_2 , CO , NO , CO_2 , H_2S , H_2O , $(\text{CH}_3)_2\text{O}$, CH_3OH , and SF_6 . All of the molecular systems studied here are simple enough to be potential candidates for

ab initio calculations of hyperpolarizabilities (calculations already exist for some), and data from various other nonlinear optical experiments are available for many of them. In addition, several of the molecules and groups of molecules have features of particular interest, to be discussed in due course.

In our experiments, the beam from a pulsed ruby laser is focused in a gas in a region of dc electric field, and the second-harmonic radiation generated at the focus is detected and measured. The problems of relating the nonlinear susceptibility of a molecular gas to the hyperpolarizability tensors of the molecules, and of determining this susceptibility from the second harmonic generated, are reviewed in chapter 2. In chapter 3, attention is turned to the experimental apparatus, and a description of the various types of experiments performed is given.

Experimental data and derived coefficients for the molecules other than halogenated methanes are presented in chapter 4. Comparisons with other experimental data and with available theoretical calculations are included, as well as discussions of specific points of interest for several of the molecules. Chapter 5 contains the data, coefficients, and comparisons with experiments and theory for the halogenated methanes.

The availability of the data for all of the halogenated methanes facilitates the critical evaluation of various

schemes for the correlation of molecular electric tensor properties among homologous molecules. In chapter 6, the Bond Additivity Approximation, a correlation scheme in which inter-bond interactions are ignored, is described with examples of its application and with notice taken of its drawbacks. An Interacting Segment Model, in which intramolecular interactions are accounted for approximately, is presented and applied to the dipole moments and to the linear and second-order polarizabilities of the halogenated methanes. The results are compared with those of bond additivity.

Chapter 7 contains a summary and conclusions concerning the data and the model.

CHAPTER 2

THE THEORY OF DCSHG IN MOLECULAR GASES

The objective of the dcSHG experiments described in this dissertation is to gain information about the nonlinear polarizabilities of isolated molecules. The experiments, however, must actually be performed on an ensemble of molecules, so that the nonlinear properties observed will be ensemble averages of those individual molecules and will therefore in general have different symmetry properties. In particular, a gas is macroscopically isotropic, even though an individual molecule of the gas may not be. In addition, dispersive effects, which can be ignored for a single molecule of dimensions much shorter than the wavelength of the fundamental or second-harmonic radiation, must be considered when the light traverses a sample of gas which is long compared with the wavelength.

In this chapter, the dcSHG process is reviewed for a microscopic system, after which the relation between microscopic and macroscopic hyperpolarizabilities in a dipolar molecular gas is examined. The chapter is concluded with a brief review of second-harmonic generation in the geometry of these experiments, including the effects of dispersion and a non-uniform dc electric field.

2.1 Microscopic Hyperpolarizabilities

Equations 1.1 and 1.2 are scalar simplifications of full tensor equations. For the general situation of applied field and induced moment with several frequency components

it is useful to express the Fourier amplitudes of the frequency and spatial components of the induced moment as functions of the Fourier amplitudes of the frequency and spatial components of the applied field. The general equation for the Fourier amplitude of the induced dipole moment per molecule at frequency ω_σ is

$$\begin{aligned} \mu_j^{\omega_\sigma} = & \sum_{n=1}^{\infty} \sum_{\substack{\omega_1 + \dots + \omega_n = \omega_\sigma \\ \omega_1 \leq \dots \leq \omega_n}} K(-\omega_\sigma; \omega_1, \dots, \omega_n) \\ & \times \chi_{j i_1 \dots i_n}(-\omega_\sigma; \omega_1, \dots, \omega_n) E_{i_1}^{\omega_1} \dots E_{i_n}^{\omega_n} \end{aligned} \quad (2.1)$$

where summation over repeated indices is implied. The $E_j^{\omega_m}$ are Fourier amplitudes of the time-dependent components of the applied electric field with frequency ω_m and polarization vector \hat{j} , given by

$$E_j^{\omega_m}(t) = \frac{1}{2} (E_j^{\omega_m} e^{-i\omega_m t} + E_j^{-\omega_m} e^{i\omega_m t}) \quad (2.2)$$

where $E^{-\omega}$ is the complex conjugate of E^ω . The definition of $K(-\omega_\sigma; \omega_1, \dots, \omega_n)$ is discussed by Orr and Ward.⁷ Basically, K includes factors from Fourier decomposition of fields and from distinguishable permutations of field frequency labels, with the results that:

1. A single ordering of field frequencies may be used, i.e., one need only write,

say, $\chi(-\omega_\sigma; \omega_1, \omega_2)$ and not $\chi(-\omega_\sigma; \omega_2, \omega_1)$
in addition;

2. $\lim_{\omega_1, \dots, \omega_n \rightarrow 0} \chi(-\omega; \omega_1, \dots, \omega_n) = \chi(0; 0, \dots, 0)$; and
3. $K(0; 0, \dots, 0) = 1$ for all orders of hyperpolarizability.

For a molecule subjected to an optical electric field \underline{E}^ω and a dc field \underline{E}^0 , the dipole moment amplitude at frequency 2ω to third order in the applied fields is, from equation 2.1,

$$\begin{aligned} \mu_i^{2\omega} = & \frac{1}{2} \chi_{ikl}(-2\omega; \omega, \omega) E_k^\omega E_l^\omega \\ & + \frac{3}{2} \chi_{ijk}(-2\omega; 0, \omega, \omega) E_j^0 E_k^\omega E_l^\omega \end{aligned} \quad (2.3)$$

where the factors $1/2$ and $3/2$ are the values of $K(-2\omega; \omega, \omega)$ and $K(-2\omega; 0, \omega, \omega)$ respectively. To get a rough idea of the relative sizes of the contributions to $\mu_i^{2\omega}$, it is useful to examine the form of time-dependent quantum-theoretical perturbation expansions⁷ for the non-resonant second- and third-order contributions to equation 2.3. These expansions contain terms like the following:

(second order term) =

$$\frac{3e^3}{\hbar^2} \frac{\langle X_i \rangle_{gm} \langle X_k \rangle_{mn} \langle X_l \rangle_{ng}}{(\omega_{mg} + 2\omega)(\omega_{ng} - \omega)} E_k^\omega E_l^\omega \quad (2.4)$$

(third order term) =

$$\frac{-4e^4}{n^3} \frac{\langle X_i \rangle_{gp} \langle X_j \rangle_{pm} \langle X_k \rangle_{mn} \langle X_l \rangle_{ng}}{(\omega_{pg} + 2\omega)(\omega_{mg} - 2\omega)(\omega_{ng} - \omega)} E_j^0 E_k^{\omega} E_l^{\omega} \quad (2.5)$$

where the ω_{rs} are molecular transition frequencies and $e\langle X_q \rangle_{rs}$ are dipole matrix elements between states. To obtain an order-of-magnitude estimate of the relative sizes of these terms, we first replace the matrix elements by a typical molecular dimension r . Further, we assume that the ω_{rs} are all much larger than ω or 2ω , and can all be replaced by one effective frequency ω_0 . Then, noting that the electron energy $\hbar\omega_0$ is approximately e^2/r and the typical intramolecular field E_{mol} is of the order e/r^2 , we see that the third-order polarization terms differ from the second-order by a factor of E^0/E_{mol} . With a typical r of 1 Å, E_{mol} is of the order of 10^7 esu; thus $\mu^{2\omega}$ (second-order) is much larger than $\mu^{2\omega}$ (third-order) for electric fields E^0 which can be sustained in gases at ordinary pressures without breakdown ($\sim 10^2$ esu). As will be seen in the next section, however, incomplete molecular alignment causes the polarizations arising from second- and third-order molecular SHG processes that are actually observed in the gas phase to be of roughly the same magnitude.

2.2 Relating Microscopic and Macroscopic Hyperpolarizabilities

In an unperturbed molecular gas, the orientation of the coordinate frame of a given molecule with respect to the laboratory coordinate frame is completely random. In what follows, the alignment of molecules by an electric field is treated classically. This approach is justified because the thermal energy kT at room temperature is sufficiently larger than the rotational constants for all dipolar molecules studied that the classical limit of orientational averaging is consistent with a quantum mechanical rotational state distribution. If the gas is subjected to a uniform electric field \underline{E} and transient effects are allowed to die out, distribution of molecular orientations will contain the Boltzmann weighting factor

$$g = \exp(-u/kT), \quad (2.6)$$

where

$$u = - \left\langle \int_0^1 \underline{\mu}(\xi \underline{E}) \cdot \underline{E} d\xi \right\rangle, \quad (2.7)$$

k is Boltzmann's constant, and the angular brackets indicate an average over a time long compared with the orientational relaxation time of the molecule. The dipole moment $\underline{\mu}$ will, in general, contain contributions from all orders of polarizability. The magnitude of u is, to a good approximation, just μE^0 , where μ is the magnitude

of the permanent dipole moment of the molecule ($\sim 10^{-18}$ esu) and E^0 is the magnitude of the dc component of \underline{E} . With an E^0 of ~ 40 esu, the orientational energy is about 4×10^{-17} erg, compared to kT of 4×10^{-14} erg at room temperature. Thus we may write

$$g \sim 1 - u/kT. \quad (2.8)$$

The orientational average of $\underline{\mu}^{2\omega}$ is given by

$$\langle \underline{\mu}^{2\omega} \rangle = \frac{\int (\underline{\mu}^{2\omega}) g \, d\Omega}{\int g \, d\Omega} \quad (2.9)$$

where integration over Ω indicates formally the integration over all orientations of molecular coordinates with respect to laboratory coordinates. In equation 2.9 $\underline{\mu}^{2\omega}$ has the form

$$\begin{aligned} \mu_i^{2\omega} = & \frac{1}{2} \chi_{ikl}(-2\omega; \omega, \omega) \phi_{Fi} \phi_{Hk} \phi_{Ml} E_H^\omega E_M^\omega \\ & + \frac{3}{2} \chi_{ijk}(-2\omega; 0, \omega, \omega) \phi_{Fi} \phi_{Gj} \phi_{Hk} \phi_{Ml} E_G^0 E_H^\omega E_M^\omega \end{aligned} \quad (2.10)$$

where i, j, k, l refer to the molecular coordinate frame, F, G, H, M refer to the laboratory frame, and the ϕ_{Nr} are direction cosines between the molecular and lab frame coordinate axes. The only terms retained in equation 2.9 are those of up to first order in E^0 and up to second order in \underline{E}^ω . The only term in u contributing to these coefficients is $\mu_j \phi_{Gj} E_G^0$ (another term of comparable size

in this experiment would be $(1/2)\chi_{kl}(-\omega;\omega)\phi_{Hk}\phi_{Ml}E_H^\omega E_M^\omega$, but it does not survive the orientational averaging). The integral in equation 2.9 has been performed⁵ and yields the result

$$\mu_F^{2\omega} = \frac{3}{2}(\chi_{FGHM}^{(3)} + \frac{1}{9kT} \mu \chi_{FGHM}^{(2)}) E_G^0 E_H^\omega E_M^\omega, \quad (2.11)$$

where

$$\chi_{FGHM}^{(3)} = \langle \phi_{Fi} \phi_{Gj} \phi_{Hk} \phi_{Ml} \rangle \chi_{ijkl}(-2\omega; 0, \omega, \omega) \quad (2.12)$$

and

$$\mu \chi_{FGHM}^{(2)} = \langle \phi_{Fi} \phi_{Gz} \phi_{Hk} \phi_{Ml} \rangle \mu_z \chi_{ikl}(-2\omega; \omega, \omega) \quad (2.13)$$

The $\langle \phi_{Fi} \phi_{Gj} \phi_{Hk} \phi_{Ml} \rangle$ are averages of products of direction cosines over all molecular orientations, which have been tabulated by Cyvin et al.,⁸ and \hat{z} is the direction of the molecular dipole moment, as discussed in section 3.2c.

It should be noted that all contributions to $\mu^{2\omega}$ of second order in the electric field average to zero in equation 2.9, so that one may write

$$\mu_F^{2\omega} = \frac{3}{2} \chi_{FGHM}^e E_G^0 E_H^\omega E_M^\omega \quad (2.14)$$

where the effective hyperpolarizability per molecule, χ^e , is given by

$$\chi_{FGHM}^e = \chi_{FGHM}^{(3)} + \frac{\mu}{9kT} \chi_{FGHM}^{(2)} \quad (2.15)$$

The isotropy of the gas phase places strong restrictions on χ^e . For example, given the coordinate transformation $X' = -X$, isotropy demands that

$$\chi_{X'YYY}^e = \chi_{XYYY}^e \quad (2.16)$$

Now considering the process

$$\langle \mu_X^{2\omega} \rangle = \frac{3}{2} \chi_{XYYY}^e E_Y^{\omega} E_Y^{\omega} \quad (2.17)$$

the electric fields in the \hat{Y} direction do not change sign under the coordinate transformation, but the dipole moment, having the parity of an electric field in the \hat{X} direction, does change sign, so that

$$\begin{aligned} -\langle \mu_X^{2\omega} \rangle &= \langle \mu_{X'}^{2\omega} \rangle = \frac{3}{2} \chi_{X'YYY}^e E_Y^{\omega} E_Y^{\omega} \\ &= \frac{3}{2} \chi_{XYYY}^e E_Y^{\omega} E_Y^{\omega} = \langle \mu_X^{2\omega} \rangle \end{aligned} \quad (2.18)$$

It follows that $\langle \mu_X^{2\omega} \rangle$, and therefore χ_{XYYY}^e , are zero. By considering similar coordinate transformations and exchange symmetry of the two electric fields at frequency ω , it follows⁵ that there are only two independent non-zero elements of χ_{FGHM}^e , and therefore of $\chi_{FGHM}^{(2)}$ and $\chi_{FGHM}^{(3)}$, and that they can be chosen to be $FGHM = YYYY$ (to be denoted as \parallel) and $FGHM = YYXX$ (to be denoted \perp). The symbols \parallel and \perp thus stand for the situations in which the applied optical electric field polarization is respectively parallel to and perpendicular to the dc field direction.

$\chi_{\parallel,\perp}^{(3)}$ and $\chi_{\parallel,\perp}^{(2)}$ can be evaluated⁵ in terms of molecular-frame

components using equations 2.12 and 2.13 to give

$$\chi_{\parallel}^{(3)} = \frac{2}{15} \chi_{\sigma\eta\sigma\eta}(-2\omega; 0, \omega, \omega) + \frac{1}{15} \chi_{\sigma\sigma\eta\eta}(-2\omega; 0, \omega, \omega) \quad (2.19)$$

$$\chi_1^{(3)} = \frac{2}{15} \chi_{\sigma\sigma\eta\eta}(-2\omega; 0, \omega, \omega) - \frac{1}{15} \chi_{\sigma\eta\sigma\eta}(-2\omega; 0, \omega, \omega) \quad (2.20)$$

$$\chi_{\parallel}^{(2)} = \frac{2}{5} \chi_{\eta\eta z}(-2\omega; \omega, \omega) + \frac{1}{5} \chi_{z\eta\eta}(-2\omega; \omega, \omega) \quad (2.21)$$

$$\chi_1^{(2)} = \frac{2}{5} \chi_{z\eta\eta}(-2\omega; \omega, \omega) - \frac{1}{5} \chi_{\eta\eta z}(-2\omega; \omega, \omega) \quad (2.22)$$

where summation over repeated indices is implied.

The nonlinear polarization of the medium is the average induced nonlinear dipole moment of each molecule times the number density of the molecules:

$$P_F^{2\omega} = \rho L \chi_{FGHM}^e E_G^0 E_H^\omega E_M^\omega \quad (2.23)$$

where L is Loschmidt's number ($2.69 \times 10^{19} \text{ cm}^{-3}$) and ρ is the number density of the gas in units of Loschmidt's number (ρ is a dimensionless quantity and is equal to 1 for an ideal gas at STP). In equation 2.23, no distinction is made between the applied electric field and the local field. The inequivalence of these fields is important in condensed phases;⁹ however, in gases at the pressures used in these experiments, intermolecular interactions are small,⁵ and the local field can be assumed to be equal to the applied field.

2.3 dcSHG in a Focused Gaussian Beam

The polarization at the optical frequency 2ω given

by equation 2.23 will emit electromagnetic radiation at that frequency. The pattern and intensity of this emission depends on the spatial distribution of \underline{E}^0 and \underline{E}^ω , and of the dispersion of the gas. Dependence of dcSHG on the parameters of this experiment is discussed by Finn⁵ and by Bigio et al.,¹⁰ and only the major points are sketched here.

The propagation of the second-harmonic beam is described by the inhomogeneous wave equation

$$\nabla \times \nabla \times \underline{E}^{2\omega}(\underline{r}) + \epsilon \frac{4\omega^2}{c^2} \underline{E}^{2\omega}(\underline{r}) = -4\pi \frac{4\omega^2}{c^2} \underline{P}^{nl}(\underline{r}) \quad (2.24)$$

where $\underline{P}^{nl}(\underline{r})$ is the driven second-harmonic polarization given by equation 2.23. The incident optical field for a lowest-order Gaussian beam propagating in the \hat{z} direction and polarized in the y direction is given by

$$\underline{E}^\omega(\underline{r}) = \hat{y} E^\omega \frac{e^{ik^\omega b \xi / 2}}{1 + i\xi} \exp\left(\frac{-k^\omega(x^2 + y^2)}{b(1 + i\xi)}\right) \quad (2.25)$$

where b is the confocal parameter, k^ω is the wave vector at frequency ω , and the dimensionless parameter ξ , equal to $2z/b$, is introduced for convenience. The second-harmonic field is assumed also to be a Gaussian beam coaxial and confocal with the incident beam, with the same b and with k^ω replaced by $k^{2\omega}$, but having an additional factor of a slowly-varying z dependence, reflecting

the (assumed) slow, uniform generation of second harmonic as the beam proceeds in the \hat{z} direction. All that is needed to complete the definition of equation 2.25 is the specification of the dc field.

In these experiments, the dc electric field is generated by maintaining a voltage difference between two long, parallel cylindrical electrodes each of radius a , with a distance l between centers, as shown in figure 1. The electric field on the z axis is calculated⁵ to be

$$\underline{E}^O(z) = \hat{y} \frac{2V_0}{d \cosh^{-1}(l/2a)} \cdot \frac{1}{(1 + 4z^2/d^2)}, \quad (2.26)$$

where

$$d = (l^2 - 4a^2)^{1/2} \quad (2.27)$$

is the distance between equivalent line charges and V_0 is the potential difference between the electrodes. The positional relationship of the dc electric field with respect to the incident beam is shown in figure 1. The beam is perpendicular to the plane of the electrode centers and equidistant from them, with the waist of the beam located a distance z_0 from the electrode plane. Since the beam is of small extent in the x and y directions near the electrodes, it is a good approximation to say that $\underline{E}^O(\underline{r}) = \underline{E}^O(z)$.

Using the aforementioned approximations, and adding those of small far-field diffraction angle, negligible

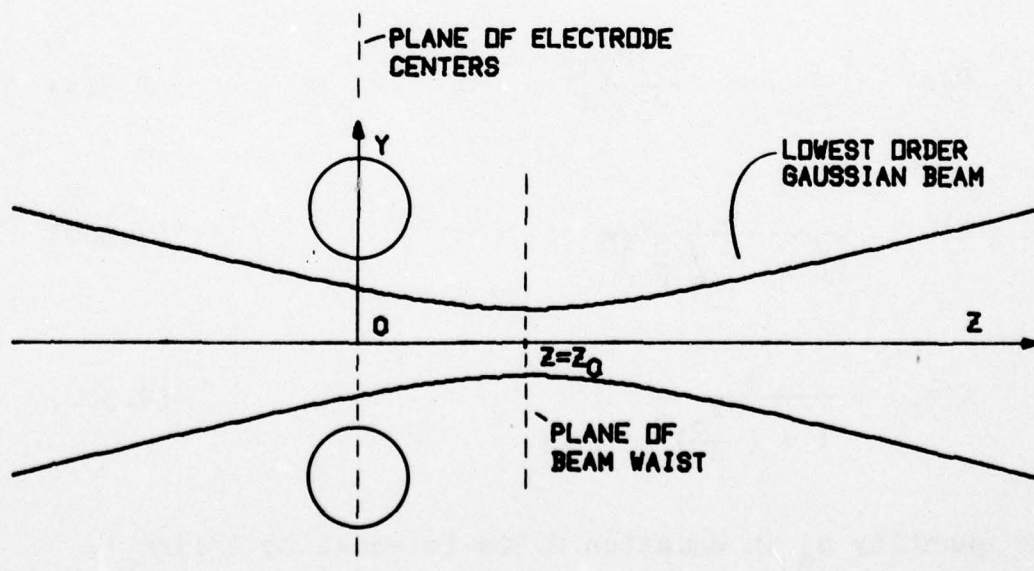
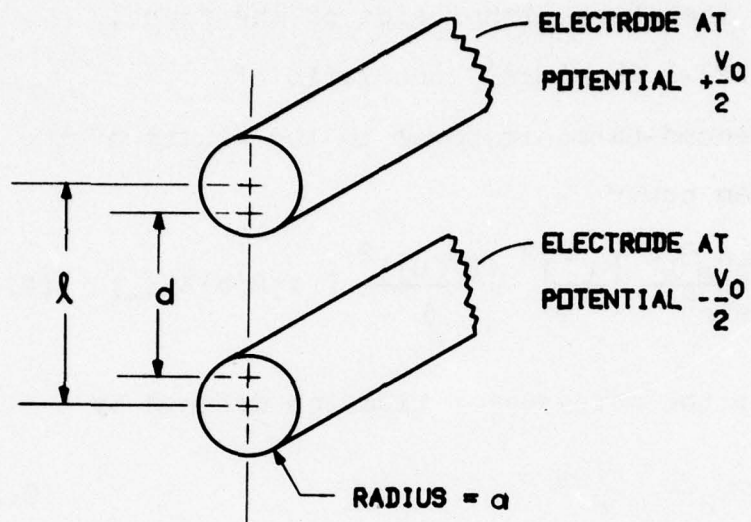


Figure 1. Electrodes and Interaction Region.

fundamental-beam depletion, and path-length in the gas much longer than b on either side of the focus, equations 2.24-2.26 yield¹¹ the ratio of generated second-harmonic power to the square of the incident-beam power:

$$\frac{P^{2\omega}}{(P^\omega)^2} = \frac{72\pi^4 \omega^3 L^2}{e^2 c^4} \left| \frac{\chi^e}{\Delta k_o} \right|^2 \frac{(E^o(0))^2}{d} \Gamma(\rho) B(b) Z(z_o) \quad (2.28)$$

Here, Δk_o is the wave-vector mismatch defined by

$$\Delta k_o = 2k_o^\omega - k_o^{2\omega} \quad (2.29)$$

where the subscript o indicates that a quantity is evaluated at $\rho = 1$. The dimensionless functions in equation 2.28 are as follows:

$$\Gamma(\rho) = \left[\frac{\rho}{\rho_o} \exp \left(\frac{\rho_o - \rho}{\rho_o} \right) \right]^2 ; \quad (2.30a)$$

$$B(b) = \frac{4}{\left(\sqrt{\frac{b}{d}} + \sqrt{\frac{d}{b}} \right)^2} ; \quad (2.30b)$$

$$Z(z_o) = \frac{1}{1 + \left(\frac{2z_o}{d} \right)^2} \quad (2.30c)$$

The quantity ρ_o in equation 2.30a is equal to $2/d|\Delta k_o|$. Maximum values of 1 are attained for the functions in equations 2.30a, b, and c for ρ equal to ρ_o , b equal to d , and z_o equal to zero, respectively. When these

conditions are met, equation 2.28 becomes

$$\frac{P^{2\omega}}{(P^\omega)^2} \sim \left| \frac{\chi^e}{\Delta k_0} \right|^2 V_o^2 \quad (2.31)$$

where this quantity is fairly insensitive to small density variations, small displacement of the focus, and small changes in the interelectrode separation. However, the experimental signal depends on such things as alignment, photomultiplier quantum efficiency, and so on, which are susceptible to slow random drifts. These factors will be discussed further in section 3.3.

We have seen that a molecular gas subjected to a dc electric field and irradiated by an optical field can have a polarization at twice the optical frequency as a consequence of the second- and third-order nonlinear polarizabilities $\chi^{(2)}$ and $\chi^{(3)}$ of the molecules. Further, we have seen how this polarization will radiate at the second harmonic frequency for a particular configuration of dc and optical fields. This effect can be exploited in measuring the components of the molecular hyperpolarizabilities. The details of such experiments are examined in the next chapter.

CHAPTER 3

THE DCSHG EXPERIMENTS

The relation embodied in equation 2.31 indicates how measurements of dcSHG in molecular gases can be used to determine the nonlinear polarizabilities of the molecule. In the first section of this chapter, the experimental apparatus for making such measurements is described. In the second section, the experiments performed with this apparatus are explained individually. The third section contains a discussion of the data and data analysis, including an indication of statistical error limits and comments on possible systematic errors.

3.1 The Experimental Apparatus

The apparatus for the dcSHG experiments is similar to that described in detail by Bigio,⁶ and is illustrated in figure 2. A brief sketch is given here of the various components, with differences from Bigio's apparatus noted.

The fundamental optical electric field is generated by a flashlamp-pumped actively Q-switched ruby laser, Korad model K-15, operating at 6943 Å. The laser cavity contains a 1.5 mm aperture to reduce higher-order transverse modes, simultaneously limiting the power to 1-2 MW in a pulse of ~ 20 ns duration. The laser is fitted at its output with a Glan-Laser polarizer, manufactured by the Karl Lambrecht Corporation, to ensure accurate linear polarization.

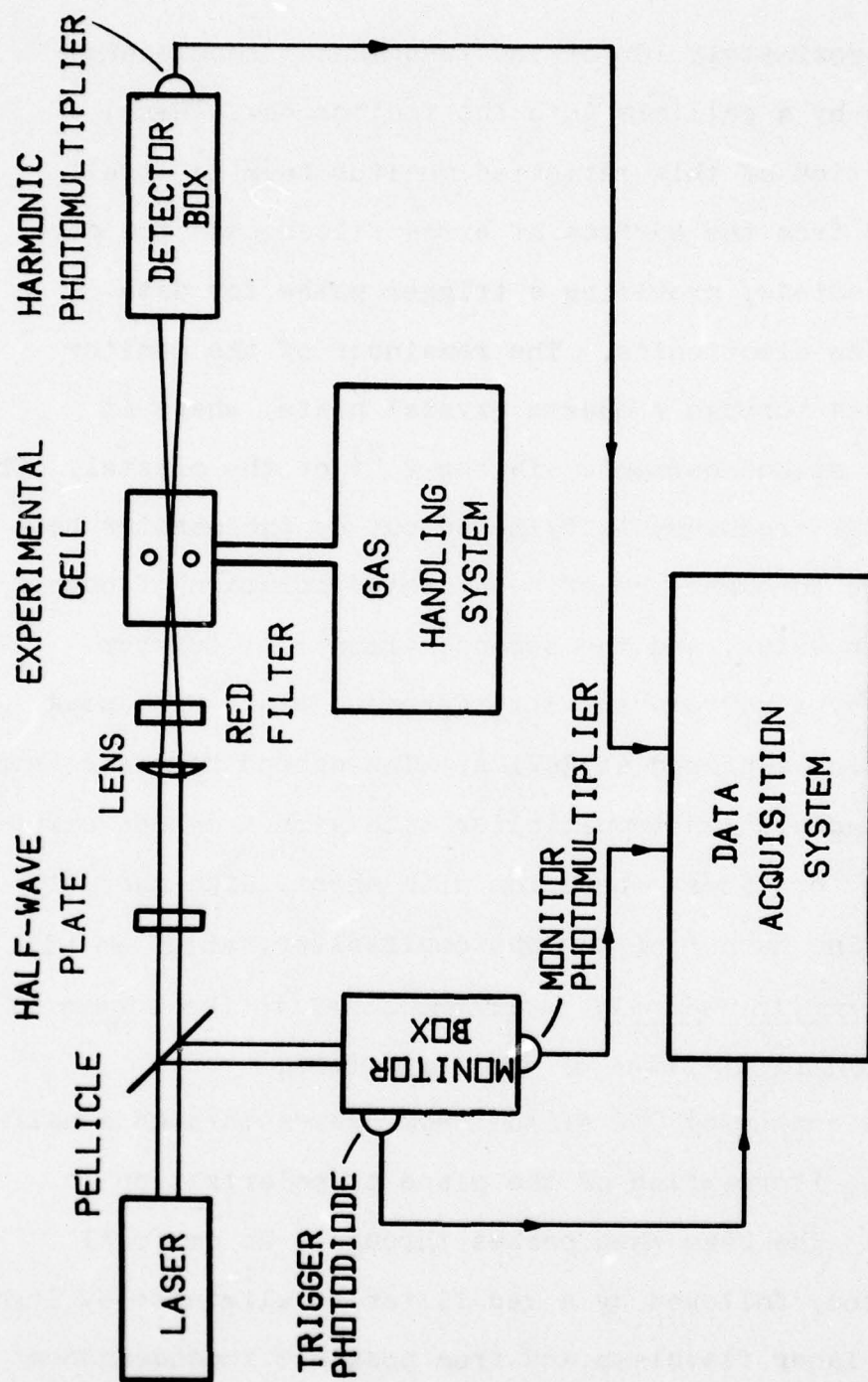


Figure 2. Schematic Diagram of Experimental Apparatus.

Approximately 10% of the fundamental beam energy is reflected by a pellicle into the monitor box. Here, a small portion of this reflected monitor beam is itself reflected from the surface of a red filter onto the face of a photodiode, providing a trigger pulse for data-acquisition electronics. The remainder of the monitor beam passes through a quartz crystal plate, where it generates second harmonic via the $\chi^{(2)}$ of the crystal. The fundamental frequency is filtered out of the monitor beam by passage through 5 cm of a saturated solution of copper sulfate in water, and the second harmonic is further isolated by a narrow-band interference filter with peak transmission centered at 3471 Å. The second harmonic beam is detected by a photomultiplier tube with a dynode circuit optimized for linear operation with short, high-current, pulses. The output of the photomultiplier, which we will call the monitor signal, is proportional to the square of the instantaneous power of the laser beam.

The remaining 90% of the beam passes through a half-wave plate if rotation of the plane of polarization is required. The beam then passes through a 26 cm focal length lens, followed by a red filter to eliminate UV light from the laser flashlamp and from possible incandescence at the surfaces of optical components, and is focused in the experimental cell.

The experimental cell is stainless steel, with

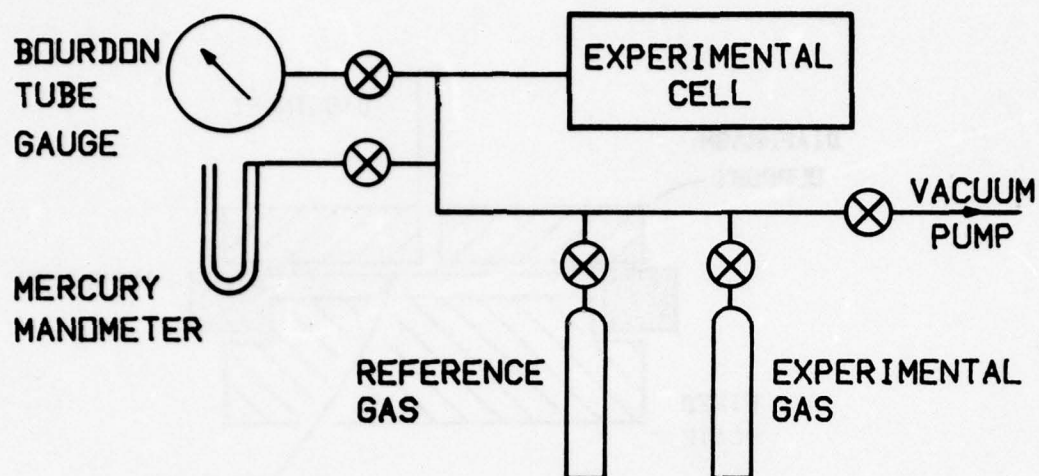
anti-reflection-coated fused silica windows sealed to it by means of o-rings. Criteria for o-ring material selection are resistance to high temperature and compatibility with the particular gas under investigation. Among materials used were silicone rubber, ethylene propylene, Teflon, and Viton. The cell houses the electrodes described in section 2.3, consisting of 2-inch long polished stainless steel rods, 1/16 inch in diameter and approximately 1/4 inch apart. The cell is wrapped with heating tapes, and its temperature is controlled to within 1°C by a proportioning controller. It can be filled with gas or vapor or evacuated through the gas-handling system described below.

The laser beam, along with the second harmonic generated in the interaction region of the cell, proceeds to the detector box, in which the fundamental is filtered out and the second harmonic is detected in the same manner as in the monitor box. The output of the detector box photomultiplier will be referred to as the harmonic signal. The harmonic and monitor signals are amplified as required and are gated by the trigger pulse to separate integrators. The integrated charges are digitized, and the digital values are punched on paper tape for later analysis by computer.

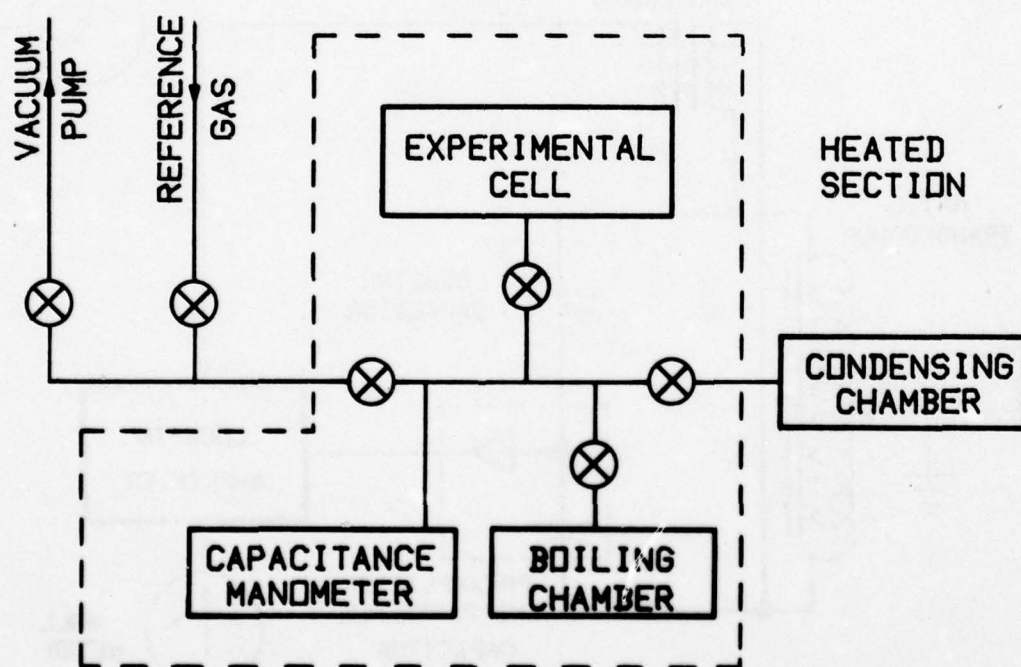
The gas handling system has been modified from that of Bigio to allow gas-phase measurements on substances which are liquids at room temperature. The room-temperature and

high-temperature gas handling systems are illustrated schematically in figure 3. The room-temperature system includes a Bourdon tube pressure gauge and mercury manometer for pressure measurement, and uses brass valves with plastic packing, with copper tubing for interconnection. In the high-temperature section, a high-temperature capacitance manometer is used to measure pressures, interconnecting tubing is made of stainless steel and is heated to temperatures above those used in the cell to ensure against condensation, and all-stainless-steel bellows valves with heated bonnets are used. The liquid sample is kept in a separately heated chamber at a temperature such that the vapor pressure is above the highest pressure to be used in the experiment. Waste vapors are condensed in a separate cooled chamber.

The capacitance manometer was constructed for these experiments to measure pressures in the range 0-2 atmospheres absolute, at temperatures in excess of 300°C. A cutaway drawing of the high-temperature pressure sensing element and a schematic diagram of the measuring circuit appear in figure 4. The pressure-dependent variable is the capacitance between a stainless steel diaphragm and a fixed metal plate. The diaphragm forms one wall of a capsule, the interior of which is connected to the vapor being measured. The other side of the diaphragm is at atmospheric pressure. The thickness of the insulator between the capsule and the fixed plate was chosen so

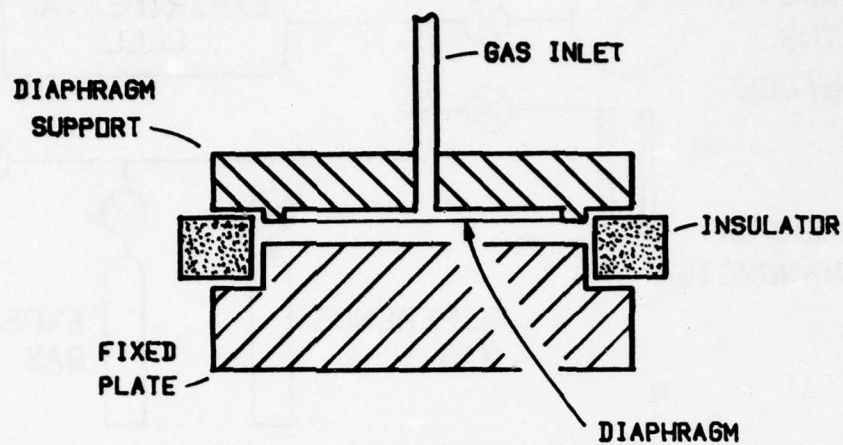


ROOM TEMPERATURE SYSTEM

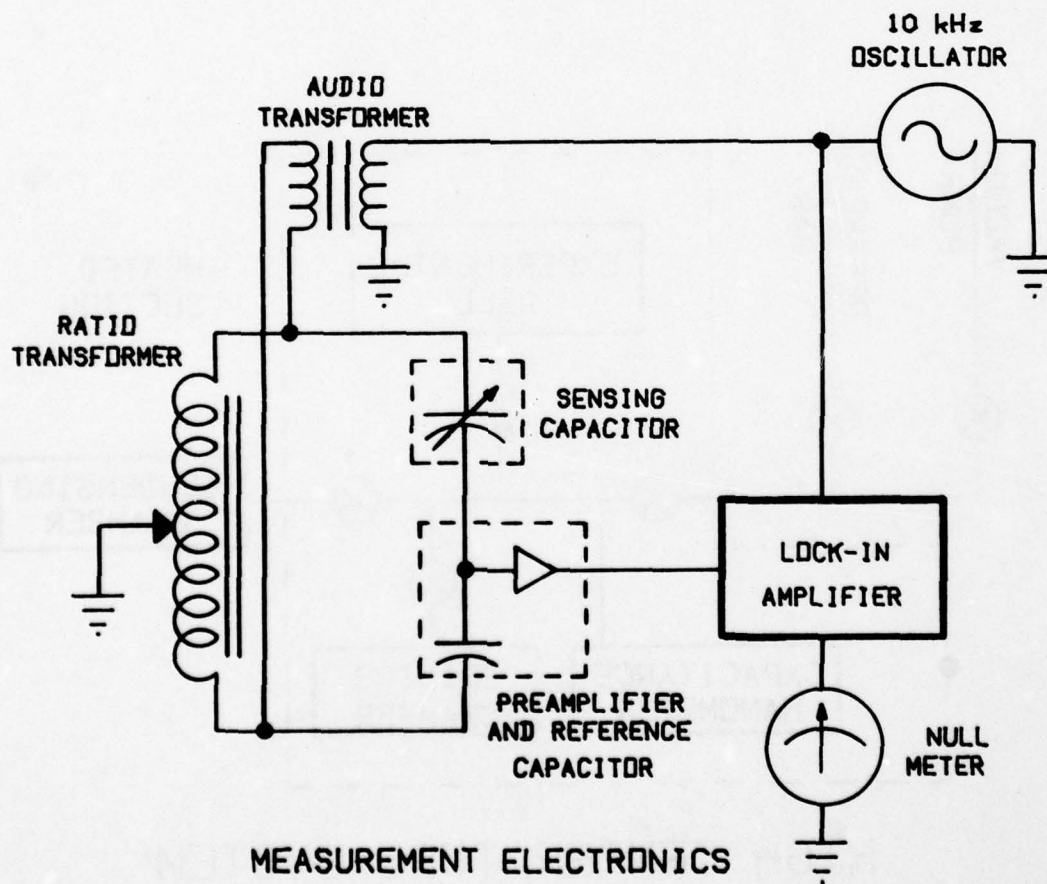


HIGH TEMPERATURE SYSTEM

Figure 3. Room-Temperature and High-Temperature Gas-Handling Systems.



PRESSURE SENSING CAPACITOR



MEASUREMENT ELECTRONICS

Figure 4. Capacitance Manometer.

that the coefficient of thermal expansion of the gap would be zero. While this goal was not achieved exactly, control of the sensor temperature to 1°C was sufficient to limit thermal drift to an acceptable level. The capacitance of the sensor head forms one leg of an ac bridge circuit; the rest of the bridge consists of a fixed silver mica capacitor and the two legs of a Singer Ratiotran ratio transformer, which is effectively an inductor with a finely variable tap. The bridge is driven with a 10 kHz sine wave from a low-distortion Wien bridge oscillator. Any out-of-null signal from the bridge is detected with a simple lock-in amplifier circuit. If y is the ratio of the inductance of the upper leg of the transformer to that of the lower leg, then when the bridge is nulled, y is proportional to C_s , the capacitance of the sensor. This capacitance unfortunately does not vary linearly with the pressure difference across the diaphragm. However, one can expand the pressure difference p as a power series in y

$$p = a_1(y-y_0) + a_2(y-y_0)^2 + a_3(y-y_0)^3, \quad (3.1)$$

and likewise y as a function of p

$$(y-y_0) = b_1p + b_2p^2 + b_3p^3 \quad (3.2)$$

where y_0 is the value of y at $p=0$, i.e., when the vapor is at atmospheric pressure. (Equations 3.1 and 3.2 are used for respectively measuring and setting pressure.)

Coefficients a_i and b_i can be chosen such that these functions fit the actual p vs. y data to better than 2 mm Hg. Drift and hysteresis amount to no more than 5 mm Hg. for absolute pressures up to 2 atm, permitting measurements of $|\Delta k_0|$, as described below, to better than 1%. The sensor element is kept continuously at a temperature higher than the maximum temperature to be used in the experimental cell. If the sensor temperature is changed, a new calibration of the a_i and b_i is made before the gauge is used again.

3.2 Experiment Descriptions

Ignoring statistical and systematic fluctuations (discussed in section 3 of this chapter) the harmonic signal is proportional to $P^{2\omega}$ and the monitor signal is proportional to $(P^\omega)^2$. We call the ratio of the harmonic to the monitor signals simply the signal, denoted by S . Given the interaction geometry of figure 1, we see from equation 2.31 that

$$S = c \left| \frac{\chi^e}{\Delta k_0} \right|^2 v_o^2 \quad (3.3)$$

with the density set to ρ_0 as discussed in section 2.3.

The following experiments exploit this relation to determine $\chi_{\parallel,1}^{(3)}$ and $\chi_{\parallel,1}^{(2)}$.

3.2a $|\chi_{\parallel}^e|$

In this experiment measurements of S for a particular gas are made alternately with measurements of S for a reference gas, all at a particular temperature. Measure-

ments relative to a reference gas are favored over absolute measurements because of difficulties in calibrating C in equation 3.3 absolutely, as discussed in section 3 of this chapter. In a typical data run at a fixed temperature, 5 subruns of 40 laser shots each, with the experimental gas in the cell, are interleaved with 5 subruns in which the reference gas is in the cell. Helium was used as the reference gas by Ward and Bigio,¹² but in their experiment, C was calibrated only at room temperature in a cell which could withstand the high pressure at optimum density for helium (approximately 600 psi). However, for substances which are liquids at room temperatures, C had to be calibrated at elevated temperatures, and for some gases investigated, the change in $|\chi^e|$ over the accessible temperature range was comparable to systematic drifts over the time required to make the measurements, so it was found desirable to calibrate C at various temperatures. For these situations S had to be measured for the reference gas in the more fragile heated cell, which contains delicate ceramic-to-metal seals, so a gas with a lower pressure at optimum density was used. Methane was chosen as the alternate reference because of its ready availability and reasonable (~ 1 atm) pressure at optimum density. Methane was compared carefully with helium (see section 4.2) in a high-pressure cell. It should be noted that neither helium nor methane has a permanent dipole moment, so that from equation 2.17 each has a χ^e which is independent of

temperature.

Using equation 3.3, with primes to indicate reference gas values, we can write

$$|\chi_{\parallel}^e(T)| = \chi_{\parallel}^{e'} \left(\frac{S(T)}{S'} \right)^{1/2} \left| \frac{\Delta k_o}{\Delta k_o'} \right|. \quad (3.4)$$

An experiment described below is used to determine Δk_o for the experimental gases and for methane. For helium, Δk_o can be determined from accurate data on the dispersion of the index of refraction:¹³

$$\Delta k_o(\text{He}) = 0.0946 \text{ cm}^{-1} \quad (3.5)$$

To establish an absolute scale for the magnitude of χ^e , we use a value calculated by Sitz and Yaris¹⁴ which is thought to be accurate to 1%:

$$\chi_{\parallel}^e = \chi_{zzzz}(-2\omega; 0, \omega, \omega) = +3.79 \times 10^{-39} \text{ esu/helium atom} \quad (3.6)$$

3.2 b Sign of χ^e

According to equation 3.3, the signal is independent of the sign of χ^e . However, the relative signs of χ^e for two different molecules can be established by measuring signals generated in binary mixtures of gases.¹⁵ If the χ^e are of opposite sign, cancellation will lead to zero signal for some ratio of gas densities. In practice, the signal is measured with a fixed density of reference gas, and the density of experimental gas is varied through a

range including the expected cancellation value. The variation of signal with density of experimental gas can be predicted⁵ for both cancellation and no cancellation, and is quite different for the two cases; in addition, as is shown in the Appendix, the cases with $\Delta k_0 > 0$ (of which none were encountered in these experiments) would exhibit variations quite different from those of normally dispersive gases.

Two possible references for absolute determination of the sign of χ^e may be employed. Either the (positive) sign of the calculated value for helium¹⁴ may be used, or one may assume that the experimentally determined (positive) sign of the Kerr coefficient for argon¹⁶ is the same as that of the dcSHG coefficient. Binary mixture experiments¹³ have verified that the dcSHG coefficients of helium and argon are of the same sign, so that there is no inconsistency in these methods.

A least-squares fit of the absolute, signed values of χ^e as a linear function of $1/T$ may now be made to determine the parameters in the \parallel version of equation 2.15, which can be written as

$$\chi_{\parallel}^e = \chi_{\parallel}^{(3)} + \frac{\mu}{9kT} \chi_{\parallel}^{(2)}. \quad (3.7)$$

The best-fit line yields the values

$$\chi_{\parallel}^{(3)} = \lim_{1/T \rightarrow 0} \chi_{\parallel}^e, \quad (3.8)$$

$$\chi_{\parallel}^{(2)} = \frac{9k}{\mu} \frac{d\chi^e}{d(1/T)} \quad (3.9)$$

We see from equation 3.7 that since the sign of $\chi^e(T)$ has been measured, the sign of $\mu\chi^{(2)}$ is determined unambiguously. We choose to assign to $\chi^{(2)}$ the sign measured for $\mu\chi^{(2)}$. This choice is the equivalent of choosing the molecular z-axis to have the same direction and sense as the permanent dipole moment; that is, the molecular z-direction is defined as the $\xrightarrow{-+}$ direction of the dipole moment. Hence, μ is equal to μ_z , which is always positive. For some of the molecules, further detailed discussion of results requires a knowledge of the direction and sense of the dipole moment in relation to molecular geometry. These cases will be examined in chapter 6.

3.2c χ_{\perp}

As noted in section 2.2, $\chi^{(3)}$ and $\chi^{(2)}$ each have two independent nonzero components, denoted by \parallel and \perp . Rather than express our results in terms of $\chi_{\perp}^{(3)}$ and $\chi_{\perp}^{(2)}$ directly, we have found it convenient to deal with the \parallel components and the ratios $R^{(2)}$ and $R^{(3)}$, which are defined as $\chi_{\parallel}^{(2)}/\chi_{\perp}^{(2)}$ and $\chi_{\parallel}^{(3)}/\chi_{\perp}^{(3)}$, respectively. If there is complete exchange symmetry among the subscripts of the molecular χ_{ijk} or χ_{ijkl} , then $R^{(2)}$ or $R^{(3)}$, respectively, will be equal to 3, as can be seen by examining equations 2.19 - 2.22. This has been shown to be the case¹⁷ to within experimental uncertainty for the inert gases. Thus, it is the deviations of $R^{(2)}$ and $R^{(3)}$ from 3 which will be of

interest experimentally.

Two methods were used to determine $R^{(2)}$ and $R^{(3)}$. Both methods involve measuring the quantity $R^e(T)$ defined by

$$R^e(T) = \chi_{\parallel}^e(T) / \chi_{\perp}^e(T) . \quad (3.10)$$

(experimental determination of this quantity involves relative measurements of the signal as a function of the angle between the beam polarization direction, as adjusted by the half-wave plate in figure 2, and the direction of the dc field, as described in detail by Bigio and Ward¹⁷). The first method is direct, and depends on the measurement of χ_{\perp}^e at various temperatures. The analogs of equations 3.8 and 3.9 are then used to determine $\chi_{\perp}^{(3)}$ and $\chi_{\perp}^{(2)}$, after which $R^{(2)}$ and $R^{(3)}$ are calculated directly. In order to get an accurate absolute scale for χ_{\perp}^e , the ratio $R^e(T)$ is measured at a single temperature. This procedure, although time-consuming, is straightforward, and was actually used for the first gases measured.

In the second method, which was used on the halogenated methanes, $R^e(T)$ is determined for two temperatures, T_L and T_H say, and then equation 3.7 and its counterpart for perpendicular components

$$\chi_{\perp}^e = \chi_{\perp}^{(3)} + \frac{\mu}{9kT} \chi_{\perp}^{(2)} \quad (3.11)$$

can be evaluated at T_L and T_H and combined with equation

3.10 to yield

$$\begin{aligned}
 R^{(2)} &\equiv \chi_{\parallel}^{(2)} / \chi_{\perp}^{(2)} \\
 &= \frac{R^e(T_L) R^e(T_H) (T_H - T_L)}{T_L T_H [R^e(T_H) - R^e(T_L)] / Q + [T_H R^e(T_H) - T_L R^e(T_L)]}
 \end{aligned}
 \tag{3.12}$$

$$\begin{aligned}
 R^{(3)} &\equiv \chi_{\parallel}^{(3)} / \chi_{\perp}^{(3)} \\
 &= \frac{R^e(T_L) R^e(T_H) (T_H - T_L)}{Q [R^e(T_L) - R^e(T_H)] + [T_H R^e(T_L) - T_L R^e(T_H)]}
 \end{aligned}
 \tag{3.13}$$

where Q , defined by

$$Q \equiv \mu \chi_{\parallel}^{(2)} / 9k \chi_{\parallel}^{(3)} \tag{3.14}$$

is minus the inverse of the $1/T$ intercept of the best-fit line to χ_{\parallel}^e vs. $1/T$, and has thus been determined by the experiments described above. Both of these methods were used on one gas as a test of consistency, and the results were found to agree within experimental uncertainty.

3.2d $|\Delta k_o|$

As mentioned in section 3.1b $|\Delta k_o|$, the magnitude of the wave vector mismatch defined in equation 2.29 must be known in order to be able to derive χ^e . $|\Delta k_o|$ is determined experimentally by observing interference between second-harmonic waves which are generated in two crystalline quartz

plates by a single collimated laser beam, in an experiment devised by Finn and Ward.¹⁸ A cell placed between the two plates contains the vapor under investigation. No dc field is applied, and the beam is not focused, so no second harmonic is generated in the gas. The only harmonic fields present are those generated in the quartz plates, and these fields do not change in amplitude with changing gas density. However, dispersion in the gas changes the relative phase of the harmonic generated at the two plates as gas density changes. Since the second harmonic leaving the second plate is the sum of the harmonic waves generated at the two plates, its intensity varies periodically as a function of the density. It is assumed here that n^ω and $n^{2\omega}$, the indices of refraction at the respective frequencies, are linear functions of density, which is a good approximation for dilute gases.¹ The magnitude of the wave vector mismatch is then given by¹⁸

$$|\Delta k_o| = \frac{2\pi M}{D\Delta\rho} \quad (3.15)$$

where $\Delta\rho$ is the density difference between two accurately located harmonic minima, M is the number of intensity maxima between the two minima, and D is the distance of experimental gas which the beam traverses between the plates.

Many of the vapors investigated have departures from ideality of $> 5\%$ at the temperatures and pressures employed, so it is important to evaluate the pressure dependence of the density correctly. We have relied upon published virial

coefficients in performing such evaluations.

3.3 Data Analysis and Typical Data

The analysis of $|\chi^e|$ data is best understood by examining a typical data run. One such run is illustrated in figure 5. The top part of the figure is a plot of the harmonic versus monitor signals for each laser shot of a single subrun. The dotted lines indicate the baseline setting for the respective signals. The value of the signal S , which is the expected value of the ratio of the harmonic to monitor channel signals, is given by

$$S = \frac{\sum_{i=1}^N (H_i - B_H)}{\sum_{j=1}^N (M_j - B_M)} \quad (3.16)$$

where H_i is the number of counts in the harmonic channel for shot i , M_j is the harmonic channel count for shot j , B_H and B_M are respectively the harmonic and monitor channel baseline settings, and N is the number of laser shots in the subrun. Equation 3.16 is the best linear least-squares fit to the data passing through the point (B_M, B_H) providing that all of the statistical fluctuation is due to photon (or, more accurately, photoelectron) statistics in the monitor channel, i.e., that σ_i^2 is proportional to M_i (since signal levels are adjusted so that $M_i \approx H_i$, assignment of fluctuations to the monitor channel does not introduce error). One can compute a variance of S from the spread in the data:

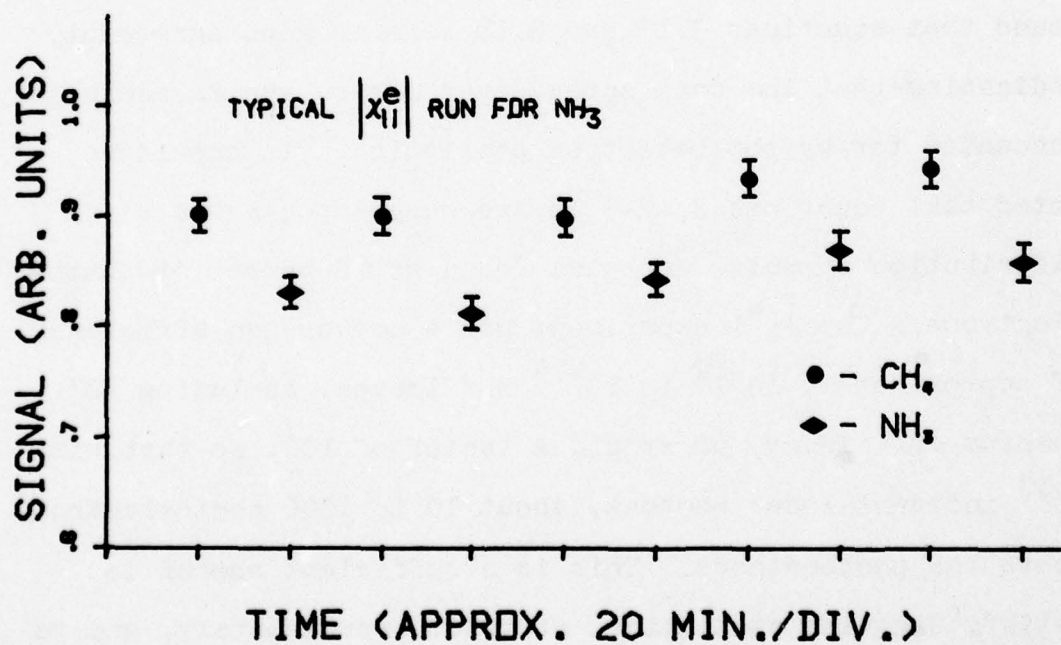
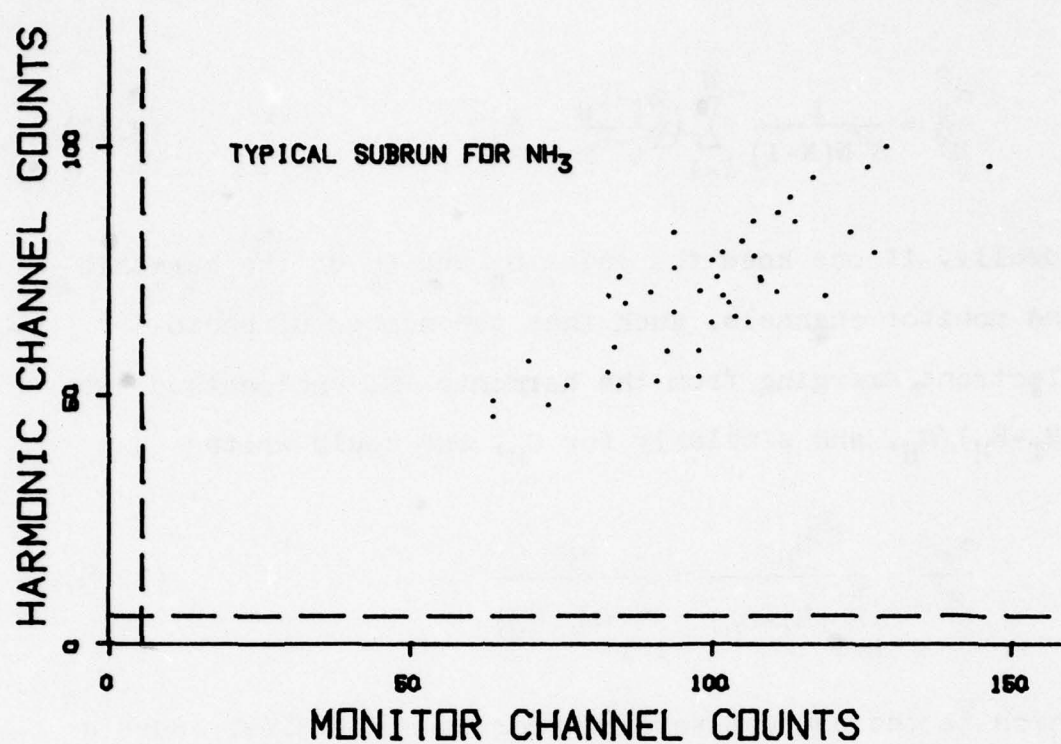


Figure 5. Typical Subrun and Typical $|\chi^e|$ Run for NH_3 .

$$\frac{\sigma_s^2}{S^2} = \frac{1}{S^2 N(N-1)} \sum_{i=1}^N \left(\frac{H_i - B_H}{M_i - B_M} - S \right)^2 \quad (3.17)$$

Ideally, if one knew the gains G_H and G_M of the harmonic and monitor channels, such that the number of photoelectrons emerging from the harmonic PMT photocathode was $(H_i - B_H)/G_H$, and similarly for G_M , one could write

$$\frac{\sigma_s'^2}{S^2} = \frac{G_H}{N \sum_{i=1}^N (H_i - B_H)} + \frac{G_M}{N \sum_{i=1}^N (M_i - B_M)} \quad (3.18)$$

which is the correct variance for equation 3.16. Such a calibration was made for several subruns, and it was found that equations 3.17 and 3.18 were in good agreement, indicating that the data spread over one subrun is adequately accounted for by photoelectron statistics. It should be noted that equations 3.16-3.18 are based upon a Gaussian distribution of pulse energies for a given number of photoelectrons. The $|\chi^e|$ experiment has a conversion efficiency of approximately 10^{-12} to 10^{-14} and losses, including PMT quantum efficiency, of around a factor of 100, so that with 10^{17} incident laser photons, about 10 to 1000 photoelectrons leave the photocathode. This is a sufficient number to satisfy Gaussian statistics, at least approximately, and to be insensitive to the details of the single-photoelectron output distribution of the photomultiplier.

The bottom part of figure 5 is a plot of a typical $|\chi^e|$ experimental run. Each point is the average, in the sense of equation 3.16, of a subrun similar to that in the top of figure 5. The error flags are the σ_s of equation 3.17. The horizontal scale is the approximate time scale of the data run. Examination of this run reveals what appears to be a drift of the signal with time, outside the limits of statistical fluctuation. Most $|\chi^e|$ runs exhibit similar drifts, and they appear to be due to slow changes in the transverse mode structure of the laser beam, drift of the beam between areas of different quantum efficiency on the photocathode of the detector, and drift of the beam focus in the region of the dc field. The beam is known¹⁰ to have components of Gaussian modes of other than the lowest order, and the dcSHG process is quite sensitive to the transverse mode structure.¹⁹ Alternating subruns of experimental gas with those of reference gas has the effect of recalibrating C in equation 3.3 at brief intervals, minimizing the effects of the drifts, and run-to-run fluctuations are consistent with the subrun statistics of equation 3.17. An absolute calibration of C, including analysis of transverse mode structure, evaluation of losses in optical components and gains and losses in detectors and electronics, and measurement of the efficiency of the quartz harmonic generator in the monitor box, yields absolute measurements⁵ of χ^e with uncertainties of about a factor of 3. This large uncertainty precludes

useful comparison with theory. Relative measurements of χ^e for pairs of molecules, on the other hand, yield results with much smaller uncertainties in the range of 1-5%. We put these results on an absolute basis without introducing a large experimental uncertainty by using an accurate calculated value for helium as described in section 3.2a.

Thus, the information obtained from the run illustrated in figure 5 is $S(T)$ for the experimental gas and S' for the reference gas, which are the averages of the respective quantities from the individual subruns. Voltages are adjusted so that $S(T)$ and S' are nearly equal, minimizing systematic errors due to baseline inaccuracies. Typical uncertainty of the ratio of $|\chi^e/\Delta k_0|$ of the experimental gas to that of the reference gas is 1%.

Figure 6 shows a typical plot of $\chi_{||}^e$ against inverse temperature. The error bars are comparable with the size of the data points, and include the uncertainty of $|\Delta k_0|$ (where applicable, the uncertainty of $\chi_{||}^e$ would also include that of $\chi_{||}^{(3)}$ of methane relative to that of helium, but the uncertainty of the calculated value for helium is not included). The line through the points is the best least-squares fit to the data, and $\chi_{||}^{(3)}$ and $\chi_{||}^{(2)}$ are derived using equations 3.8 and 3.9, respectively, with μ obtained from the literature. Uncertainties are determined for $\chi^{(2)}$ and $\chi^{(3)}$ from the uncertainties of the χ^e and μ data by standard methods.²⁰

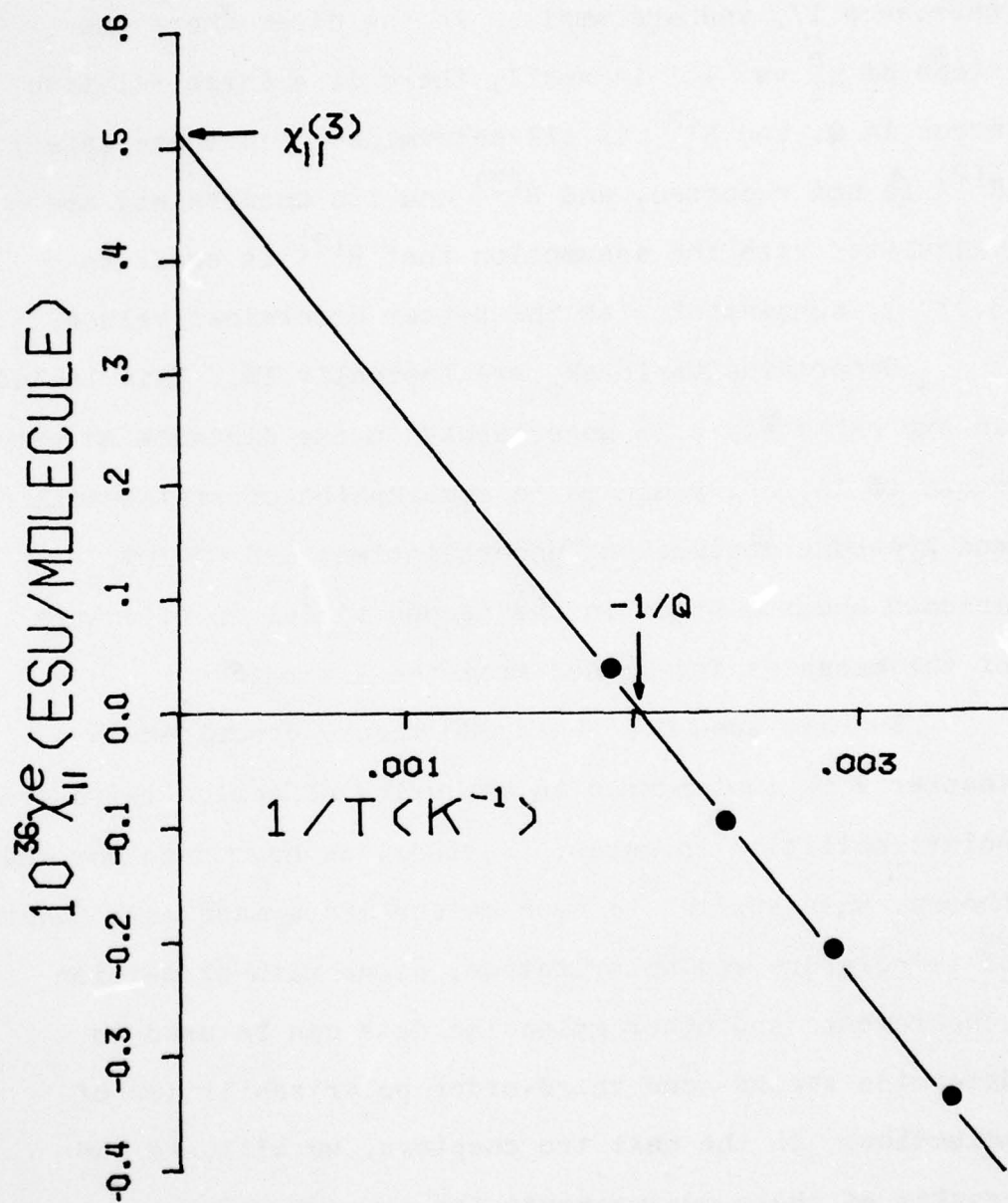


Figure 6. χ_{\parallel}^e versus $1/T$ for NH_3 .

$R^e(T)$ is determined with a statistical accuracy of 1 to 3%. Systematic effects in $R^e(T)$ are discussed in reference 17, and are small. In the cases where the slope of $\chi_{||}^e$ vs. $1/T$ is small, there is a large relative error in Q , and $R^{(2)}$ is ill-determined. In these cases, $R^{(2)}$ is not reported, and $R^{(3)}$ and its uncertainty are calculated with the assumption that $R^{(2)}$ is equal to 3.0 ± 0.3 , consistent with the better determined values.

Uncertainties in Δk_0 are typically 1%. This includes an approximately 0.5% uncertainty in the distance Δp between measured intensity minima (a combination of statistical and pressure measurement uncertainties) and 5%-10% assumed uncertainties in the second virial coefficients of the gases as determined from the literature.

We have seen how the dcSHG theory described in chapter 2 is implemented in measuring effective third-order polarizabilities in gases. Further, we have seen how the theory, when applied to such measurements made as a function of temperature and polarization, along with dispersion measurements and other molecular data can be used to determine second- and third-order polarizabilities of molecules. In the next two chapters, we will see the results of these measurements for several molecular gases.

CHAPTER 4

EXPERIMENTAL RESULTS FOR ASSORTED SMALL MOLECULES

We have applied the experimental techniques presented in chapter 3 to a number of molecules. These can be divided into two broad categories — chloro- and fluoro-substituted (halogenated) methanes, and "other" molecules. The halogenated methane data will be presented in chapter 5, and will be further examined in conjunction with the model discussed in chapter 6.

The assorted "other" molecules were selected for a number of reasons: data from other nonlinear optical experiments exist for several; theoretical results are available for a few; and interesting correlations can be applied to some groups of them. All of these molecules share the property of being relatively small, simple systems for which hyperpolarizability calculations in the domain of molecular orbital theory are feasible.

The experimental parameters and data for these gases are presented in section 1. Also shown there are the derived hyperpolarizabilities and ratios, along with other experimental hyperpolarizability data and theoretical estimates. In section 2, special points of interest for certain of the molecules are discussed.

4.1 Experimental Parameters, Data, and Derived Quantities

The experimental parameters and data for the molecules not possessing permanent dipole moments, and therefore having χ^e which are independent of temperature, are displayed in table 1. The values of E^0 are the field strengths on the z axis between the electrodes, as calculated from equation 2.26 with $z = 0$, for typical voltages V_0 . Values of Δk_0 were all negative for these gases, and were obtained from experimental data with the aid of the virial data referenced in the table. χ_{\parallel}^e and R^e were measured at room temperature (approximately 20°C) and optimum density ρ_{opt} . The uncertainties listed for χ_{\parallel}^e are standard deviations.

Similar parameters and data for the dipolar molecules are shown in table 2. The temperature T_0 at which R^e was measured is also listed for these molecules. In addition, since χ_{\parallel}^e and R^e are both temperature-dependent, their slopes with respect to $1/T$ and their infinite-temperature limits are indicated. The first method of section 3.2c was used to determine $R^{(2)}$ and $R^{(3)}$, so that only one value of R^e appears for each gas. In the cases of CO, NO, and H_2S , there was insufficient signal to recover statistically meaningful values for χ_1^e ; however, for these gases R^e did not differ significantly from 3.0 at room temperature, and there was no indication of unusual behavior of χ_1^e .

The values of $\chi_{\parallel}^{(3)}$ and $R^{(3)}$ for both dipolar and non-dipolar molecules as derived from the experimental data are shown in table 3, along with results from other

Table 1.

	E^O (esu)	ρ_{opt}	$-\Delta k_O^a$ ($-\text{cm}^{-1}$)	$10^{36} \chi_{ }^e$ (esu)	R^e
H ₂	35	2.97	1.27 \pm .01	.0652 \pm .0008	2.86 \pm .03
N ₂	36	1.86	1.89 \pm .02	.0866 \pm .0010	3.00 \pm .06
O ₂	48	1.46	2.41 \pm .02	.0953 \pm .0016	2.97 \pm .07
CO ₂	43	1.05	3.36 \pm .03	.1119 \pm .0013	2.81 \pm .06
SF ₆	58	1.08	3.47 \pm .03	.130 \pm .002	2.97 \pm .07

a) Using virial data from:
 Reference 42 (H₂, N₂, O₂); K. E. MacCormack and W. G. Schneider, J. Chem. Phys. 18, 1269 (1950) (CO₂); and
 H. P. Clegg, J. S. Rowlinson, and J. R. Sutton, Trans. Faraday Soc. 51, 1327 (1955) (SF₆).

Table 2.

E	T _o	° _{opt}	-Δk _o (cm ⁻¹)	a	10 ³⁶ Lim x ^e 10 ³⁶ $\frac{dx^e}{dT^{-1}}$	R ^e (T _o)	10 ³⁶ Lim x ^e 10 ³⁶ $\frac{dx^e}{dT^{-1}}$	b	10 ³⁶ $\frac{dx^e}{dT^{-1}}$
(esu)	(°K)				(esu)	(esu °K)	(esu)	(esu)	(esu °K)
CO	43	293	1.05	3.35±.03	.144±.004	11.6±1.2	2.94±.03	—	—
NO	23	293	1.29	2.72±.03	.235±.007	18.8±2.2	3.24±.06	—	—
H ₂ S	29	293	0.36	9.73±.10	.865±.022	-34±7	2.82±.04	—	—
NH ₃	31	293	0.65	5.40±.05	.511±.009	-248±5	2.41±.06	.161±.006	-88±4
H ₂ O	23	419	1.53	2.44±.02	.194±.010	-141±5	3.40±.07	.006±.012	-45±5
(CH ₃) ₂ O	21	293	0.40	8.92±.09	.529±.011	-302±5	3.07±.04	.177±.009	-100±4
CH ₃ OH	40	393	0.73	5.02±.07	.385±.011	-207±12	2.98±.06	.132±.009	-71±4

a) Using virial data from:

S. H. Maron and D. Turnbull, Ind. Eng. Chem. 33, 408 (1941) (H₂S); J. S. Rowlinson, Trans. Faraday Soc. 45, 974 (1949) (NH₃); R. M. Kennedy, M. Sagenkahn, and J. G. Aston, J. Am. Chem. Soc. 63, 2267 (1941) [(CH₃)₂O]; E. P. Bartlett, H. C. Hetherington, H. K. Kvalnes, and T. H. Tremearne, J. Am. Chem. Soc. 52, 1374 (1930) (CO); Reference 42 (NO); and L. S. Marks and H. N. Davis, Tables and Diagrams of the Thermal Properties of Saturated and Superheated Steam (Longmans, Green and Co., New York, 1929) (H₂O).

b) Measurement of these quantities for H₂S, CO, and NO was impractical because of insufficient signal, as discussed in the text.

Table 3.

	$R^{(3)}$	$10^{36} \chi_{\parallel}^{(3)}$ (esu)	Other $\chi_{\parallel}^{(3)}$ Data			
			dcSHG	TWM ^a	Kerr	THG ^b Theory
H ₂	2.86 ± .03	.0652 ± .0008	.079 ^d		.047 ^e ± .005	.080 ± .012 .034 ^h
N ₂	3.00 ± .06	.0866 ± .0010		.104	.12 ^f ± .01	.107 ± .017 .071 ⁱ
O ₂	3.12 ± .07	.0953 ± .0016	.11 ^d	.100		
SF ₆	2.97 ± .07	.130 ± .002	.20	.192	.20 ^g ± .02	
CO ₂	2.81 ± .08	.1119 ± .0013		.192	.75 ^f ± .16	.156 ± .023
CO	2.92 ^c ± .15	.144 ± .004		.138		
NO	3.32 ^c ± .15	.235 ± .007		.322		
H ₂ S	2.84 ^c ± .11	.865 ± .022				
NH ₃	3.19 ± .11	.511 ± .009				
H ₂ O	2.94 ± .55	.194 ± .010				
(CH ₃) ₂ O	2.99 ± .15	.529 ± .011				
CH ₃ OH	2.90 ± .21	.385 ± .011				

- a) Three-wave mixing (TWM) data from reference 43 normalized using the dcSHG coefficient for argon from reference 13.
- b) Third-harmonic generation (THG) data from J.F. Ward and G.H.C. New, Phys. Rev. 185, 57 (1969).
- c) Derived assuming $R^{(2)} = 3.0 \pm 0.3$.
- d) Data from reference 4, normalized using the dcSHG coefficient for argon from reference 13.
- e) A.D. Buckingham and B.J. Orr, Proc. Roy. Soc. A 305, 259 (1968).
- f) Reference 21.
- g) A.D. Buckingham and D.A. Dunmur, Trans. Faraday Soc. 64, 1776 (1968).
- h) $\chi_{zzzz}(0;0,0,0)$ from reference 44.
- i) $\chi_{zzzz}(0;0,0,0)$ from reference 22.

gas-phase experiments, and available theoretical estimates. $R^{(3)}$ does not differ significantly from 3.0, the value which would apply in the limit of small dispersion in the molecular $\chi^{(3)}$. This result is not surprising since all of the experimental frequencies involved are far from molecular resonances. The other experimental gas-phase data for $\chi_{\parallel}^{(3)}$ are from other dcSHG experiments and from three-wave mixing (TWM), Kerr effect, and third-harmonic generation (THG) experiments. These data tend to be slightly larger than our values, but not unreasonably so in view of experimental uncertainties and the likelihood of small effects due to dispersion. A possible exception is $\chi^{(3)}$ for CO_2 , for which the Kerr effect measurement of Buckingham *et al.*²¹ is much larger than other values, whereas their data for N_2 and SF_6 agree acceptably with the others.

The theoretical values of $\chi_{\parallel}^{(3)}$ listed for H_2 and N_2 are the molecular χ_{zzzz} only. The value listed for N_2 is preliminary, and it is anticipated²² that the calculation will be refined and extended to the other components of χ_{ijkl} for the gases investigated in this dissertation and in reference 12.

Values for $\chi_{\parallel}^{(2)}$ and $R^{(2)}$, as derived from the experimental data and from literature values for permanent dipole moments, are shown in table 4, along with other experimental data and with theoretical results. Comments on the single other experiment, a dcSHG measurement in

Table 4.

	$10^{18} \mu^a$ (esu)	$R^{(2)}$	$10^{30} \chi''$ (esu)	theory		Other expt.
				SE	HF	CHF
CO	.112 \pm .005	—	+ .129 \pm .014	-.0435 ^b +.095 ^c	+ .879 ^d +.420 ^d +.387 ^d -.438 ^e	
NO	.15872 \pm .00002	—	+ .147 \pm .017	-.0477 ^b		
H ₂ S	.974 \pm .005	—	-.043 \pm .009			
NH ₃	1.474 \pm .009	2.82 \pm .08	-.209 \pm .005	-.0564 ^b		+ .0444 ^f +.0651 ^f +.0190 ^f -.0156 ^g -.0408 ^g -.0525 ^f -.0792 ^f -.0219 ^f +.0516 ^g +.0480 ^g
H ₂ O	1.86 \pm .02	3.12 \pm .38	-.094 \pm .004	-.120 ^b	+ .0906 ^e	
(CH ₃) ₂ O	1.307 \pm .010	3.02 \pm .10	-.287 \pm .005			
CH ₃ OH	1.71 \pm .02	2.92 \pm .18	-.150 \pm .009			

Footnotes for Table 4.

- a) Electric dipole moment in Debye units from references 45 and 46.
- b) N. S. Hush and M. L. Williams, Theoret. Chim. Acta (Berlin) 25, 346 (1972).
- c) $\chi_{zzz}^{(2)}(0;0,0)$ from reference 44.
- d) Reference 23.
- e) S. P. Liebmann and J. W. Moskowitz, J. Chem. Phys. 54, 3622 (1971).
- f) Reference 24.
- g) Reference 25.
- h) Refractivity virial data from reference 47.

liquid H_2O , is deferred to the next section.

The theoretical results are from molecular orbital calculations, and are listed according to the general method employed, either "semi-empirical" (SE), uncoupled Hartree-Fock (HF), or coupled Hartree-Fock (CHF). Wide discrepancies in magnitude, and even sign differences, occur between the results of different authors using various techniques. For example, in H_2O , the theoretical results for $10^{30} \chi_{\parallel}^{(2)}$ range from -0.12 to +0.09 and in CO , they vary from -0.44 to +0.88. In addition, results by the same authors vary considerably depending on the number and nature of the basis functions used.^{23,24,25} Our data, with an uncertainty of less than 21% in the worst case, and 3-12% for the rest, can provide a stringent test of molecular orbital calculations for these molecules.

4.2 Discussion of Results for Particular Molecules

Certain of the 12 molecules considered in this chapter warrant particular attention, and they are discussed in this section in turn.

4.2a H_2 , N_2 , and O_2

Because of the relative simplicity of the homonuclear diatomic molecule, it seems reasonable to attempt to predict $\chi^{(3)}$ for H_2 , N_2 , and O_2 using an adaptation of an approximation due to Dawes²⁶ which meets with some success in predicting the variation of $\chi^{(3)}$ among the inert gases.^{13,26} In the Dawes approximation, the perturbation

expansion⁷ for χ_{ijkl} , obtained by summing terms such as that in equation 2.5, is reduced to a single term in a manner analogous to the linear polarizability. A single effective state frequency ω_0 is substituted for transition frequencies ω_{ij} in order to factor out the term ω_0^{-5} . Next, the approximation is made that

$$\langle r^2 \rangle_{gg} = \omega_0^{-1} \sum_i \omega_{gi} \langle \underline{r} \rangle_{gi} \cdot \langle \underline{r} \rangle_{ig} \quad (4.1)$$

where g refers to the ground state. Finally, the assumption is made that $\chi^{(3)}$ is the sum of N_0 identical "one electron" expressions, where N_0 is an effective electron number. The resulting expression is proportional to a sum like that on the right-hand side of equation 4.1, and the Thomas-Reiche-Kuhn sum rule²⁷ is invoked to collapse it to a single term. The N_0 and ω_0 are then taken to be the values used to fit the dispersion of the linear index of refraction. In the case of homopolar diatomic molecules, one can use data on the anisotropy of the linear molecular polarizability to fit two effective electron numbers (which can be thought of as the numbers of electrons oscillating respectively parallel to and perpendicular to the internuclear axis). The expression arrived at after averaging over molecular orientations is

$$\chi_{\parallel}^{(3)} = \frac{N_{\parallel} e^4}{\hbar m^2 \omega_0^5} \times \frac{[1-4r^4 - \delta(\frac{2}{3} + \frac{8}{45}r - \frac{17}{45}r^2 - \frac{31}{45}r^3 + \frac{26}{45}r^4 + 8r^5 - 16r^6)]}{(1-4r^2)^2(1-r^2)^2} \quad (4.2)$$

in which the quantities are as follows: δ is $1-(N_{\perp}/N_{\parallel})$, where N_{\parallel} and N_{\perp} are the effective electron numbers in the parallel and perpendicular directions, respectively; r is the ratio ω/ω_0 , where ω is the field frequency; and e is the charge, and m the mass, of the electron. Since the Dawes approximation reproduces the values of $\chi_{\parallel}^{(3)}$ for the inert gases only to an overall multiplicative factor, it is necessary to normalize the Dawes values of $\chi_{\parallel}^{(3)}$ for the homopolar diatomic molecules to that for helium. Table 5 shows the results of the application of equation 4.2 to H_2 , N_2 , and O_2 , with values of N_0 and ω_0 obtained from reference 28 and polarizability anisotropy data from reference 29. While far from a good fit, the Dawes approximation values are of the correct order of magnitude, and display the correct direction of variation from molecule to molecule. Even when normalized to $\chi_{\parallel}^{(3)}$ of N_2 , the Dawes values for H_2 and O_2 do not agree convincingly with the experimental values. However, because of the severity of the approximations, and the increased complexity of homonuclear diatomic molecules over that of inert gas

Table 5.

	ω_0 (10^{16} sec^{-1})	N_{\parallel}	N_{\perp}	$\chi_{\text{Dawes}}^{(3)}$ (ref. He)	$\chi_{\text{Dawes}}^{(3)}$ (ref. N_2)	$\chi_{\parallel}^{(3)}$ (expt.)
H ₂	2.21	1.96	1.36	.089	.067	.065
N ₂	2.59	5.85	4.03	.114	(.086)	.086
O ₂	2.25	4.56	2.41	.163	.124	.096

All $\chi^{(3)}$ values are in units of 10^{-36} esu.

atoms, it is not astonishing that the Dawes approximation should be less applicable to these molecules.

4.2b NH₃

The permanent electric dipole moment of the static pyramidal NH₃ configuration was used in table 4. The ground-vibrational state of NH₃ is inversion-split by the energy ϵ corresponding to the frequency of tunneling of the N atom through the center of the triangle formed by the three H nuclei. This splitting is small, however, and it can be shown that for

$$\epsilon^2/(kT)^2 \ll 1 \quad (4.3)$$

ammonia behaves like a gas of ordinary dipolar molecules. At room temperature the value of $\epsilon^2/(kT)^2$ is about 2×10^{-5} , so the inequality 4.3 is well satisfied. Indeed, the fact that χ^e is a linear function of $1/T$ in the range of temperatures used here (see figure 5) confirms the ordinary behavior of ammonia.

The ammonia molecule also illustrates dramatically the fact that the differences of $R^{(2)}$ and $R^{(3)}$ from 3.0, while small, are indeed non-zero. If $R^{(2)}$ and $R^{(3)}$ were equal, then $R^e(T)$ would have to be a constant function of temperature, equal to $R^{(2)}$ (and to $R^{(3)}$), as can be seen from equations 3.7 and 3.10-3.13. However, as shown in tables 2, 3, and 4, R^e is significantly different from $R^{(2)}$ and $R^{(3)}$, so that the latter two quantities cannot

be equal (in particular, they cannot both be equal to 3.0) indicating that the effects of dispersion in various components of χ_{ijk} and χ_{ijkl} , while they might be small, cannot be neglected entirely.

4.2c H₂O

Levine and Bethea³⁰ have measured $\chi_{||}^e$ in water and in water-methanol and water-dioxane solutions by the method of dcSHG in the liquid phase. Because the details of intermolecular interactions in strongly associating liquids are not well understood,⁹ Levine and Bethea were not able to extract precise isolated-molecule values of $\chi_{||}^{(2)}$ and $\chi_{||}^{(3)}$ for water from their data. By postulating a model of the interactions, however, they arrive at the expression for $\chi_s^{(2)}$, the second-order polarizability per molecule of water in solutions, of

$$\chi_s^{(2)} = (\chi_{||}^{(2)} + \chi_{hb}^{(2)}) + \chi_{dip}^{(2)}(1-g) \quad (4.4)$$

where $\chi_{||}^{(2)}$ is the value for an isolated molecule (corresponding to our gas-phase value), $\chi_{hb}^{(2)}$ is the second order nonlinearity due to hydrogen bonding among the water and solvent molecules, $\chi_{dip}^{(2)}$ is the effective second-order hyperpolarizability induced in the molecule by the interaction of the molecular $\chi^{(3)}$ with the average electric field due to the permanent dipole moments of surrounding molecules, and g is the Kirkwood-Frölich correlation parameter, having to do with short-range

molecular alignment. They derive values of $\chi_s^{(2)}$ from their data using an estimate for the gas-phase value of $\chi_{\parallel}^{(3)}$ consistent with our measured value. They calculate values of g for mixtures from data on the dielectric constants of mixtures. Their derived values of $\chi_s^{(2)}$ range from about $1/2$ to $1/8$ of our $\chi_{\parallel}^{(2)}$ value, and they find that in this range, $\chi_s^{(2)}$ varies approximately as $(1-g)$. This behavior along with equation 4.4, implies that

$$\chi_{\parallel}^{(2)} + \chi_{hb} = 0 \quad (4.5)$$

to within the broad uncertainty limits of the data and model. Such a cancellation would be interesting, in that it would suggest that hydrogen bonding might cause H and O atoms to be arranged with a high degree of short-range symmetry. For example, an O atom might be surrounded by four H atoms in a T_d symmetry, while an H atom could lie between two O atoms in a $C_{\infty v}$ symmetry. The value of $\chi_{\parallel}^{(2)}$, as defined by equation 2.21, is zero for both of these symmetries.²

In this chapter we have presented experimental parameters and data for χ^e and R^e , and their temperature dependence, from which we have extracted $\chi_{\parallel}^{(3)}$, $\chi_{\parallel}^{(2)}$, $R^{(3)}$, and $R^{(2)}$ values for a number of simple molecules. Our data are largely consistent with other experimental values that are available for comparison. Where the values disagree, we feel that our data are less subject to errors

in measurement and interpretation. Our experiments have an inherently high signal-to-noise ratio, and systematic errors are compensated for in a straightforward manner, with calibration an integral part of the experiment. In addition, the molecular observables are derived from the experimental data in an unambiguous manner, without having to estimate contributions to the effects either from other processes or from intermolecular interactions. While we have commented upon particular features of some of the molecules here, we defer a discussion of water, methanol, and dimethyl ether as a group to the section on the Bond Additivity Approximation in chapter 6.

CHAPTER 5

EXPERIMENTAL RESULTS FOR SOME HALOGENATED METHANES

The halogenated methanes investigated here are all of the form CX_nY_{4-n} , with $n = 1-4$ and $X, Y = F, Cl, H$. The second- and third-order polarizabilities $\chi^{(2)}$ and $\chi^{(3)}$ for some of the molecules have been measured by Bigio and Ward.¹² The capability of making gas-phase measurements in substances which are liquids at room temperature has allowed us to complete the series with measurements of $\chi^{(2)}$ and $\chi^{(3)}$ for CCl_4 , $CHCl_3$, CH_2Cl_2 , CH_3Cl , CCl_2F_2 and CCl_3F . In addition, we have made an especially precise measurement of $\chi_{||}^{(3)}$ for CH_4 , since it was used here as a reference gas. The data presented in this chapter have appeared in The Physical Review, Section A.³¹

The experimental parameters, and experimental data on dispersion, effective hyperpolarizabilities, and effective ratios, are shown in table 6. These data are similar in nature to those presented in tables 1 and 2. However, for these molecules, the second method discussed in section 3.2c for determining $R^{(2)}$ and $R^{(3)}$ was used. Thus, there are two values listed for R^e , as well as two values for the temperatures at which the R^e were measured, for each gas (except for the non-dipolar molecules CH_4 and CCl_4 , for which a single value of R^e suffices).

The results for $\chi_{||}^{(3)}$ and $R^{(3)}$ are shown in table 7, along with other gas-phase experimental data. Again, $R^{(3)}$

Table 6.

	E^0 (esu)	$T_L - T_H$ (°K)	ρ_{opt}	$-\Delta k_O^a$ (cm ⁻¹)	$10^{36} \lim_{T \rightarrow 0} \chi_{ }^e$ (esu)	$10^{36} \frac{d\chi_{ }^e}{dT^{-1}}$ (esu °K)	$R^e(T_L)$	$R^e(T_H)$
CCl ₄	30	387 ...	0.192	19.3 ± 0.2	1.37 ± 0.02	0	3.02 ± 0.09	...
CHCl ₃	38	384 -485	0.238	15.6 ± 0.2	1.12 ± 0.03	+4 ± 9	2.99 ± 0.05	...
CH ₂ Cl ₂	30	386 -498	0.314	11.8 ± 0.1	0.92 ± 0.03	+22 ± 13	3.02 ± 0.08	...
CH ₃ Cl	16	293 -488	0.497	7.75 ± 0.07	0.57 ± 0.03	+87 ± 9	2.96 ± 0.04	3.00 ± 0.09
CH ₄	28	293 ...	0.909	4.08 ± 0.04	0.263 ± 0.003	0	3.05 _b ± 0.05	...
CCl ₂ F ₂	45	293 -478	0.379	9.8 ± 0.1	0.61 ± 0.01	-106 ± 3	3.15 ± 0.09	2.96 ± 0.06
CCl ₃ F	37	323 -477	0.254	14.6 ± 0.1	0.96 ± 0.03	-49 ± 15	3.02 ± 0.07	3.00 ± 0.07

Footnotes for Table 6.

- a) Using virial data from: J.D. Lambert, G.A.H. Roberts, J.S. Rowlinson, and V.J. Wilkinson, Proc. R. Soc. London Ser. A 196, 113 (1949) ($\text{CCl}_4, \text{CHCl}_3$); P.G.T. Fogg, P.A. Hanks, and J.D. Lambert, Proc. R. Soc. London A 219, 490 (1953) (CH_2Cl_2); H.G. Tanner, A.F. Benning, and W.F. Mathewson, Ind. Eng. Chem. 31, 878 (1939) (CH_2Cl); W.S. Haworth and L.E. Sutton, Trans. Faraday Soc. 67, 2907 (1971) (CCl_2F_2); and reference 42 ($\text{CCl}_3\text{F}, \text{CH}_4$).
- b) Taken from reference 12.

Table 7.

	$R(3)$	$\chi_{ }(3)$	Other $\chi(3)$ data		
			dcSHG	TWM	Kerr
CCl_4	3.02 ± 0.09	1.37 ± 0.02	1.7 ^c	1.7 ^c	1.66 $\pm 0.05^e$
CHCl_3	2.96 ^a $\pm 0.05^a$	1.12 ± 0.03		1.19 ^c	
CH_2Cl_2	3.02 ^a $\pm 0.09^a$	0.92 ± 0.03			
CH_3Cl	3.28 ± 1.03	0.57 ± 0.03			
CH_4	3.05 ^b $\pm 0.05^b$	0.263 ± 0.003	0.32 ^c	0.34 ^c 0.19 ^d	0.242 ^f $\pm 0.012^f$
CCl_2F_2	3.55 ± 0.35	0.61 ± 0.01			
CCl_3F	3.39 ± 2.92	0.96 ± 0.03			

- a) Using the assumption $R^{(a)} = 3.0 \pm 0.3$.
b) From reference 12.
c) Data from reference 4 normalized using the dcSHG coefficient for argon from reference 13.
d) Data from reference 43 normalized using the dcSHG coefficient for argon from reference 13.
e) Reference 48.
f) A.D. Buckingham and B.J. Orr, Trans. Faraday Soc. 65, 673 (1969).

is not significantly different from 3.0, and as before, for cases in which $R^{(2)}$ cannot be accurately determined, $R^{(3)}$ is calculated by assuming the value $R^{(2)} = 3.0 \pm 0.3$. Other experimental data are from TWM, THG, and Kerr effect measurements, and there is excellent agreement between these data and ours. A number of measurements have been made of the third-order nonlinearity of CCl_4 in the liquid phase for various processes, such as dcSHG, Kerr effect, and ellipse rotation. Much of this information has been reviewed by Levine and Bethea,³² who use Onsager local-field factors⁹ to extract estimates for $\chi_{\parallel}^{(3)}$ of the isolated molecule. They arrive at estimates which are typically within 15% of our experimental result. There are currently no ab initio calculations of $\chi^{(3)}$ available for these molecules.

Results for $\chi_{\parallel}^{(2)}$ and $R^{(2)}$ are shown in table 8, along with dipole moments and measurements of $\chi_{\parallel}^{(2)}$ from other sources. $R^{(2)}$ is subject to large uncertainties, and in fact could not be assigned a meaningful value in the case of CHCl_3 and CH_2Cl_2 (for which the change in χ^e over the temperature range used was very small). For the other molecules, $R^{(2)}$ does not differ significantly from 3.0. The sign of $\chi_{\parallel}^{(2)}$, assigned according to the conventions of section 3.2b, is negative for CCl_2F_2 and CCl_3F , as it is¹² for CClF_3 and for $\text{CH}_n\text{F}_{4-n}$, $n = 1-3$, but it is positive for $\text{CH}_n\text{Cl}_{4-n}$ (however, negative and zero values of $\chi_{\parallel}^{(2)}$ are

Table 8.

	μ^a	$R^{(2)}$	$\chi^{(2)}$	Other $\chi^{(2)}$ data		
				Kerr	dcSHG+TWM	Other
CHCl_3	1.04	...	$+0.005$ ± 0.011	-0.5^b ± 0.4	0.47^d	$+13^e$ $+101^f$
CH_2Cl_2	1.60	...	$+0.017$ ± 0.010	$+0.5^b$ $\pm 0.7^c$ -3.3^c		-3.5 $\pm 1.0^g$
CH_3Cl	1.90	2.73 ± 0.48	$+0.057$ ± 0.006	$+0.0^b$ ± 0.5		-4^h
CCl_2F_2	0.51	2.68 ± 0.17	-0.258 ± 0.008			
CCl_3F	0.46	2.70 ± 1.62	-0.132 ± 0.041			

a) Electric dipole moments in Debye units from reference 45 and 46.
b) Reference 48.

c) Data from H.A. Stuart, Die Struktur des Freienmoleküls (Springer-Verlag, Berlin, 1952) as cited in reference 2.

d) Data from reference 4 normalized using the dcSHG coefficient for argon from reference 13.

e) Depolarization of Rayleigh scattering in the liquid from reference 2.

f) Depolarization of Rayleigh scattering in the liquid from S. Kielich, Acta Phys. Pol. 22, 299 (1962).

g) Kerr effect in solution from reference 2.

h) Refractivity virial data from reference 47.

within the uncertainty limits for CHCl_3). The uncertainties of other published gas-phase measurements of $\chi_{\parallel}^{(2)}$ are large, so although the other data tend to be larger in magnitude than our values, they are not necessarily inconsistent. A possible exception is the value from the dcSHG and TWM experiments of Mayer et al.⁴ for CHCl_3 , which differs from our result by 40 times our experimental uncertainty. It should be noted that $\chi_{\parallel}^{(2)}$ is obtained by Mayer et al. from the difference between the results of the dcSHG and TWM experiments, which require independent calibrations with different sets of frequencies, whereas in our method, only relative measurements of signal as a function of temperature are made, all at the same set of frequencies. If $10^{30}\chi_{\parallel}^{(2)}$ were 10 times our uncertainty, or approximately 0.1 esu, there would have been an easily-seen 15% change in our experimental signal over the temperature range 319-500°K, rather than the ~ 1% change actually observed.

The methods for extracting isolated-molecule values of $\chi_{\parallel}^{(2)}$ from measurements in the liquid phase are indirect, involving estimation of poorly-understood effects due to intermolecular interactions. The agreement between these data and our measurements is poor.

There are currently no ab initio calculations of $\chi_{\parallel}^{(2)}$ for any of these halogenated methanes.

We have presented experimentally determined temperature-dependent values of χ_{\parallel}^e and R^e for some halogenated methanes, as well as the derived $\chi^{(3)}$, $\chi^{(2)}$, $R^{(3)}$, and $R^{(2)}$ values, and compared them with other available experimental data. Again, our values are for the most part consistent with other data, and where this is not the case, we feel that our values are the more reliable, as discussed in chapter 4. In the next chapter, we will investigate correlation of some of these properties, along with other electric tensor properties, among the molecules of the complete halogenated methane series.

CHAPTER 6

CORRELATION OF ELECTRIC TENSOR PROPERTIES

AMONG SIMILAR MOLECULES

Molecular electric tensor properties $\underline{\alpha}$, $\underline{\chi}^{(2)}$, $\underline{\chi}^{(3)}$, and so on are ultimately determined by the changes in electronic wave functions due to applied electric fields, and can be written formally in terms of time-dependent perturbation theory expressions.⁷ Such expressions, while correct in principle, generally defy evaluation because of the difficulty of finding molecular wave functions. However, the obvious structural similarity among the molecules within certain groups suggests that the electric tensor properties of the molecules in a given group might be correlated. In such correlations, the electric tensor properties of the set of molecules are calculated from a smaller set of parameters. For the cases discussed here, the parameters are interpreted physically as the electric tensor properties of the bonds or structural groups in the molecules, and the predicted tensor properties for a given molecule are expressed as a function of the properties of the component segments and the geometry of the molecule.

In section 1, we examine the Bond Additivity Approximation (BAA), in which the electric tensor properties of a molecule are assumed to be the sums of respective properties associated with its component bonds

or structural groups. In section 2, an Interacting Segment Model (ISM) of these properties is proposed, with the aim of avoiding some of the drawbacks of the BAA while retaining much of its simplicity. In section 3, the ISM is applied to the permanent dipole moments μ , linear polarizabilities α , and second order polarizabilities $\chi^{(2)}$ of the halogenated methanes in order to obtain a clearer picture of the contributions of bond interactions to the electric tensor properties of this set of similar molecules. Much of the material in this chapter has appeared in The Journal of Chemical Physics.³³

6.1 The Bond Additivity Approximation

The concept of assigning separate electric tensor properties to the bonds (such as the C-Cl bond in CH_3Cl) and/or functional groups (such as the CH_3 , or methyl, group in CH_3OH) of a molecule, and summing the respective properties over the segments (bonds and groups) to determine the overall properties of the molecule, is called the Bond Additivity Approximation. This model has been widely (although not universally) accepted by chemists and physicists for more than fifty years,³⁴ largely because of its simplicity. The BAA has found use in, for example, resolving questions about molecular geometry.

In the BAA, the i th segment in a molecule is

assigned tensor properties $\underline{\chi}_i^{(n)}$, $n = 0, 1, \dots$, where $\underline{\chi}_i^{(0)}$ is the permanent electric dipole moment, $\underline{\chi}_i^{(1)}$ the linear polarizability, and so on (we will use $\underline{\chi}^{(0)}$ and $\underline{\chi}^{(1)}$ interchangeably with $\underline{\mu}$ and $\underline{\alpha}$, respectively, as appropriate). The BAA value $\underline{\chi}^{(n) '}$ for the molecular tensor is found by adding the respective segment tensors:

$$\underline{\chi}^{(n) ' } = \sum_i \underline{\chi}_i^{(n)} \quad (6.1)$$

The segment tensors are here assumed to be independent of their environment so that, for example, $\underline{\chi}_i^{(n)}(\text{C-Cl})$ in CH_3Cl is equal to $\underline{\chi}_i^{(n)}(\text{C-Cl})$ in CCl_4 (in the coordinate system of the bond). In actuality, the quantities which are to be reproduced by any model such as this are scalar observables related to the electric tensors (for example, we know $\chi_{\parallel}^{(2)}$, rather than $\chi_{ijk}^{(2)}$). The relation between each tensor property and its associated observable will be defined when it is introduced.

We have two sets of molecules on which to test bond additivity. The first set has only two segment types, and consists of only three molecules—water (H_2O), dimethyl ether ($(\text{CH}_3)_2\text{O}$), and methanol (CH_3OH). The second set has three types of segments, and consists of twelve halogenated methanes. We will discuss the smaller set of molecules first because of their structural simplicity.

The three molecules in the first set may be characterized as an oxygen atom with two groups attached. The groups may both be hydrogen atoms, or both CH_3 groups, or one hydrogen atom and one methyl group, constituting water, dimethyl ether, and methanol, respectively.

We will write the properties associated with the O-H bond as $\underline{\chi}^{(n)}(\text{O-H})$, and those associated with the O-C bond and CH_3 group collectively as $\underline{\chi}^{(n)}(\text{O-CH}_3)$. As discussed later, the question of the location within the segment at which the properties act is not important in the BAA, and will be ignored here. The symmetry axis of the CH_3 group is considered to be along the O-C internuclear axis, so that the (O-CH_3) segment symmetry axis will also be in this direction. The two properties of these molecules that we will examine first are: the isotropic linear polarizability α , defined by

$$\alpha = \frac{1}{3}(\alpha_{xx} + \alpha_{yy} + \alpha_{zz}); \quad (6.2)$$

and $\chi_{\parallel}^{(3)}$ which, as we have already seen in equation 2.19, is a twice-contracted fourth-rank tensor. Both of these quantities transform as scalars, and therefore the segment quantities add very simply:

$$\alpha(\text{H}_2\text{O}) = 2\alpha(\text{O-H}) \quad (6.3)$$

$$\alpha((\text{CH}_3)_2\text{O}) = 2\alpha(\text{O-CH}_3) \quad (6.4)$$

$$\alpha(\text{CH}_3\text{OH}) = \alpha(\text{O-H}) + \alpha(\text{O-CH}_3) \quad (6.5)$$

which means that BAA predicts the isotropic linear polarizability per molecule of methanol to be the simple average of those of water and dimethyl ether. The same statement, along with the analogs of equations 6.3-6.5, apply to $\chi_{\parallel}^{(3)}$:

$$\chi_{\parallel}^{(3)}(\text{H}_2\text{O}) = 2\chi_{\parallel}^{(3)}(\text{O-H}) \quad (6.6)$$

$$\chi_{\parallel}^{(3)}((\text{CH}_3)_2\text{O}) = 2\chi_{\parallel}^{(3)}(\text{O-CH}_3) \quad (6.7)$$

$$\chi_{\parallel}^{(3)}(\text{CH}_3\text{OH}) = \chi_{\parallel}^{(3)}(\text{O-H}) + \chi_{\parallel}^{(3)}(\text{O-CH}_3) \quad (6.8)$$

We choose $\alpha(\text{O-H})$, $\alpha(\text{O-CH}_3)$, $\chi_{\parallel}^{(3)}(\text{O-H})$, and $\chi_{\parallel}^{(3)}(\text{O-CH}_3)$ to satisfy equations 6.3, 6.4, 6.6, and 6.7, respectively, and predict α and $\chi_{\parallel}^{(3)}$ for CH_3OH from equations 6.5 and 6.8. The results of this fitting along with the experimental values are shown in table 9. The prediction for $\alpha(\text{CH}_3\text{OH})$ is well within the uncertainty limits expected for these data ($\sim 3\text{-}10\%$). This is not surprising, since the BAA has been applied successfully to α in many cases.³⁴ The prediction for $\chi_{\parallel}^{(3)}(\text{CH}_3\text{OH})$, while slightly outside the uncertainty limits of the experimental value, it is still not unreasonable. Thus, it appears that bond additivity also works well for $\chi_{\parallel}^{(3)}$.

Table 9.

	$10^{24}\alpha(\text{expt})$ (esu)	$10^{24}\alpha(\text{BAA})$	$10^{30}\chi''(3)(\text{expt})$	$10^{36}\chi''(3)(\text{BAA})$
H_2O	1.45 ^a		.194 \pm .010	
$(\text{CH}_3)_2\text{O}$	5.27 ^b		.529 \pm .011	
CH_3OH	3.27 ^b	3.36	.385 \pm .011	.361 \pm .008

a) Reference 49.

b) From linear index of refraction data of reference 28.

The situation is somewhat more complicated for the permanent dipole moment (here the observable μ is the magnitude of $\underline{\mu}$, the dipole moment vector). In H_2O and $(\text{CH}_3)_2\text{O}$, symmetry dictates that $\underline{\mu}$ must lie in the plane of the segments and along the bisector of the angle between them. Thus from the vectorial addition of $\underline{\mu}$, we find that

$$\mu(\text{O-H}) = \frac{\mu(\text{H}_2\text{O})}{2\cos(\theta/2)} \quad (6.9)$$

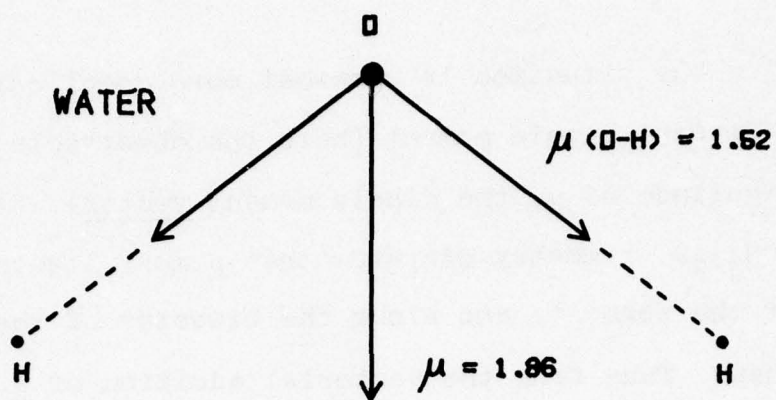
$$\mu(\text{O-CH}_3) = \frac{\mu((\text{CH}_3)_2\text{O})}{2\cos(\varphi/2)} \quad (6.10)$$

where θ is the angle³⁵ between (O-H) bonds in H_2O , and φ is the angle between (O-C) bonds in $(\text{CH}_3)_2\text{O}$. These bond moments may be added vectorially at the proper angle to obtain the predicted dipole moment for CH_3OH . The process, angles involved, and experimental values are shown in figure 7. The magnitude of the predicted moment is within 10% of the experimental value, although it is not within the approximately 1% experimental uncertainty. In addition, the orientation of the molecular moment is within 10 degrees of the experimentally determined orientation.³⁶

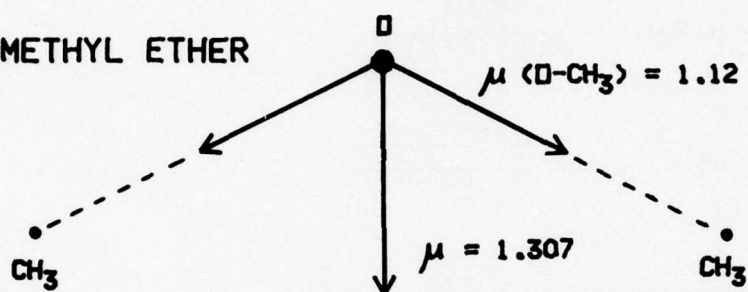
In applying the BAA to $\chi_{\parallel}^{(2)}$ for these molecules, we are hampered by the lack of symmetry about the plane bisecting the angle between the two segments in CH_3OH .

74

WATER



DIMETHYL ETHER



METHANOL

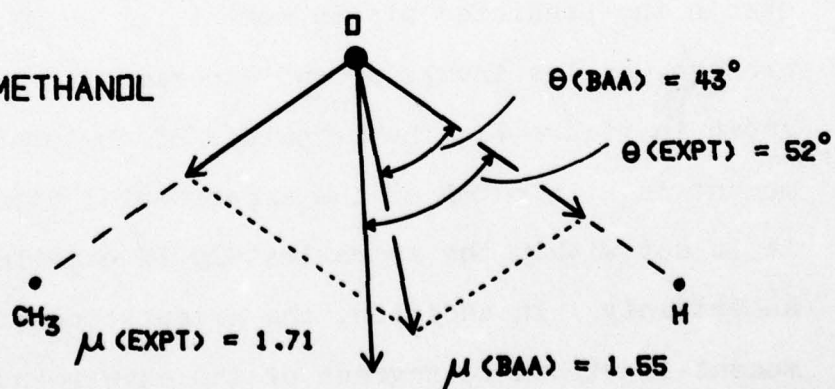


Figure 7. BAA Applied to μ for H_2O , $(\text{CH}_3)_2\text{O}$, and CH_3OH .

From equation 2.22, we see that $\chi_{\parallel}^{(2)}$ is the z component of the vector $\chi_{\eta\eta}$, where the z axis is along the dipole moment. In H_2O and $(\text{CH}_3)_2\text{O}$ this vector, which we shall call $\underline{\chi}_v^{(2)}$, is parallel to $\underline{\mu}$ by symmetry, so for these molecules

$$|\chi_{\parallel}^{(2)}| = |\underline{\chi}_v^{(2)}| \quad (6.11)$$

and equations analogous to 6.9 and 6.10 hold:

$$\chi_{\parallel}^{(2)}(\text{O-H}) = \frac{\chi_{\parallel}^{(2)}(\text{H}_2\text{O})}{2\cos(\theta/2)} \quad (6.12)$$

$$\chi_{\parallel}^{(2)}(\text{O-CH}_3) = \frac{\chi_{\parallel}^{(2)}((\text{CH}_3)_2\text{O})}{2\cos(\varphi/2)} \quad (6.13)$$

By vector addition, we can determine the direction and magnitude of $\underline{\chi}_v^{(2)}(\text{CH}_3\text{OH})$. However, the lack of symmetry in CH_3OH means that equation 6.11 does not hold.

Instead, we must use the more general relation

$$\chi_{\parallel}^{(2)} = \frac{\underline{\mu}}{|\underline{\mu}|} \cdot \underline{\chi}_v^{(2)} \quad (6.14)$$

where the direction defined by $\underline{\mu}/|\underline{\mu}|$ is that determined from experiment. The procedure and results are illustrated in figure 8. The predicted value of $\chi_{\parallel}^{(2)}$ for CH_3OH and the experimental value agree within 18%, somewhat outside

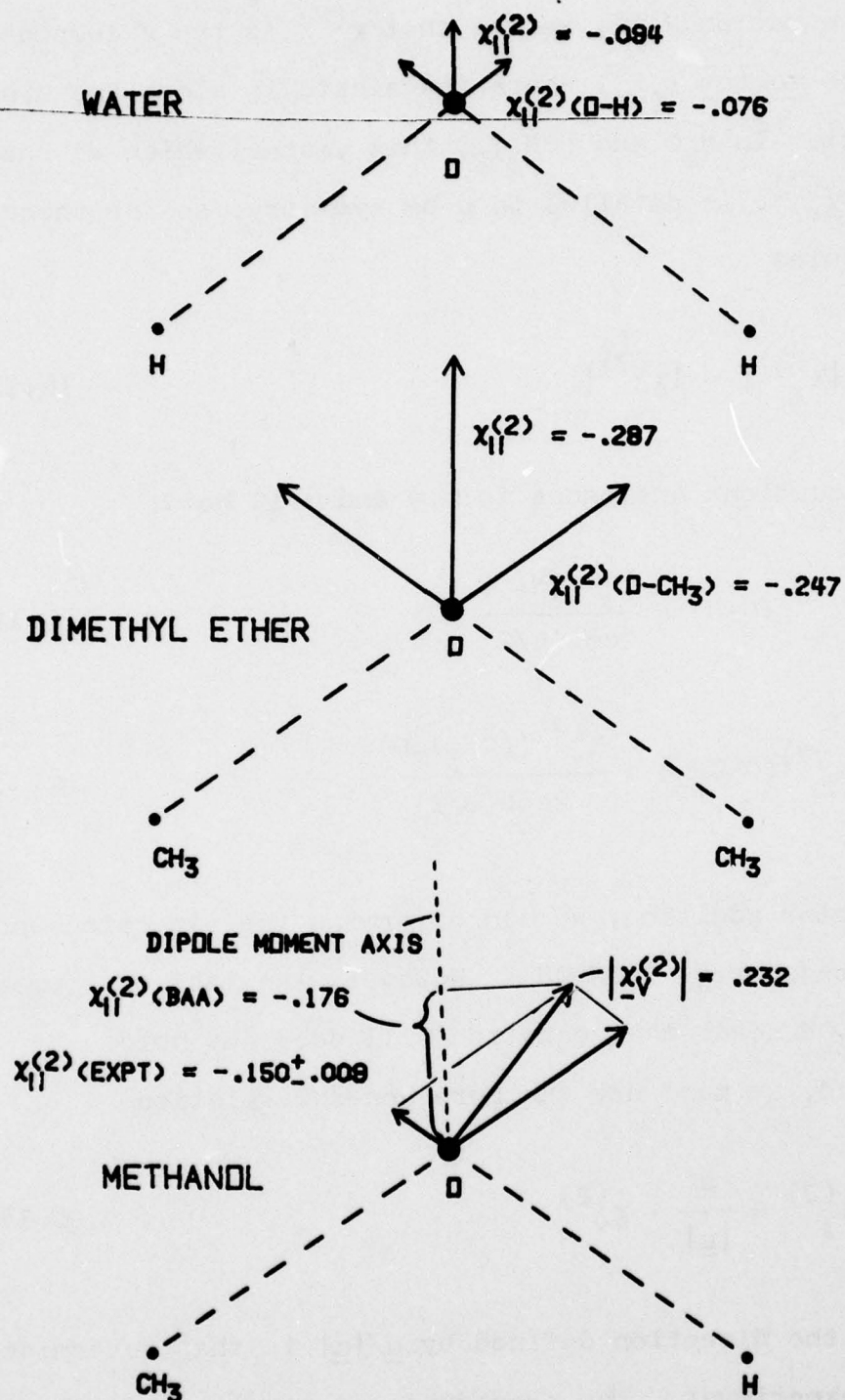


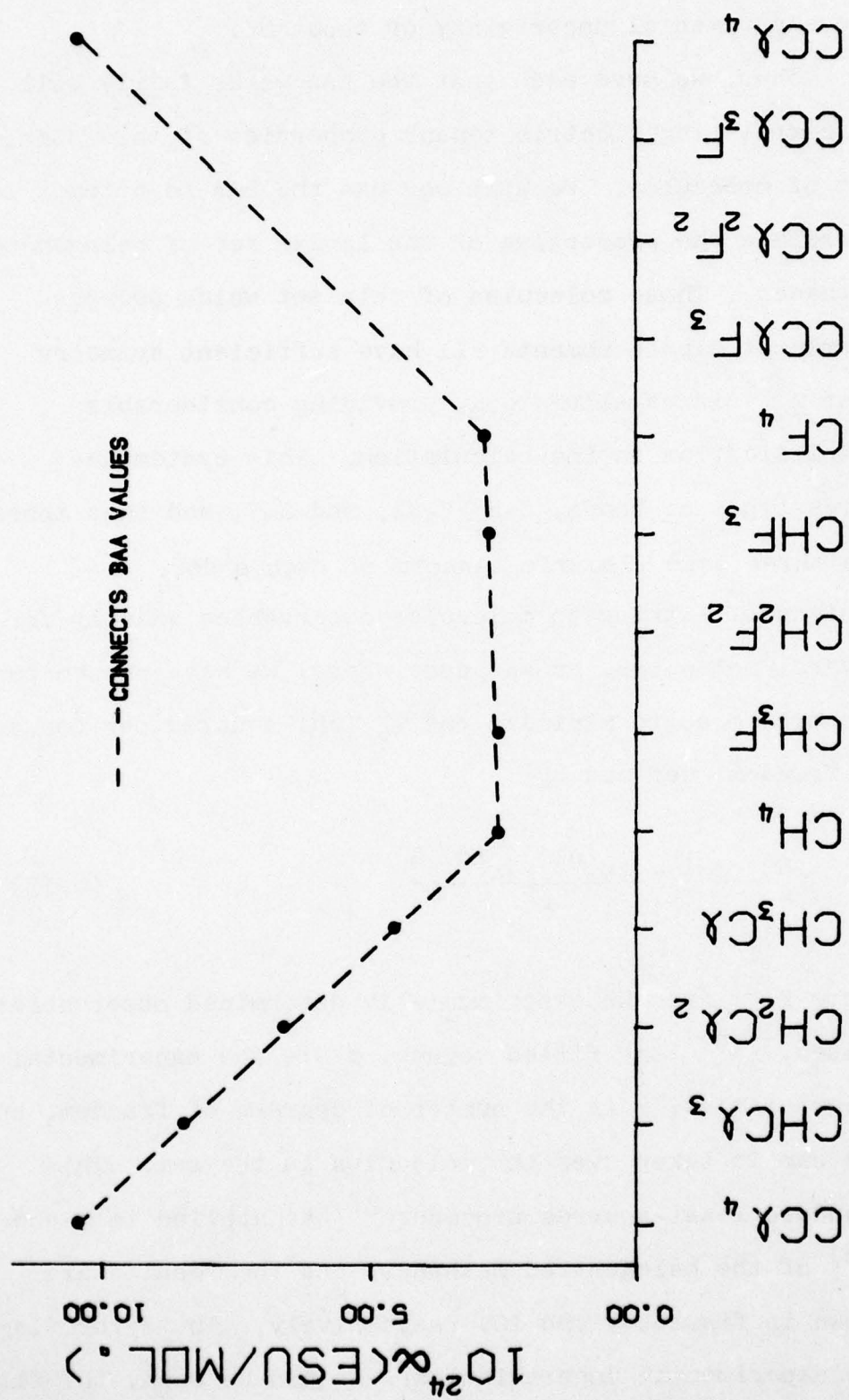
Figure 8. BAA Applied to $\chi_{11}^{(2)}$ for H_2O , $(\text{CH}_3)_2\text{O}$, and CH_3OH .

the experimental uncertainty of about 6%.

Thus, we have seen that the BAA works fairly well in correlating electric tensor properties of this simple set of molecules. We will now use the BAA to attempt to correlate the properties of the larger set of halogenated methanes. Those molecules of this set which possess permanent dipole moments all have sufficient symmetry that $\chi_v^{(2)}$ is parallel to $\underline{\mu}$, providing considerable simplification in the calculation. This system has three types of bonds, C-H, C-Cl, and C-F, and thus there are three bare electric tensors of each order. Instead of fitting to molecular observables exactly for several molecules, as was done above, we have chosen bond tensors so as to minimize the χ_v^2 (chi-squared per degree of freedom) defined by

$$\chi_v^2 = v^{-1} \sum_i \frac{(\chi^{(n)'} - \chi^{(n)})^2}{\sigma^2} \quad (6.15)$$

where $\chi^{(n)}$ are the experimentally determined observables values, $\chi^{(n)}'$ the fitted values, σ are the experimental uncertainties, v is the number of degrees of freedom, and the sum is taken over the molecules in the set. This standard least-squares procedure³⁷ was applied to α and $\chi_{||}^{(3)}$ of the halogenated methanes, and the results are shown in figures 9 and 10, respectively. The error flags are experimental uncertainties. As can be seen, the fits

Figure 9. BAA Applied to α for the Halogenated Methanes.

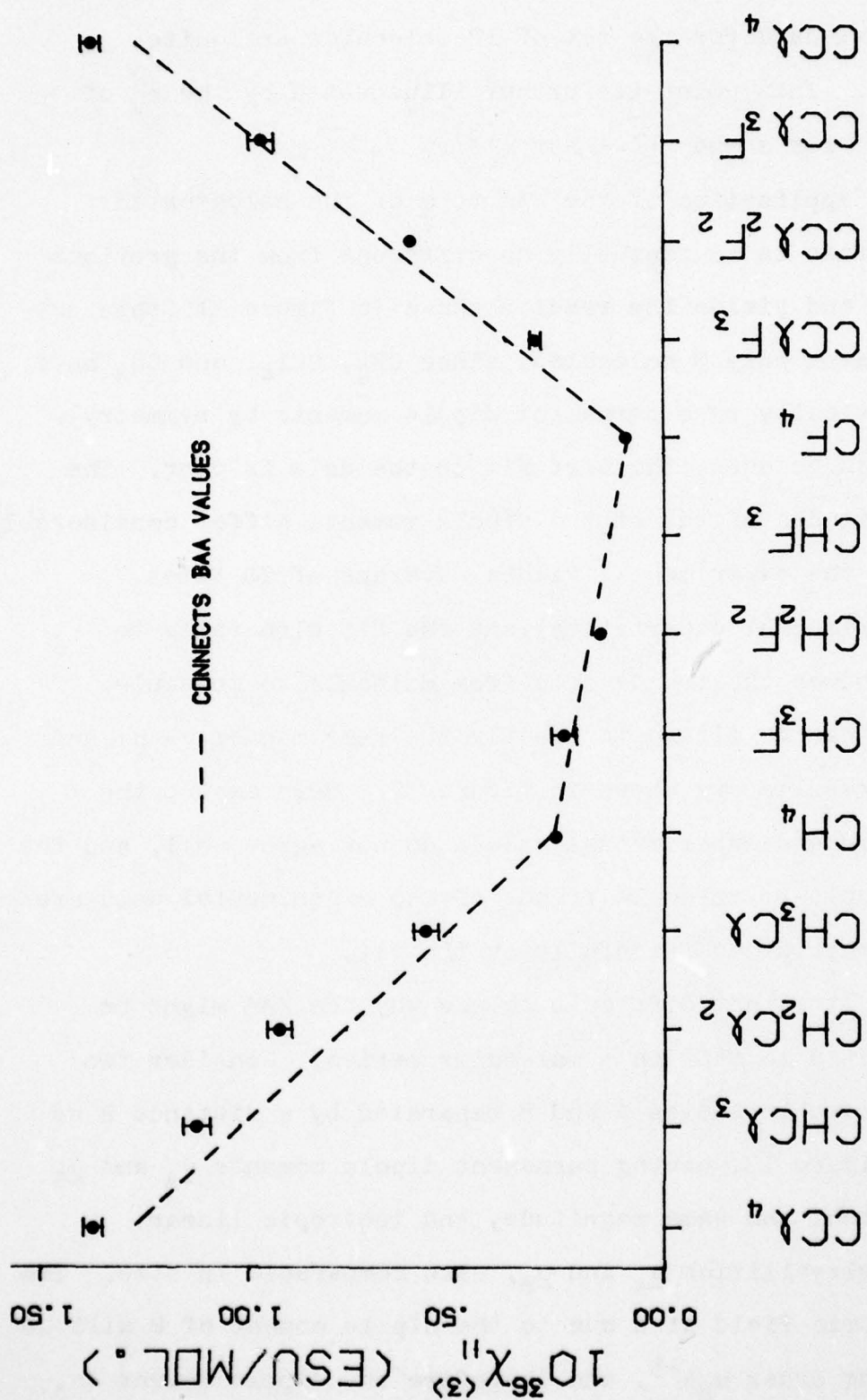


Figure 10. BAA Applied to $X_{II}^{(3)}$ for the Halogenated Methanes.

to the data for the set of 12 molecules are quite good. This point is further illustrated by the χ^2_v of 0.5 for α and 17.4 for $\chi_{||}^{(3)}$.

Application of the BAA to $\underline{\mu}$ of the halogenated methanes is conceptually no different from the previous case and yields the results shown in figure 11 (this set contains only 9 molecules, since CF_4 , CCl_4 , and CH_4 have identically zero permanent dipole moments by symmetry). As can be seen, the best fit to the data is poor. The magnitudes of the fitted dipole moments differ considerably from the experimental values (average of 20 times experimental uncertainty), and the fit also fails to reproduce the trends of μ from molecule to molecule. $\chi_{||}^{(2)}$ can be fitted in exactly the same manner as μ , and the results are shown in figure 12. Here again, the fitted and experimental values do not agree well, and the molecule-to-molecule trends of the experimental data are not reproduced faithfully by the fit.

It is not difficult to see why the BAA might be expected to fail in a molecular series. Consider two polarizable bodies A and B separated by a distance R as in figure 13, having permanent dipole moments $\underline{\mu}_A$ and $\underline{\mu}_B$ of about the same magnitude, and isotropic linear polarizabilities $\underline{\alpha}_A$ and $\underline{\alpha}_B$, also comparable in size. The electric field at A due to the dipole moment of B will be of the order $\mu_B R^{-3}$, and therefore the dipole moment $\Delta\mu_A$

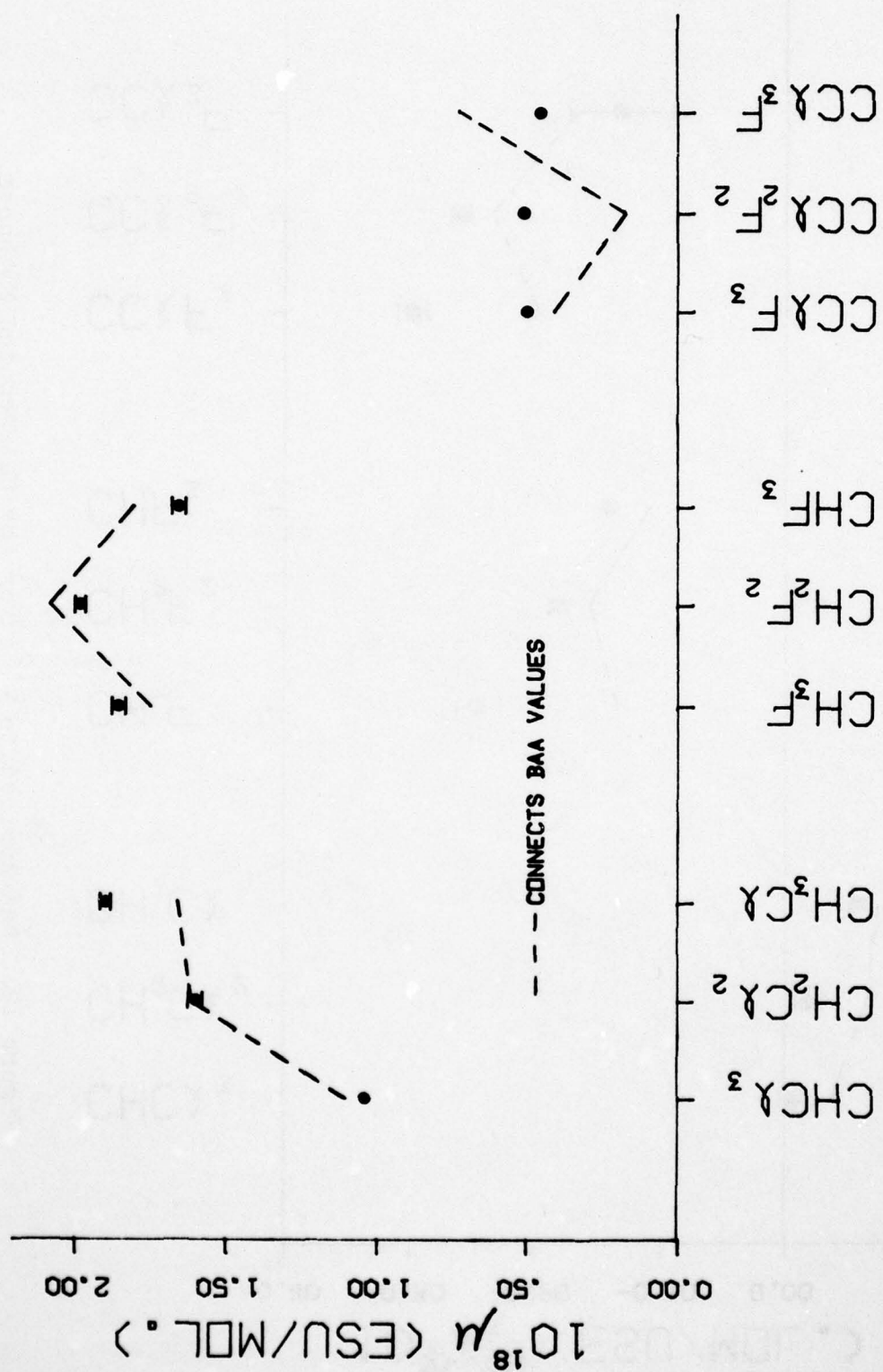


Figure 11. BAA Applied to μ for the Halogenated Methanes.

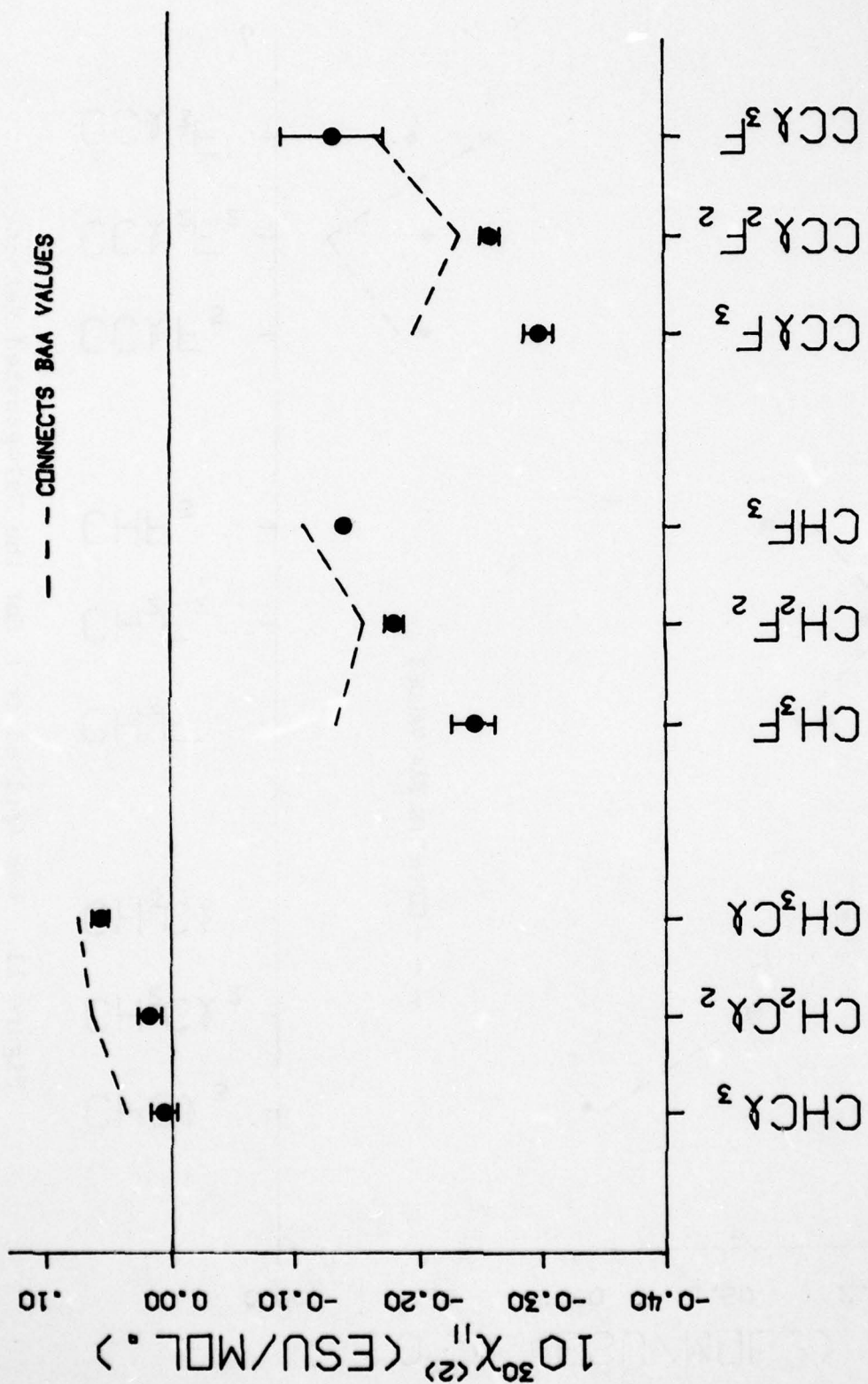


Figure 12. BAA Applied to $\chi''(2)$ for the Halogenated Methanes.

AD-A066 726

MICHIGAN UNIV ANN ARBOR DEPT OF PHYSICS
NONLINEAR OPTICAL POLARIZABILITIES OF MOLECULES.(U)
JAN 78 C K MILLER

F/G 20/3

UNCLASSIFIED

AFOSR-TR-79-0365

AFOSR-77-3225

NL

2 OF 2
ADA
066726

11



END
DATE
FILMED

5-79
DOC

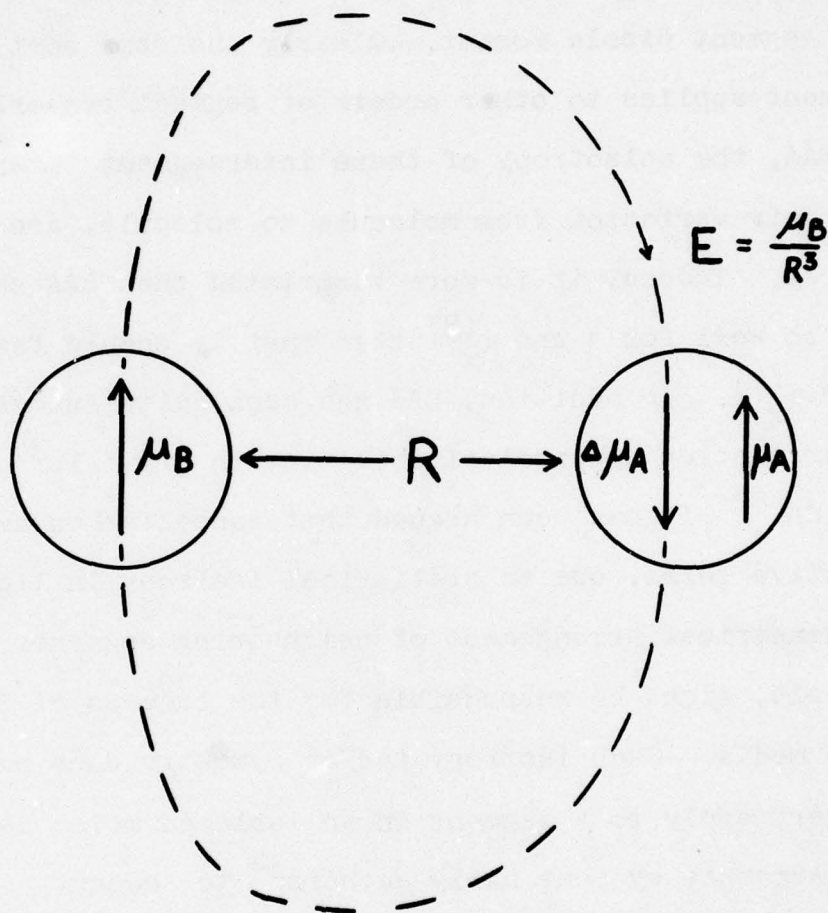


Figure 13. Interaction Between Neighboring Polarizable Dipolar Bodies.

induced in A due to μ_B will be approximately $\mu_B \alpha_A R^{-3}$. Molecular polarizabilities are of the order 10^{-24} cm^3 , and typical inter-segment distances in molecules are 10^{-8} cm , so the factor $\alpha_A R^{-3}$ is of order 1, and $\Delta\mu_A$ is of the order of a segment dipole moment. Clearly the same sort of argument applies to other orders of segment tensors. In the BAA, the anisotropy of these intersegment interactions, and their variation from molecule to molecule, are ignored. Indeed, it is more surprising that BAA should work so well for α and $\chi_{\parallel}^{(3)}$ than that it should fail for μ and $\chi_{\parallel}^{(2)}$. In addition, BAA has been quite successful in correlating hyperpolarizabilities in crystals³⁸ and liquids.³² It has been argued that cancellation among inductive terms, due to statistical isotropy in liquids or symmetrical arrangement of neighboring segments in crystals, might be responsible for the success of BAA in these media. Such isotropy and/or symmetry does not, however, apply to a segment in an isolated molecule.

Attempts by some early authors³⁴ to account approximately for inductive effects among the C-H, C-Cl, and C-F bond dipole moments of the halogenated methanes met with limited success in predicting the molecular dipole moments. However, iterative methods were used in that work. We will consider a self-consistent approach to calculating inter-segment interactions in molecules.

6.2 The Interacting Segment Model

We wish to develop an Interacting Segment Model (ISM) which considers bond interaction contributions to the electric tensor properties of structurally similar molecules, without completely discarding the simplicity of the BAA. A molecular group-dipole interaction model bearing formal similarity to our ISM has recently been developed by Sundberg.³⁹

All segment electric tensor properties in the BAA have two characteristics in common. These are additivity, as expressed by equation 6.1, and transferability, meaning that bond properties are independent of molecular environment. In the ISM, we assign these characteristics to two different sets of tensors. We suppose that in the absence of intersegment interactions, a segment i can be characterized by a set of "bare" segment parameters $\underline{\mu}_i, \underline{\alpha}_i, \chi_i^{(2)}, \chi_i^{(3)}, \dots$; these parameters are to be thought of as the electric tensor properties of an isolated segment so that, for example, a C-X bond, X = halogen, has rotational symmetry about the bond axis. These bare parameters are defined to be transferable from molecule to molecule. When intersegment interactions are included, the segment i is characterized by a set of "dressed" parameters $\hat{\underline{\mu}}_i, \hat{\underline{\alpha}}_i, \hat{\chi}_i^{(2)}, \hat{\chi}_i^{(3)}, \dots$; these tensor properties have been modified by interactions with neighboring segments, and will possess a symmetry dictated by the

arrangement of surrounding segments, which will in general be lower than that of the bare parameters.

These tensors are assigned the characteristic of additivity and so conform to equation 6.1, which now takes the form

$$\underline{\chi}^{(n)'} = \sum_1 \underline{\hat{\chi}}_1^{(n)} \quad (6.16)$$

where the sum is over all segments in the molecule.

It is appropriate at this point to adopt the dispersionless limit, that is, to assume that all $\underline{\chi}^{(n)}$ are equal to their dc values. As we have seen, the fact that $R^{(2)}$ and $R^{(3)}$ are very nearly 3.0 implies that dispersion is not important in these molecules, and by neglecting its effect, we will realize a significant simplification in the mathematics. In this limit, we can write the dipole moment of segment i in the presence of an external electric field \underline{E} as

$$\begin{aligned} \mu_i(\underline{E}) &= \underline{\hat{\mu}}_i + \underline{\hat{\alpha}}_i \underline{E} + \underline{\hat{\chi}}_i^{(2)} \underline{E}^2 + \underline{\hat{\chi}}_i^{(3)} \underline{E}^3 + \dots \\ &= \sum_{n=0}^{\infty} \underline{\chi}_i^{(n)} \underline{E}^n \end{aligned} \quad (6.17)$$

where \underline{E}^n is a tensor of rank n , the direct product of \underline{E} with itself n times, and $\underline{\chi}_i^{(n)} \underline{E}^n$ is the inner product of the $(n+1)$ th rank tensor $\underline{\chi}_i^{(n)}$ with \underline{E}^n . Thus, equation 6.17 is equivalent to equation 2.1 for dc field, except that it is applied here to a segment, rather than to a

complete molecule. One can also express $\underline{\mu}_i(\underline{E})$ in terms of the total electric field \underline{E}_i at segment i , consisting of the external field \underline{E} and the fields at segment i due to permanent and induced dipoles at neighboring segments. Since the interactions are included in the electric field, this expression involves bare segment tensors and is written as

$$\begin{aligned}\underline{\mu}_i(\underline{E}) &= \underline{\mu}_i + \underline{\alpha}_i \underline{E}_i + \underline{\chi}_i^{(2)} \underline{E}_i^2 + \underline{\chi}_i^{(3)} \underline{E}_i^3 + \dots \\ &= \sum_{n=0}^{\infty} \underline{\chi}_i^{(n)} \underline{E}_i^n\end{aligned}\quad (6.18)$$

In equations 6.17 and 6.18, we have assumed that all intersegment interactions are electrostatic in origin, and we have ignored all non-classical short-range interactions. To obtain simple expressions for \underline{E}_i , we further assume that all tensors for a given segment are localized within the segment at a single point, called the "active center", and that contributions from segment electric multipoles of order higher than dipole can be ignored. This point localization, which was not required by the BAA, finds some justification in localized molecular orbital calculations,³⁴ but it is still a major simplification. Such drastic approximations can only be justified by the ability of the model to reproduce experimentally observed molecular tensor properties, given

a single set of bare parameters which are transferable from molecule to molecule. With these approximations, the electric field $\Delta \underline{E}^{(ij)}$ at segment i due to the dipole $\underline{\mu}_j(\underline{E})$ at segment j is $\underline{T}_{ij} \underline{\mu}_j(\underline{E})$ or, more explicitly,

$$\Delta E_{\xi}^{(ij)} = T_{ij\xi\nu} \mu_{j\nu}(\underline{E}) \quad (6.19)$$

Hereinafter, Latin indices refer to segment numbers and Greek indices stand for spatial coordinates, and summation is implied over repeated Greek indices only. The tensor \underline{T}_{ij} is defined by

$$\begin{aligned} T_{ij\xi\eta} &= [3R_{ij\xi}R_{ij\eta} - \delta_{\xi\eta}R_{ij}^2] R_{ij}^{-5}, \quad j \neq i \\ &= 0, \quad j = i \end{aligned} \quad (6.20)$$

where \underline{R}_{ij} is the distance vector between active centers i and j , and $\delta_{\xi\eta}$ is the Kronecker delta.

The total electric field at segment i can then be written

$$\underline{E}_i = \underline{E} + \sum_j \underline{T}_{ij} \underline{\mu}_j(\underline{E}) \quad (6.21)$$

Substituting equation 6.17 into equation 6.21 yields an expression for \underline{E}_i in terms of the applied field \underline{E} , the dressed tensors $\hat{\chi}_j^{(n)}$, and the geometrical factors \underline{T}_{ij} . Further substitution of equation 6.21 into equation 6.18

results in a polynomial in \underline{E} which can be compared term-by-term with equation 6.17 to yield expressions for $\hat{\underline{x}}_j^{(m)}$ in terms of the \underline{T}_{ij} , $\underline{x}_i^{(p)}$ of all orders p , and $\hat{\underline{x}}_i^{(n)}$ for $n \leq m$. Before writing down these results, we introduce further notation conventions:

1. The expression $\langle \underline{T} \cdot \hat{\underline{x}}^{(n)} \rangle_i$ stands for the sum over j of the inner product of \underline{T}_{ij} and $\hat{\underline{x}}_j^{(n)}$;
2. All products of such terms (including the m -fold product $\langle \underline{T} \cdot \hat{\underline{x}}^{(n)} \rangle_i^m$) are direct products;
3. The product of a bare parameter with a term such as one of those in 1 and 2 above is an inner product.

Using these conventions, results for the dressed parameters are written as

$$\hat{\underline{\mu}}_i = \underline{\mu}_i + \underline{\alpha}_i \langle \underline{T} \cdot \hat{\underline{\mu}} \rangle_i + \underline{x}_i^{(2)} \langle \underline{T} \cdot \hat{\underline{\mu}} \rangle_i^2 + \underline{x}_i^{(3)} \langle \underline{T} \cdot \hat{\underline{\mu}} \rangle_i^3 + \dots, \quad (6.22)$$

$$\hat{\underline{\alpha}}_i = (\underline{\alpha}_i + 2\underline{x}_i^{(2)} \langle \underline{T} \cdot \hat{\underline{\mu}} \rangle_i + 3\underline{x}_i^{(3)} \langle \underline{T} \cdot \hat{\underline{\mu}} \rangle_i^2 + \dots)(1 + \langle \underline{T} \cdot \hat{\underline{\alpha}} \rangle_i), \quad (6.23)$$

$$\begin{aligned} \hat{\underline{x}}_i^{(2)} = & \underline{\alpha}_i \langle \underline{T} \cdot \hat{\underline{x}}^{(2)} \rangle_i + \underline{x}_i^{(2)} [2 \langle \underline{T} \cdot \hat{\underline{\mu}} \rangle_i \langle \underline{T} \cdot \hat{\underline{x}}^{(2)} \rangle_i + (1 + \langle \underline{T} \cdot \hat{\underline{\alpha}} \rangle_i)^2] \\ & + 3\underline{x}_i^{(3)} \langle \underline{T} \cdot \hat{\underline{\mu}} \rangle_i [\langle \underline{T} \cdot \hat{\underline{\mu}} \rangle_i \langle \underline{T} \cdot \hat{\underline{x}}^{(2)} \rangle_i + (1 + \langle \underline{T} \cdot \hat{\underline{\alpha}} \rangle_i)^2] + \dots, \end{aligned} \quad (6.24)$$

$$\begin{aligned}
\hat{\underline{\chi}}_i^{(3)} = & \underline{\alpha}_i \langle \underline{T} \cdot \hat{\underline{\chi}}^{(3)} \rangle_i + 2\underline{\chi}_i^{(2)} [\langle \underline{T} \cdot \hat{\underline{\mu}} \rangle_i \langle \underline{T} \cdot \hat{\underline{\chi}}^{(3)} \rangle_i + (1 + \langle \underline{T} \cdot \hat{\underline{\alpha}} \rangle_i) \langle \underline{T} \cdot \hat{\underline{\chi}}^{(2)} \rangle_i] \\
& + \underline{\chi}_i^{(3)} [3 \langle \underline{T} \cdot \hat{\underline{\mu}} \rangle_i^2 \langle \underline{T} \cdot \hat{\underline{\chi}}^{(3)} \rangle_i + 6 \langle \underline{T} \cdot \hat{\underline{\mu}} \rangle_i (1 + \langle \underline{T} \cdot \hat{\underline{\alpha}} \rangle_i) \langle \underline{T} \cdot \hat{\underline{\chi}}^{(2)} \rangle_i \\
& + (1 + \langle \underline{T} \cdot \hat{\underline{\alpha}} \rangle_i)^3] + \dots \quad (6.25)
\end{aligned}$$

Terms not explicitly included in equations 6.22-6.25 are those containing $\underline{\chi}_i^{(n)}$ with $n > 3$. The dimensional arguments in the previous section and in section 2.1 would seem to suggest that for all orders n there will be terms in $\underline{\chi}^{(n)}$ which will be comparable in magnitude with the leading terms in these equations. However, we adopt the hypothesis that higher-order $\underline{\chi}^{(n)}$ are overestimated by the dimensional arguments. Also, cancellation in the tensor sum over bonds $\langle \underline{T} \cdot \hat{\underline{\chi}}^{(2n)} \rangle$, where $\hat{\underline{\chi}}^{(2n)}$ is an even-order electric-tensor which vanishes in a centro-symmetric system, will reinforce this tendency (contributions to $\hat{\underline{\chi}}^{(n)}$ which contain $\underline{\chi}^{(m)}$, $m > n$, must have at least a factor $\langle \underline{T} \cdot \hat{\underline{\mu}} \rangle_i^{m-n}$).

The task that remains is to determine sets of dressed and undressed molecular tensors from molecular observables, using the expressions developed in this section. We now consider this problem for the permanent dipole moments $\underline{\mu}$, linear polarizabilities $\underline{\alpha}$, and second-order polarizabilities $\underline{\chi}^{(2)}$ of the halogenated methanes.

6.3 Application of the ISM to Electric Tensor Properties of the Halogenated Methanes

Equations 6.22-6.25 form a coupled non-linear system. Our goal is to find a set of bare bond tensors which, when substituted into these equations, reproduce the molecular observables. We will, however, make some simplifying assumptions before doing so.

Our first step is to exclude $\underline{\chi}^{(3)}$ from the fitting procedure, eliminating equation 6.25 from the set. Since only the isotropic parts of the molecular $\underline{\chi}^{(3)}$ s are known, it is felt that anisotropies of the bare parameters $\underline{\chi}_i^{(3)}$ would be ill-determined by fitting. Thus the bare $\underline{\chi}_i^{(3)}$ will be considered to be isotropic, with

$$\chi_{zzzz}^{(3)}(\text{C-X}) = \frac{1}{4}\chi_{\parallel}^{(3)}(\text{CX}_4), \quad \text{X} = \text{F, Cl, H} \quad (6.26)$$

Secondly, we invoke our hypothesis that terms containing tensor sums $\langle \underline{T} \cdot \underline{\hat{\chi}}^{(2n)} \rangle$ will be reduced in magnitude owing to cancellation in the sums. We will ignore any terms containing even-order polarizabilities in expressions for $\underline{\hat{\chi}}^{(n)}$ with odd n , and we will discard terms containing more than one even-order factor in expressions for $\underline{\hat{\chi}}^{(m)}$ with even m . Thus, the equations for $\underline{\hat{\alpha}}_1$ will contain no even-order factors, and terms in the equations for $\underline{\hat{\mu}}_1$ and $\underline{\hat{\chi}}_1^{(2)}$ will have no more than one even-order factor. With this restriction, we rewrite equations 6.22-6.24:

$$\hat{\underline{\mu}}_i = \underline{\mu}_i + \underline{\alpha}_i \langle \underline{T} \cdot \hat{\underline{\mu}} \rangle_i ; \quad (6.27)$$

$$\hat{\underline{\alpha}}_i = \underline{\alpha}_i + \underline{\alpha}_i \langle \underline{T} \cdot \hat{\underline{\alpha}} \rangle_i ; \quad (6.28)$$

$$\begin{aligned} \hat{\chi}_i^{(2)} = & \chi_i^{(2)} + \underline{\alpha}_i \langle \underline{T} \cdot \hat{\chi}^{(2)} \rangle_i + \chi_i^{(2)} \langle \underline{T} \cdot \hat{\underline{\alpha}} \rangle_i (2 + \langle \underline{T} \cdot \hat{\underline{\alpha}} \rangle_i) \\ & + 3\chi_i^{(3)} \langle \underline{T} \cdot \hat{\underline{\mu}} \rangle_i (1 + \langle \underline{T} \cdot \hat{\underline{\alpha}} \rangle_i)^2 . \end{aligned} \quad (6.29)$$

In employing this approximation, we have gained a significant advantage. While equations 6.22-6.24 were coupled, 6.27-6.29 are independent in the following sense: $\underline{\alpha}_i$ can be selected to fit molecular $\underline{\alpha}$ values using equation 6.28, without reference to $\underline{\mu}$ or $\chi^{(2)}$; $\underline{\mu}_i$ can then be found so as to fit molecular values by means of equation 6.27, using the $\underline{\alpha}_i$ calculated in the previous step; and finally, $\chi_i^{(2)}$ can be selected to fit molecular $\chi^{(2)}$ values, making use of equation 6.29 and the $\hat{\underline{\mu}}_i$, $\underline{\alpha}_i$, and $\hat{\underline{\alpha}}_i$ already determined. The steps in this procedure are elaborated upon below.

Before equations 6.27-6.29 can be used for calculations, the \underline{T}_{ij} must be evaluated, i.e., active center locations must be selected. We have arbitrarily chosen as the distance from the carbon nucleus to the C-X bond active center the average C-X bond length,³⁵ and for angles we use experimentally determined bond angles.³⁵ These values are shown in table 10. We have explored

Table 10.

<u>Molecule</u>	<u>Bond Angles ^a</u>
CCl_4	$\angle \text{Cl-C-Cl} = 109^\circ 28'$ ^b
CHCl_3	$\angle \text{H-C-Cl} = 108^\circ$
CH_2Cl_2	$\angle \text{H-C-H} = 112^\circ$
	$\angle \text{Cl-C-Cl} = 111^\circ 48'$
CH_3Cl	$\angle \text{Cl-C-H} = 108^\circ$
CH_4	$\angle \text{H-C-H} = 109^\circ 28'$ ^b
CH_3F	$\angle \text{F-C-H} = 108^\circ 49'$
CH_2F_2	$\angle \text{H-C-H} = 111^\circ 54'$
	$\angle \text{F-C-F} = 108^\circ 30'$
CHF_3	$\angle \text{H-C-F} = 110^\circ 8'$
CF_4	$\angle \text{F-C-F} = 109^\circ 28'$ ^b
CClF_3	$\angle \text{Cl-C-F} = 110^\circ 20'$
CCl_2F_2	$\angle \text{Cl-C-Cl} = 108^\circ 30'$
	$\angle \text{F-C-F} = 109^\circ 30'$
CCl_3F	$\angle \text{F-C-Cl} = 107^\circ 12'$
<u>Bond</u>	<u>Bond Radius (\AA) ^a</u>
C-F	1.36
C-Cl	1.77
C-H	1.1

^aFrom reference 35.^bTetrahedral symmetry.

other reasonable choices for bond radii, with results qualitatively similar to those shown here.

It is desirable to rewrite equation 6.28 so that $\hat{\underline{\alpha}}_i$ is not functionally dependent upon $\hat{\underline{\alpha}}_j$. We write

$$\sum_j \{ \delta_{ij} - \alpha_{i-T_{ij}} \} \hat{\underline{\alpha}}_j = \underline{\alpha}_i \quad (6.30)$$

where $\alpha_{i-T_{ij}}$ is an inner product and the δ_{ij} are tensors such that

$$\delta_{ij\xi\eta} = \delta_{ij}\delta_{\xi\eta} \quad (6.31)$$

We then take the inverse \underline{M} of the matrix quantity {...} in equation 6.30 to obtain the expression

$$\hat{\underline{\alpha}}_i = \sum_j \underline{M}_{ij} \underline{\alpha}_j \quad (6.32)$$

This is identical to the result of Applequist et al. obtained in investigations of the polarizability of methane. Their \underline{B}_{ij} correspond to the negative of the inner product \underline{M}_{ij} . Equation 6.16 is used to obtain tensors $\underline{\alpha}'$, and standard non-linear least-squares fitting techniques³⁷ are used to adjust $\underline{\alpha}_i$ to get the best fit of the $\underline{\alpha}'$ to molecular observables. In addition to the isotropic polarizabilities α defined by equation 6.2, there are two other observables derivable from $\underline{\alpha}$. These

are κ^2 , defined by

$$\kappa^2 = \frac{1}{18\alpha^2} [(\alpha_{xx} - \alpha_{yy})^2 + (\alpha_{yy} - \alpha_{zz})^2 + (\alpha_{zz} - \alpha_{xx})^2], \quad (6.33)$$

obtained from measurements of the depolarization of Rayleigh scattering, and a quantity which we shall call $\Delta\alpha_K$, defined by

$$\Delta\alpha_K = \frac{3}{2}(\alpha_{zz} - \alpha), \quad (6.34)$$

which is extracted from measurements of the temperature dependence of the dc Kerr effect. For this last observable, the z axis is along the dipole moment, so that in order to obtain corresponding $\Delta\alpha_K'$ values from the $\underline{\alpha}'$, it is necessary to relate this axis to molecular geometry. Those halogenated methanes of this set which possess dipole moments have either C_{2v} or C_{3v} symmetry, and the dipole moment must lie along the major symmetry axis.

Once the $\underline{\alpha}_i$ are determined, the \underline{M}_{ij} are fixed and equation 6.27 may be manipulated to yield

$$\hat{\underline{\mu}}_i = \sum_j \underline{M}_{ij} \underline{\mu}_j. \quad (6.35)$$

A simple linear least-squares procedure is then used to fit the resulting $\underline{\mu}'$ to the molecular $\underline{\mu}$ values. In order to fit $\underline{\mu}'$ to $\underline{\mu}$ unambiguously, it is necessary to know the

sense of the dipole moment in relation to molecular geometry. It is taken here to be in the sense ${}^{-}\text{F}_n\text{CCl}_{4-n}^{+}$, ${}^{+}\text{H}_n\text{CCl}_{4-n}^{-}$, or ${}^{+}\text{H}_n\text{CF}_{4-n}^{-}$, which is consistent with the experimentally determined⁴¹ polarities ${}^{+}\text{HCF}_3^{-}$ and ${}^{+}\text{H}_3\text{CCl}^{-}$.

The $\hat{\underline{\mu}}_i$ thus determined, along with the tensors \underline{M}_{ij} and the previously determined $\hat{\underline{\alpha}}_i$, appear in the expression obtained by solving equation 6.29 for $\hat{\chi}_i^{(2)}$:

$$\hat{\chi}_i^{(2)} = \sum_j \underline{M}_{ij} (\chi_j^{(2)} + 3\chi_j^{(3)} \langle \underline{T} \cdot \hat{\underline{\mu}} \rangle_j) (1 + \langle \underline{T} \cdot \hat{\underline{\alpha}} \rangle_j)^2. \quad (6.36)$$

Again, all that is required is a linear least-squares fit of the resulting $\chi_{\parallel}^{(2)}$ to the molecular $\chi_{\parallel}^{(2)}$ values.

The results of fitting these functions to experimental data are shown in figures 14, 15, and 16, which may be compared with the BAA fits in figures 11, 9, and 12, respectively. The qualitative nature of the fit to the dipole moments, shown in figure 14, is not dramatically better than that provided by the BAA. There is, however, some improvement, particularly for the small dipole moments of the $\text{CCl}_n\text{F}_{4-n}$ molecules. The fit to the isotropic part of $\underline{\alpha}$, shown in figure 15, remains excellent. In addition, there is a qualitatively good fit to most of the $\Delta\alpha_K$ and κ^2 data. The $\chi_{\parallel}^{(2)}$ fit shown in figure 16 is, like the μ fit, not strikingly improved over bond additivity. Again, however, there is some degree of qualitative improvement, this time in the $\text{CH}_n\text{Cl}_{4-n}$ and

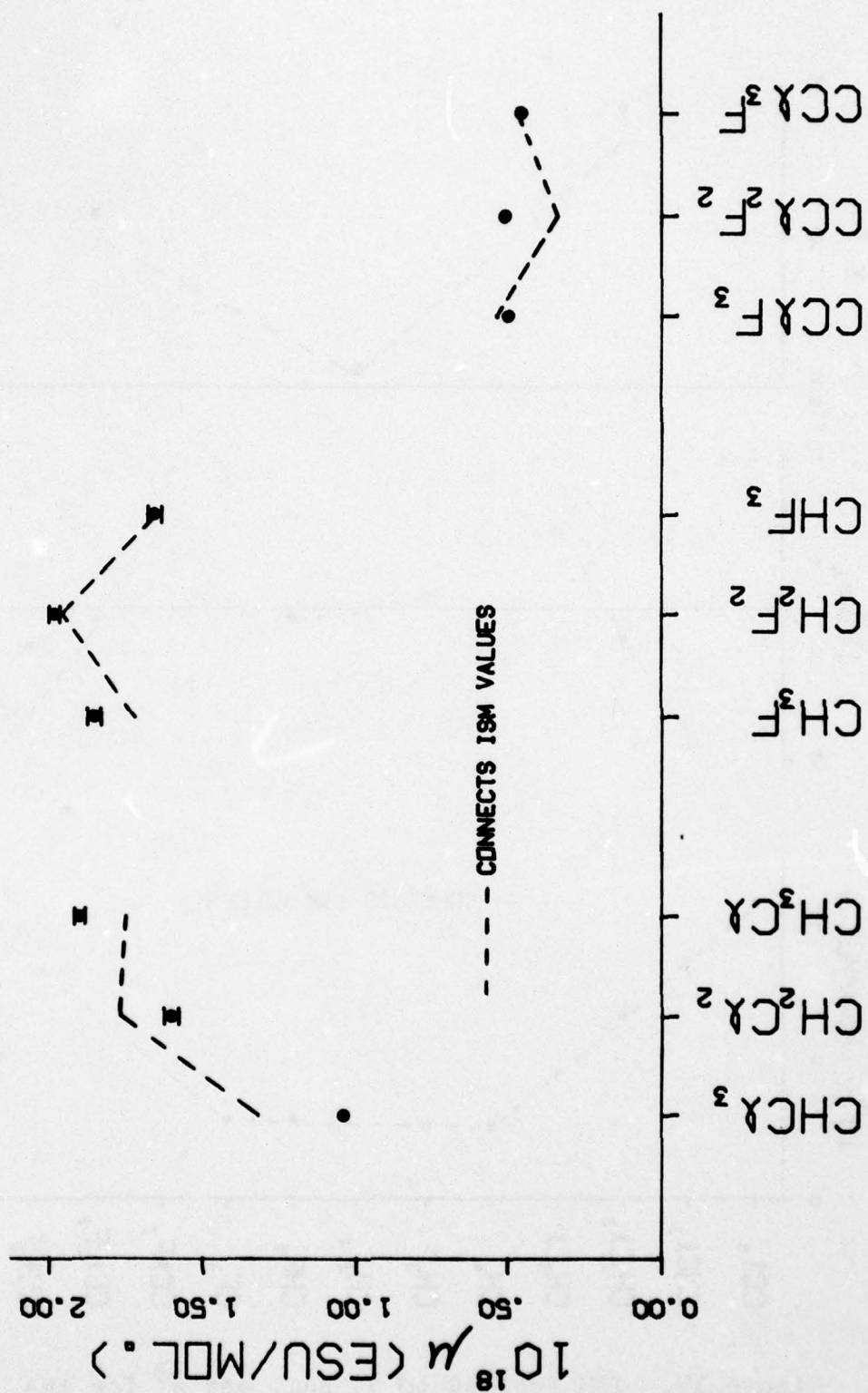


Figure 14. ISM Applied to μ for the Halogenated Methanes.

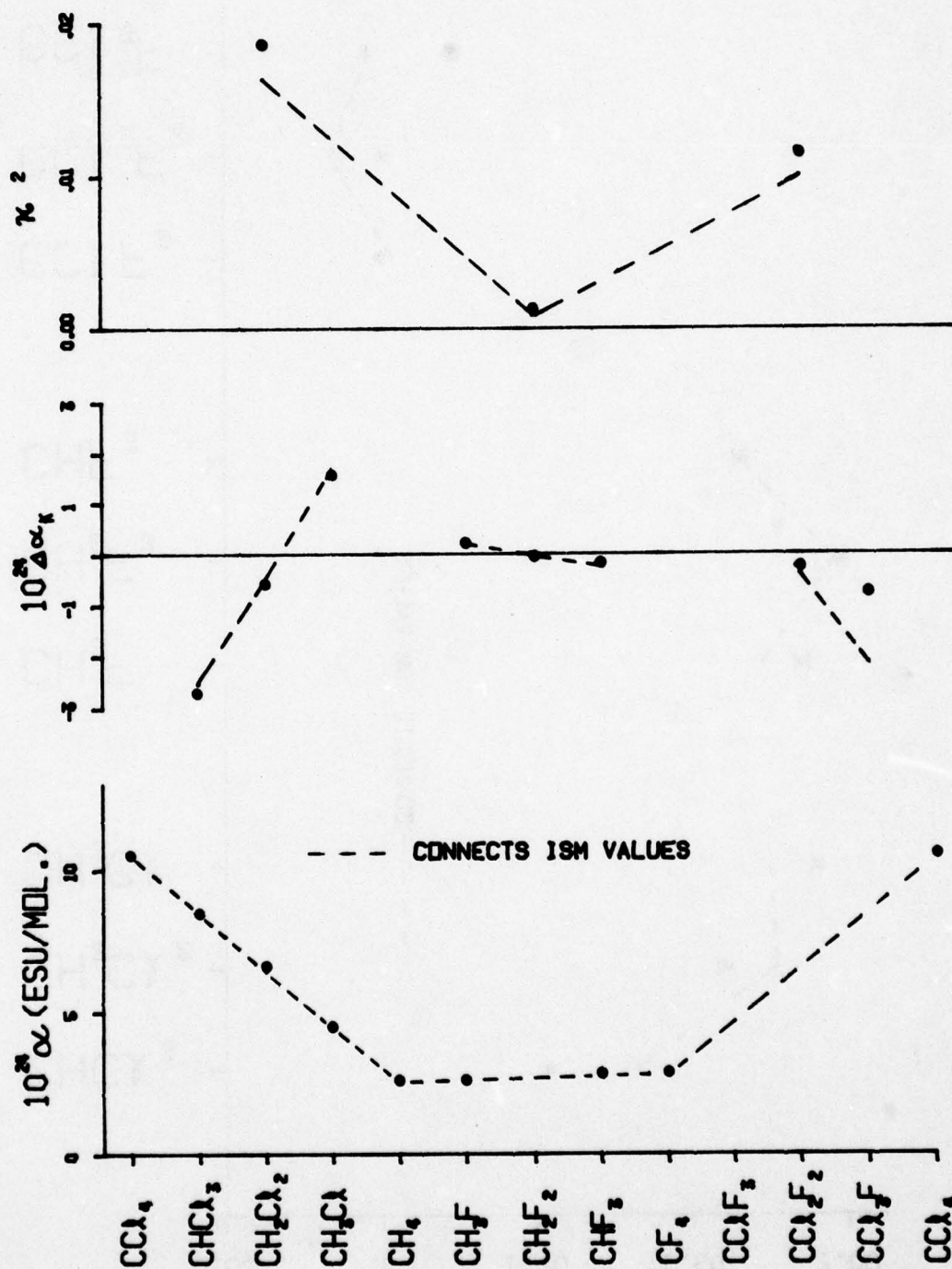


Figure 15. ISM Applied to α , $\Delta \alpha_k$, and κ^2 for the Halogenated Methanes.

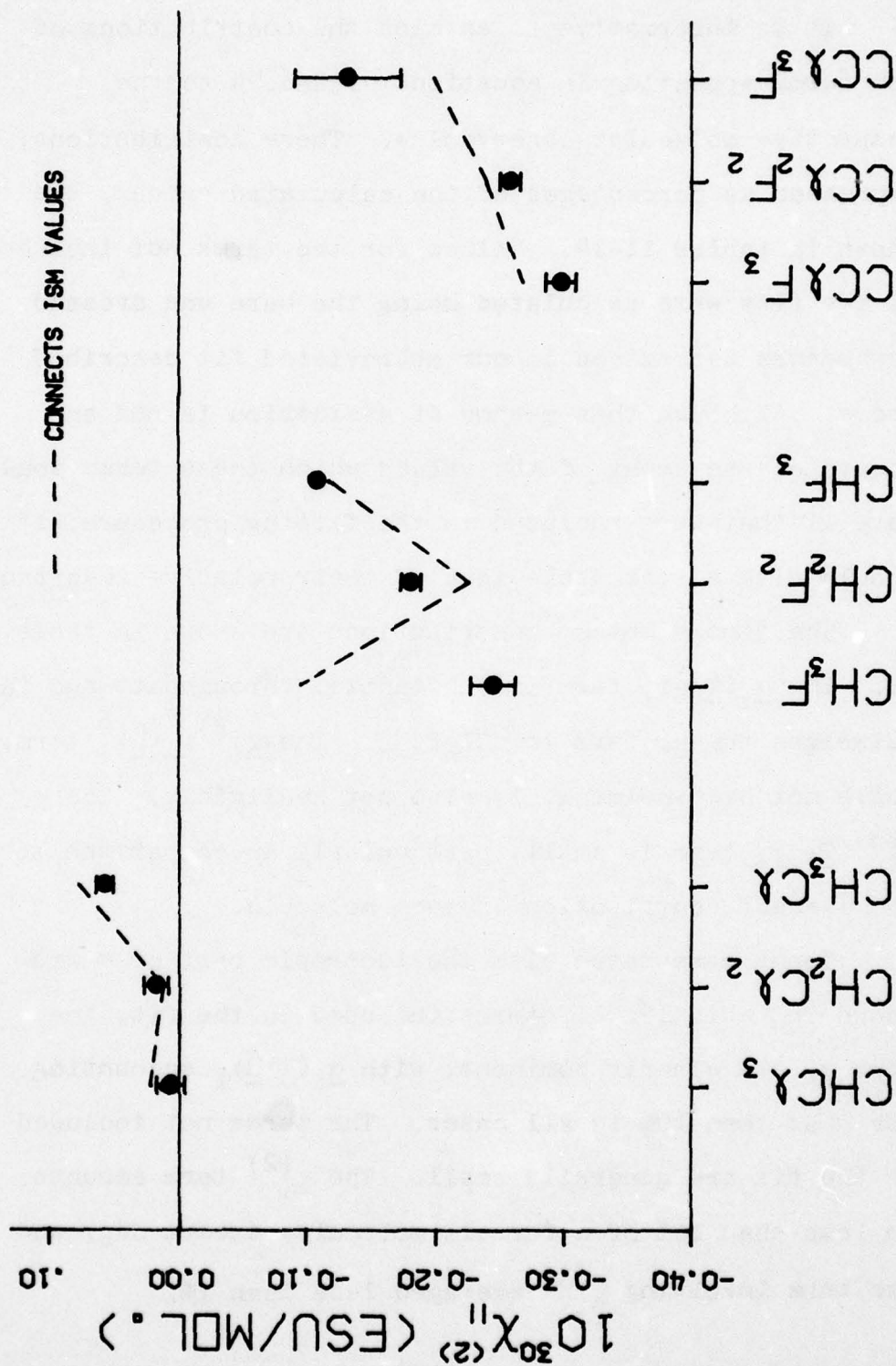


Figure 16. ISM Applied to $x_{(2)}^{(2)}$ for the Halogenated Methanes.

$\text{CCl}_n\text{F}_{4-n}$ molecules.

It is informative to examine the contributions of the terms appearing in equations 6.22-6.24 to the respective molecular observables. These contributions, expressed as percentages of the calculated values, are shown in tables 11-14. Values for the terms not included in the fits were calculated using the bare and dressed parameters determined in our abbreviated fit described above. Although this method of evaluation is not an accurate assessment of the values which these terms would have if they were included in the fitting procedure, it should give a reasonable idea of their relative importance.

The dipole moment contributions are shown in table 11. The $\underline{\alpha}_i \langle \underline{T} \cdot \underline{\hat{\mu}} \rangle_i$ term is substantial throughout, and far outweighs the $\underline{\mu}_i$ term in $\text{CCl}_n\text{F}_{4-n}$. The $\chi_i^{(2)} \langle \underline{T} \cdot \underline{\hat{\mu}} \rangle_i^2$ term, while not overwhelming, is also not negligible. The $\chi_i^{(3)} \langle \underline{T} \cdot \underline{\hat{\mu}} \rangle_i^3$ term is small, particularly in comparison to the largest contribution in each molecule.

Terms associated with the isotropic part of $\underline{\alpha}$ are shown in table 12. Of terms included in the fit, the bare $\underline{\alpha}_i$ are clearly dominant, with $\underline{\alpha}_i \langle \underline{T} \cdot \underline{\hat{\alpha}} \rangle_i$ accounting for less than 10% in all cases. The terms not included in the fit are generally small. The $\chi_i^{(2)}$ term amounts to less than 10% of α for all molecules except CH_4 , and the term involving $\chi_i^{(3)}$ averaged less than 1%.

Table 11.

Molecule	$10^{18} \mu$ (esu)	$10^{18} \mu'$ (esu)	Terms included in fit (% of μ')		Terms ignored in fit (% of μ')		
			μ_1	$\alpha_1 \langle T \cdot \hat{\mu} \rangle_1$	$X_1^{(2)} \langle T \cdot \hat{\mu} \rangle_1^2$	$X_1^{(3)} \langle T \cdot \hat{\mu} \rangle_1^3$	
CHCl_3	1.04	1.31	134	-34	-34	2	2
CH_2Cl	1.60	1.76	130	-30	-34	2	2
CH_3Cl	1.90	1.75	125	-25	-32	3	3
CH_3F	1.85	1.72	78	22	-37	8	8
CH_2F_2	1.98	1.95	82	18	-42	9	9
CHF_3	1.65	1.65	84	16	-49	11	11
CClF_3	0.50	0.54	-116	216	63	18	18
CCl_2F_2	0.51	0.34	-275	375	52	26	26
CCl_3F	0.46	0.47	-68	168	29	10	10

Table 12.

Molecule	Terms contributing to fit			Terms ignored in fit		
	$10^{24}\alpha$ (esu)	$10^{24}\alpha'$ (esu)	$(\% \alpha')$	$(\% \alpha')$		
				α_i	$\alpha_i \langle \underline{T} \cdot \hat{\underline{\alpha}} \rangle_i$	$\frac{2\chi_i^{(2)} \langle \underline{T} \cdot \hat{\underline{\mu}} \rangle_i}{3\chi_i^{(3)} \langle \underline{T} \cdot \hat{\underline{\mu}} \rangle_i}$ $\times (1 + \langle \underline{T} \cdot \hat{\underline{\alpha}} \rangle_i)$
CCl_4	10.50	10.53	91	9	2	—
CHCl_3	8.50	8.48	92	8	1	—
CH_2Cl_2	6.60	6.47	93	7	5	—
CH_3Cl	4.55	4.50	94	6	7	1
CH_4	2.60	2.59	94	6	40	3
CH_3F	2.61	2.66	94	6	7	1
CHF_3	2.80	2.79	95	5	-5	1
CF_4	2.85	2.85	95	5	-9	—

Values of $\Delta\alpha_K$ from the various terms are shown in table 13. The α_i and $\alpha_i \langle T \cdot \hat{\alpha} \rangle_i$ terms both make large contributions to this observable. The contributions from the $\chi_i^{(2)}$ term, which was not included in the fit, are large, particularly for the $\text{CH}_n\text{F}_{4-n}$ molecules. The contributions from the term involving $\chi_i^{(3)}$ are much smaller.

Contributions to the $\chi_{||}^{(2)}$ fit from terms in the expression for $\hat{\chi}_i^{(2)}$ are shown in Table 14. Contributions are generally huge compared to the $\chi_{||}^{(2)}$ values. In addition, the neglected terms involving $\chi_i^{(2)}$ are large. The terms involving $\chi_i^{(3)}$ which were not included in the fit are small except in the case of CH_2Cl_2 . All of the contributions are large for this molecule. This situation is not surprising when we look at the $\hat{\chi}_i^{(2)}$ for the individual bonds. The dressed bond tensors are large, but they cancel to less than a part in 200 when combined to form a molecular $\chi_{||}^{(2)}$. However, the individual terms do not each cancel, and so appear as large, conflicting molecular contributions. In the case of CH_2Cl_2 , for example, the neglected contribution involving $\chi_i^{(2)}$ is less than 10% of $\hat{\chi}_i^{(2)}$ in each of the two bond types in the molecule, yet when summed over the molecule, it is over 6 times the total $\chi_{||}^{(2)}$. This situation occurs, to some degree, in all of the molecules in this set, not only for $\chi_{||}^{(2)}$, but for μ and $\Delta\alpha_K$ as well. In view of the

Table 13.

Molecule	Terms included in fit			Terms ignored in fit (% $\Delta\alpha'_K$)		
	$10^{24} \Delta\alpha_K$ (esu)	$10^{24} \Delta\alpha'_K$ (esu)	(% $\Delta\alpha'_K$)			
				α_i	$\alpha_i \langle T \cdot \hat{d} \rangle_i$	$2\bar{\chi}_i^{(2)} \langle T \cdot \hat{\mu} \rangle_i$ $\times (1 + \langle T \cdot \hat{d} \rangle_i)$
CHCl ₃	-2.70	-2.53	21	79	24	—
CH ₂ Cl ₂	-0.60	-0.57	6	94	2	-2
CH ₃ Cl	1.54	1.60	31	69	32	4
CH ₃ F	0.20	0.19	88	12	624	16
CH ₂ F ₂	-0.02	-0.02	-15	115	148	7
CHF ₃	-0.18	-0.22	73	27	568	-14
CCl ₂ F ₂	-0.25	-0.39	7	93	12	-3
CCl ₃ F	-0.75	-2.11	18	82	-2	—

Table 14.

Molecule	$10^{30} \chi_{ }^{(2)}$ (esu)	$10^{30} \chi_{ }^{(2)'} $ (esu)	Terms included in fit (% of $\chi_{ }^{(2)'} $)				Terms ignored in fit (% of $\chi_{ }^{(2)'} $)	
			a	b	c	d	e	f
CHCl_3	.005	.020	695	-549	-449	403	-258	4
CH_2Cl_2	.017	.011	1855	643	-5025	2626	-635	-56
CH_3Cl	.057	.076	277	49	-502	276	89	-13
CHF_3	-.244	-.097	225	-149	25	-1	120	4
CH_2F_2	-.180	-.225	111	-39	50	-22	45	—
CHF_3	-.108	-.118	190	-34	21	-78	88	4
CClF_3	-.296	-.268	151	73	-67	-57	-8	1
CCl_2F_2	-.258	-.239	201	1	-43	-60	-2	—
CCl_3F	-.132	-.199	174	63	25	36	-1	—

Definition of $\chi_{\parallel}^{(2)}$ Terms for Table 14

a) $\underline{\chi}_i^{(2)}$

b) $\underline{\chi}_i^{(2)} \langle \underline{T} \cdot \underline{\hat{a}} \rangle_i$

c) $\underline{a}_i \langle \underline{T} \cdot \underline{\hat{x}}^{(2)} \rangle_i$

d) $3\underline{\chi}_i^{(3)} \langle \underline{T} \cdot \underline{\hat{\mu}} \rangle_i (1 + \langle \underline{T} \cdot \underline{\hat{a}} \rangle_i)^2$

e) $2\underline{\chi}_i^{(2)} \langle \underline{T} \cdot \underline{\hat{\mu}} \rangle_i \langle \underline{T} \cdot \underline{\hat{x}}^{(2)} \rangle_i$

f) $3\underline{\chi}_i^{(3)} \langle \underline{T} \cdot \underline{\hat{\mu}} \rangle_i^2 \langle \underline{T} \cdot \underline{\hat{x}}^{(2)} \rangle_i$

degree of cancellation, it is somewhat surprising that the fits are as good as they are.

In summary, we have constructed a model of electric tensor properties in which inter-bond interactions are taken into account. We include only electrostatic dipolar interactions, ignoring short-range non-classical forces and all higher order multipole moments. Further, we assume that all tensor properties of a bond are located at a single point, the position of which is arbitrary, although consistent with physical intuition. The model meets with several difficulties in implementation. Some of the observables are small differences resulting from incomplete cancellation of large bond tensors. This is the case for μ and $\chi_{\parallel}^{(2)}$ and, to some degree, for $\Delta\alpha_K$ and κ^2 . In addition, the $\chi_{\parallel}^{(2)}$ and higher order quantities are increasingly complicated and difficult to calculate. To eliminate coupling between the coefficients, it was necessary to truncate the expressions for the dressed tensors in a consistent manner, leaving what is in some sense a "first level" of interactions.

Despite the foregoing difficulties, our model still provides a fit to the experimental data which is somewhat better than that of the BAA. In particular α , which BAA fits very well, is fit equally well by the ISM. Thus we have established that the fact that isotropic properties are well fit by the BAA is not sufficient to imply that bond-bond interactions have a negligible

effect on molecular electric tensor properties. A posteriori evaluation of neglected terms indicates some trend toward decrease in the "odd-parity" contributions involving $\chi_i^{(2)}$, and such terms involving $\chi_i^{(3)}$ are shown to be much less important.

In view of these encouraging signs, we plan to extend our calculations to include the terms neglected here, including equation 6.25. We feel that there is reason to hope that such a fitting procedure, although formidable to implement, would arrive at a self-consistent set of bare bond parameters yielding a good fit to the experimental data and giving a satisfactory picture of inter-bond interactions.

CHAPTER 7

SUMMARY AND CONCLUSIONS

The objectives of the research presented here have been: measurement of the third order polarizability $\chi^{(3)}$ and, where appropriate, the second order polarizability $\chi^{(2)}$ of a number of simple molecules of potential or demonstrated theoretical and experimental interest, using the technique of dc-electric-field-induced optical second-harmonic generation (dcSHG); measurements of $\chi^{(2)}$ and $\chi^{(3)}$ for those molecules of the set CX_nY_{4-n} , $n = 1-4$, $X, Y = F, Cl, H$, for which measurements did not already exist; and development of a model to describe trends in the dipole moment, linear polarizability, and hyperpolarizabilities for series of structurally related molecules, including the effects of inter-bond interactions, with application to the halogenated methanes.

A review of second- and third-order electric tensor properties was presented. Also reviewed was the dcSHG process in gases for a particular electric field configuration, with the treatment extended to include anomalously dispersive gases.

The measurements were performed using an apparatus consisting of a pulsed, Q-switched ruby laser and associated optics and electronics, along with an experimental cell and gas handling system designed to permit temperature-dependent measurements in the gas phase

on substances which are liquids at room temperature.

The hyperpolarizabilities measured for the assorted small molecules were compared with other gas-phase experimental data and with theoretical results, wherever such data were available. Our values agreed acceptably with most other experimental data. In cases where large discrepancies occurred, it was felt that, because of the nature of the experiments, our data were the more reliable. Agreement with theoretical estimates for $\chi^{(2)}$ was poor, but calculations by various authors also disagreed strongly with each other. A quantum-mechanical approximation, formulated by Dawes to predict $\chi^{(3)}$ for the inert gases, was applied to H_2 , N_2 , and O_2 , but agreement with experiment was poor. Measurements of $\chi^{(2)}$ and $\chi^{(3)}$ were also made for several halogenated methanes, and these results, too, were compared with other experimental data. Agreement with other $\chi^{(3)}$ data is excellent. The $\chi^{(2)}$ from other gas-phase measurements tend to be larger than our values, but for the most part there is no serious inconsistency. Agreement with $\chi^{(2)}$ values extracted from liquid phase measurements is poor, but this is not unexpected, since the derivation of values from liquid measurements is indirect. There were no theoretical $\chi^{(2)}$ or $\chi^{(3)}$ values available for these molecules. However, it is anticipated that new theoretical techniques will lead to accurate calculations

for many of the molecules for which we have made measurements. Our data will provide a stringent test of the validity of such calculations.

Correlation of molecular electric tensor properties among molecules of similar structure was discussed. The Bond Additivity Approximation, or BAA, was applied to μ , α , $\chi_{||}^{(2)}$, and $\chi_{||}^{(3)}$ of the set H_2O , $(CH_3)_2O$, and CH_3OH , and was found to agree well with experimental data. This was also the case when the BAA was applied to α and $\chi_{||}^{(3)}$ for the halogenated methanes. However, the BAA did not reproduce well the variation from molecule to molecule of the experimental μ or $\chi_{||}^{(2)}$ values. A model of molecular electric tensor properties including the effects of dipolar electrostatic interaction among bonds was introduced. A simplified version of the model was applied to α , μ , and $\chi_{||}^{(2)}$ of the halogenated methanes, with a modest improvement over BAA, including the case of α , in which BAA worked well. We conclude that the success of BAA in dealing with isotropic properties does not imply that interactions among bonds can be neglected. It was found that higher order terms in our model tended to make smaller contributions to the observables. It is felt that the results warrant the effort to implement the full bond-interaction model, including all relevant contributions.

APPENDIX

APPENDIX

DCSHG IN ANOMALOUSLY DISPERSIVE GASES

The development in chapter two of an expression for second harmonic generation as a function of experimental geometry required a choice of sign to be made for the wave-vector mismatch Δk . The choice leading to equation 2.28 is $\Delta k < 0$, which is appropriate for gases of normal dispersion. We demonstrate here that the occurrence of a positive Δk would be readily detectable in a binary mixture experiment with a normally dispersive gas.

The wave-vector mismatch Δk enters into the derivation of equation 2.28 in the integral

$$I = \int_{-\infty}^{\infty} \frac{e^{i\Delta k z'}}{1 + i \frac{2z'}{b}} \frac{1}{1 + \left(2 \frac{(z' - z_0)}{d}\right)^2} dz' \quad (A1)$$

where the limits of integration are appropriate to harmonic generation in an infinite medium, which is a good approximation here. For $\Delta k < 0$, the integration is performed by the method of residues, considering as the contour the real axis and a semicircle at infinity in the lower half-plane. The only contribution to this integral is the single pole in the lower half-plane due to the dc field. For $\Delta k > 0$, the contour of the integral must be completed in the upper half-plane, in which both the dc field and

the optical field have poles. This integration can be done, yielding an expression for $S_>$, the value of $P^{2\omega}/(P^\omega)^2$ for $\Delta k > 0$, which is

$$S_> = S_< \frac{1}{(z_0^2 + (\frac{b-d}{2})^2)} \left\{ d^2 e^{-(b-d)|\Delta k|} + 2d e^{-(b-d)|\Delta k|/2} [z_0 \sin(|k|z_0) - (\frac{b+d}{2}) \cos(|\Delta k|z_0)] + z_0^2 + (\frac{b+d}{2})^2 \right\} \quad (A2)$$

where $S_<$ is the expression for $P^{2\omega}/(P^\omega)^2$ from equation 2.28. It should be noted that only the magnitude of Δk appears in equation 2.28. The expression for $S_>$ has independent maxima at $z_0 = 0$ and $b = d$, as does $S_<$, so again it is appropriate to work at these values of b and z_0 . It would appear at first glance that equation A2 has a singularity at $z_0 = 0$ and $b = d$. However, $S_>$ with $z_0 = 0$ approaches a finite limit as b approaches d , and this is the same limit approached by $S_>$ with $b = d$ as z_0 approaches zero. The limit is

$$S_> = (1 + d|\Delta k|)^2 S_<. \quad (A3)$$

With this expression, we are now in a position to predict the signal for binary mixtures of gases.

Suppose that we have two gases, labeled 1 and 2, such that $(\Delta k_o)_2 < 0$, and the sign of $\chi_{\parallel 2}^e$ (which we shall call simply χ_2) is known. We will refer to the $|\chi_{\parallel}^e|$ measured for gas 1 by the method described in section 3.2a as $|\tilde{\chi}_1|$. If $(\Delta k_o)_1$ is negative

$$|\chi_1| = |\tilde{\chi}_1| \quad , \quad (\Delta k_o)_1 < 0 \quad (A4)$$

However, if $(\Delta k_o)_1$ is positive, then

$$|\chi_1| = |\tilde{\chi}_1|/3 \quad , \quad (\Delta k_o)_1 > 0 \quad (A5)$$

The factor of three arises from the fact that the measurement is done with $\rho = \rho_o$. The optimum density ρ_o is defined by

$$\rho_o = \frac{2}{d|\Delta k_o|} \quad (A6)$$

where

$$|\Delta k_o| = |\Delta k|/\rho \quad . \quad (A7)$$

From equation A3 we see that for positive Δk_o , measurement at ρ_o leads to a factor of 9 greater signal for a given $|\chi_{\parallel}^e|$ than in the case of negative Δk_o . This factor is not accounted for in the procedure of section 3.2a.

For a mixture of gases, the effective third-order polarizability χ_M is given by

$$\chi_M = \frac{\chi_1 \rho_1 + \chi_2 \rho_2}{\rho_1 + \rho_2} \quad (A8)$$

and the wave-vector mismatch Δk_M by

$$\Delta k_M = \rho_1 (\Delta k_o)_1 + \rho_2 (\Delta k_o)_2 \quad (A9)$$

For $\Delta k_M < 0$, equation 2.28 can be used to find the form of the signal $S_{M<}$ generated in the mixture:

$$S_{M<} = C |\chi_1 \rho_1 + \chi_2 \rho_2|^2 \exp(-d |\Delta k_M|) . \quad (A10)$$

where C is a constant independent of the gases.

In practice, a fixed amount ρ_2 of gas 2 is placed in the cell, and the variation of the signal S_M is measured as the density ρ_1 of gas 1 is increased. Combining equations A3, A4, A5, and A10 we get

$$S_M = S_o |\tilde{\chi}_1 \rho_1 + \chi_2 \rho_2|^2 \exp(-d |\Delta k_M|) , \quad (\Delta k_o)_1 < 0$$

$$S_M = S_o \left| \frac{1}{3} \tilde{\chi}_1 \rho_1 + \chi_2 \rho_2 \right|^2 \exp(-d |\Delta k_M|) , \quad (\Delta k_o)_1 > 0 ,$$

$$\rho_1 \leq \left| \frac{(\Delta k_o)_2}{(\Delta k_o)_1} \right| \rho_2$$

$$S_M = S_0 \left| \frac{1}{3} \tilde{\chi}_1 \rho_1 + \chi_2 \rho_2 \right|^2 \exp(-d|\Delta k_M|)(1+d|\Delta k_M|), (\Delta k_0)_1 > 0,$$

$$\rho_1 > \left| \frac{(\Delta k_0)_2}{(\Delta k_0)_1} \right| \rho_2$$

(A11)

where S_0 is a factor normalizing the computed S_M values to the measured signal value at $\rho_1 = 0$. S_M can be plotted for four different cases, as follows:

1. $(\Delta k_0)_1 < 0$, χ_1 and χ_2 of opposite sign. As ρ_1 increases, the signal will decrease until cancellation occurs at

$$\rho_1 = \left| \frac{\chi_2}{\tilde{\chi}_1} \right| \rho_2. \quad (A12)$$

The signal will increase again, and then decay exponentially.

2. $(\Delta k_0)_1 < 0$, χ_1 and χ_2 same sign. As ρ_1 increases, signal increases to a maximum and then falls off exponentially. We choose ρ_2 to maximize the difference in signal between case 1 and case 2 at the expected cancellation density. As Finn⁵ has shown, this density is

$$\rho_2 = \frac{2}{d} \frac{1}{\left| \frac{\chi_2}{\tilde{\chi}_1} \right| + |(\Delta k_0)_1| + |(\Delta k_0)_2|} \quad (A13)$$

3. $(\Delta k_o)_1 > 0$, χ_1 and χ_2 of opposite sign. As ρ_1 increases, the signal may increase at first, but will then decrease to zero at

$$\rho_1 = 3 \left| \frac{\chi_2}{\chi_1} \right| \rho_2 . \quad (A14)$$

It then increases again, and finally falls off exponentially. Note that the expected cancellation density is three times that of case 1.

4. $(\Delta k_o)_1 > 0$, χ_1 and χ_2 of the same sign. As ρ_1 increases, the signal increases rapidly, and reaches a maximum much larger than that of case 2. Beyond the maximum, the signal decreases exponentially.

Plots of the expected signal for these four cases, along with experimental data, are shown in figure 17. Gas 2 in both plots is methane. In the upper plot, gas 1 is water vapor, and in the lower plot, gas 1 is methylene chloride vapor. The data show unambiguously that $\chi_{||}^e(\text{H}_2\text{O})$ is of opposite sign to $\chi_{||}^e(\text{CH}_4)$, $\chi_{||}^e(\text{CH}_2\text{Cl}_2)$ is of the same sign as $\chi_{||}^e(\text{CH}_4)$, and Δk_o for both gases is negative.

We have shown that a binary mixture experiment can be used to determine the sign of Δk_o for a gas simultaneously with the determination of the sign of $\chi_{||}^e$. Such experiments have shown that $\Delta k_o < 0$ for all of the gases that we have investigated.

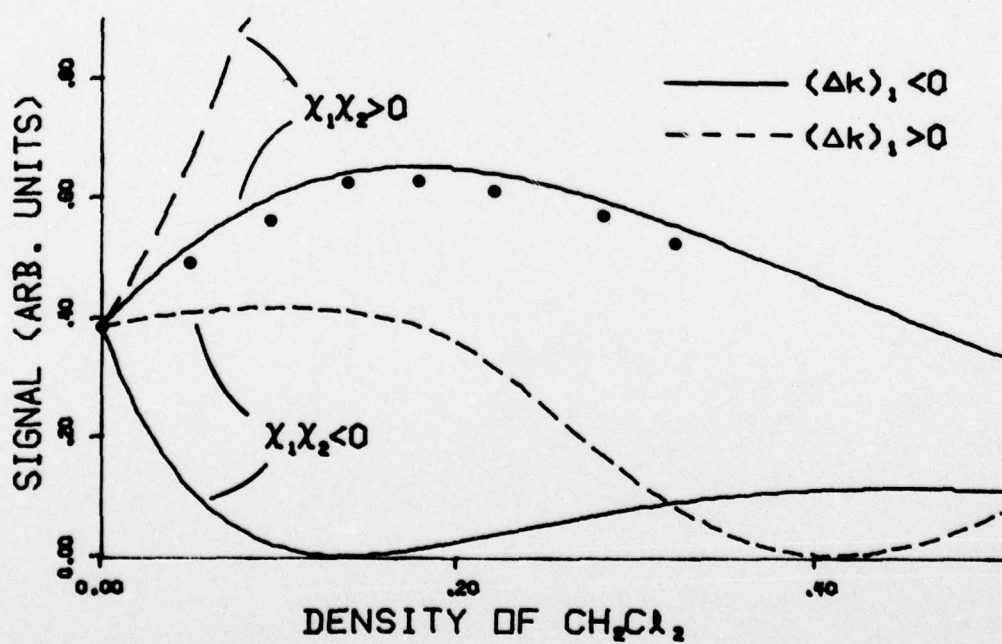
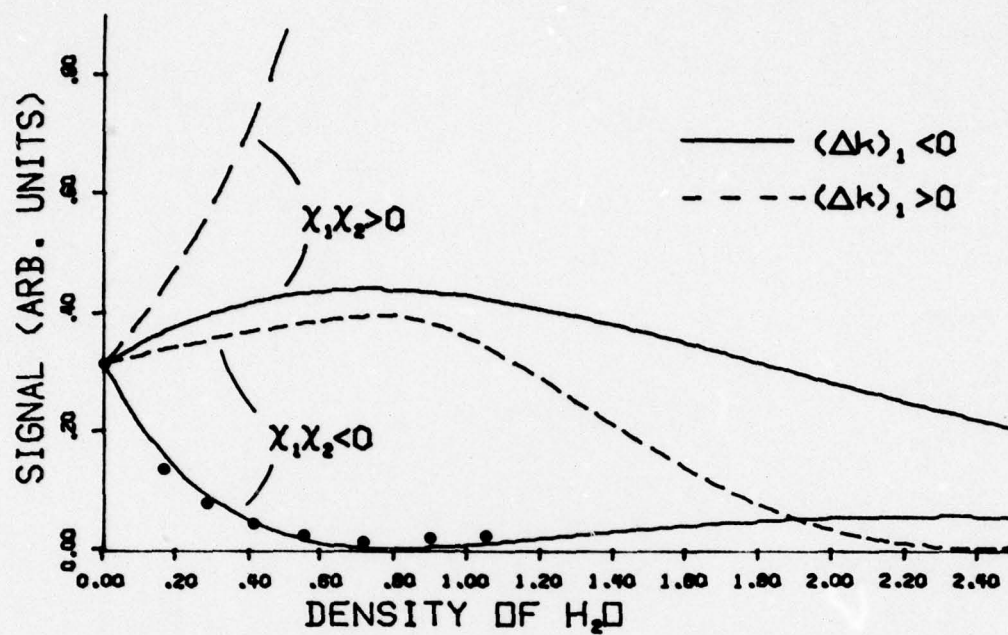


Figure 17. Signal vs. Density for Binary Mixtures.

REFERENCES

REFERENCES

1. M. P. Bogaard and B. J. Orr, International Review of Science. Physical Chemistry, Series 2, Vol. 2, edited by A. D. Buckingham (Butterworths, London, 1975), p.149.
2. A. D. Buckingham and B. J. Orr, Q. Rev. Chem. Soc. 21, 195 (1967).
3. Several review articles are available to introduce the reader to the myriad nonlinear optical and electro-optical phenomena; for example:
Reference 1.
P. A. Franken and J. F. Ward, Rev. Mod. Phys. 35, 23 (1963).
R. W. Minck, R. W. Terhune and C. C. Wang, Appl. Opt. 5, 1595 (1966).
Y. R. Shen, Rev. Mod. Phys. 48, 1 (1976).
4. G. Mayer, Compt. Rend. Acad. Sci. (Paris) 276B, 54 (1968).
G. Hauchecorne, F. Kerherve and G. Mayer, J. Phys. (Paris) 32, 47 (1971).
5. R. S. Finn, Thesis (University of Michigan, Ann Arbor) (1971).
6. I. J. Bigio, Thesis (University of Michigan, Ann Arbor) (1974).
7. B. J. Orr and J. F. Ward, Mol. Phys. 20, 513 (1971).
8. S. J. Cyvin, J. E. Rauch and J. C. Decius, J. Chem. Phys. 43, 4083 (1965).
9. C. J. F. Böttcher, Theory of Electric Polarization, 2nd ed. (Elsevier, Amsterdam, 1973).
10. I. J. Bigio, R. S. Finn, and J. F. Ward, Appl. Opt. 14, 336 (1975).
11. This expression appears in references 5, 6, and 10 with an erroneous factor of 1/2. This factor does not affect the results in these references, since only relative measurements were involved.
12. J. F. Ward and I. J. Bigio, Phys. Rev. A 11, 60 (1975).

13. R. S. Finn and J. F. Ward, Phys. Rev. Lett. 26
285 (1971).
14. P. Sitz and R. Yaris, J. Chem. Phys. 49, 3546
(1968).
15. R. S. Finn and J. F. Ward, J. Chem. Phys. 60, 454
(1974).
16. A. D. Buckingham and D. A. Dunmur, Trans. Faraday
Soc. 64, 1776 (1968).
17. Irving J. Bigio and J. F. Ward, Phys. Rev. A 9, 35
(1974).
18. R. S. Finn and J. F. Ward, Appl. Opt. 11, 2103 (1972).
19. Jayanta K. Guha, Appl. Opt. 15, 2381 (1976).
20. Hugh D. Young, Statistical Treatment of Experimental
Data, (McGraw-Hill, New York, 1962).
21. A. D. Buckingham, M. P. Bogaard, D. A. Dunmur,
C. P. Hobbs, and B. J. Orr, Trans. Faraday
Soc. 66, 1548 (1970).
22. R. Bartlett and I. Shavitt (private communication).
23. J. M. O'Hare and R. P. Hurst, J. Chem. Phys. 46,
2356 (1967).
24. P. Lazzeretti and R. Zanasi, Chem. Phys. Lett. 39,
323 (1976).
25. G. P. Arrighini, M. Maestro, and R. Moccia, Symp.
Faraday Soc. 2, 48 (1968).
26. E. L. Dawes, Phys. Rev. 169, 47 (1968).
27. E. Merzbacher, Quantum Mechanics, 2nd edition (Wiley,
New York, 1970).
28. International Critical Tables, edited by E. W.
Washburn (McGraw-Hill, New York, 1930) Vol. VIII.
29. N. J. Bridge and A. D. Buckingham, Proc. R. Soc.
(London) Ser. A 295, 334 (1966).
30. B. F. Levine and C. G. Bethea, J. Chem. Phys. 65,
2429 (1976).

31. C. K. Miller and J. F. Ward, Phys. Rev. A 16, 1179 (1977).
32. B. F. Levine and C. G. Bethea, J. Chem. Phys. 63, 2666 (1975).
33. C. K. Miller, B. J. Orr, and J. F. Ward, J. Chem. Phys. 67, 2109 (1977).
34. Numerous references are cited in Reference 33 regarding the history and previous application of the BAA, cautions about and estimates of the magnitudes of inter-bond interactions, and theoretical support for the localization of molecular properties in bonds.
35. L. E. Sutton et al., Tables of Interatomic Distances and Configurations in Molecules and Ions (Chemical Society, London, 1958); Interatomic Distances Supplement, (Chemical Society, London, 1965).
36. Eugene V. Ivash and David M. Dennison, J. Chem. Phys. 21, 1804 (1953).
37. P. R. Bevington, Data Reduction and Error Analysis for the Physical Sciences (McGraw-Hill, New York, 1969).
38. B. F. Levine, Phys. Rev. B 7, 2600 (1973).
39. K. R. Sundberg, J. Chem. Phys. 66, 114, 1475 (1977).
40. J. Applequist, J. R. Carl, and K.-K. Fung, J. Am. Chem. Soc. 94, 5168 (1972).
41. D. van der Hart and W. H. Flygare, Mol. Phys. 18, 77 (1970).
W. H. Flygare and R. C. Benson, Mol. Phys. 20, 225 (1971).
42. J. H. Dymond and E. B. Smith, The Virial Coefficients of Gases (Clarendon, Oxford, 1969).
43. W. G. Rado, Appl. Phys. Lett. 11, 123 (1967).
44. A. D. McLean and M. Yoshimine, J. Chem. Phys. 46, 3682 (1967).

45. Landolt-Börnstein, Zahlenwerte und Funktionen, Neue Serie, Gruppe II, Atom- und Molekularphysik, Band 6 (Springer-Verlag, Berlin, 1974).
46. R. D. Nelson, D. R. Lide, and A. A. Maryott, Selected Values of Electric Dipole Moments for Molecules in the Gas Phase, NSRDS-NBS 10 (U.S. Dept. of Commerce, Washington, 1967).
47. A. R. Blythe, J. D. Lambert, P. J. Petter, and H. Spoel, Proc. R. Soc. (London) Ser. A 255, 427 (1960).
48. M. P. Bogaard, B. J. Orr, A. D. Buckingham, and G. L. D. Ritchie (unpublished), as cited in Reference 31.
49. G. D. Zeiss and W. J. Meath, Mol. Phys. 30, 161 (1975).